HVDC CORONA INDUCED FIRE UNDER DC POWER LINES

by

CLEMENT MALAMBA SIAME
209511568

Dissertation

Submitted in partial fulfillment of the requirements for the degree

Master of Science in Electrical Engineering

School of Engineering

University of KwaZulu–Natal

As the candidate's supervisor I agree to the submission of this dissertation

Date of Submission:_____

Supervisor:_____
Andrew Swanson

DECLARATION OF PLAGIARISM

I, Clement Malamba Siame., declare that

1. The research reported in this dissertation, except where otherwise indicated, is my original research.

2. This dissertation has not been submitted for any degree or examination at any other university.

3. This dissertation does not contain other persons' data, pictures, graphs or other information, unless specifically acknowledged as being sourced from other persons.

4. This dissertation does not contain other persons' writing, unless specifically acknowledged as being sourced from other researchers. Where other written sources have been quoted, then:

a. Their words have been re-written but the general information attributed to them has been referenced

b. Where their exact words have been used, then their writing has been placed in italics and inside quotation marks, and referenced.

5. This dissertation does not contain text, graphics or tables copied and pasted from the Internet, unless specifically acknowledged, and the source being detailed in the dissertation and in the References sections.

Signed

……

ACKNOWLEDGEMENTS

Thanks go firstly to the heavenly father who granted me a moment in an ocean of time to produce this work. I wish to dedicate this work to my late father, Francis G Siame, who at a tender age of my life taught me to understand that a person in life can show you the way but the journey is yours. With these worlds, I would like to appreciate the invaluable contribution from my co-supervisors, Professor Ijumba and Dr. Chetty for the valuable guidance they provided to me during my studies. I would further like to appreciate the assistance given by Ms Leena Rajpal, Mr. Aaron Mutombo and Ms Charlain King, from the HVDC Centre. To the academic support staff, Ms Fiona Higginson and Ms Kim Henry, I wish to say thank you for your valuable support.

My heart filled sincere gratitude goes to my supervisor, Andrew Swanson, for having taken time to provide the guidance and support I so much needed. I wish also to appreciate friends that encouraged me; Kasumpa, Titi, Ojo and Brian. Finally, the deepest debt of my gratitude goes to my family and above all my Wife, Lister, and the Children for their love, patience and encouragement in a space of time that seemingly appeared endless.

ABSTRACT

This dissertation is about investigations on the influence of the electric field and ion current flow on the combustion of dry grass under HVDC power lines. The main objective is to show that a bush fire can actually occur when a critical electric field induced on dry grass under the HVDC power transmission line is reached. The coupling of the electric field to the dry grass as well as the space charge is the main components of this critical electric field. The ion current through a sample of dry grass was measured under an indoor HVDC test line. The maximum critical field on the surface of the conductor at which the dry grass under the line ignites was determined to be 15.86 kV/cm for a two wire conductor bundle and 36.895 kV/cm for a four wire conductor bundle at the applied voltage above 300 kV.

The current through the grass was measured and the corona activity on the conductor was captured by using the CoroCam1 in order to see the corona inception points. The corona activity against grass height was correlated in order to see what effect grass height has on the flammability of grass. The surface temperature of the grass was measured with a thermal scanner from which it was determined that grass ignites at a temperature of about 80 ^{0}C. A monopole indoor HVDC test line was used for the above tests. The test line was energized by a power supply consisting of a two-stage Cockcroft-Walton generator to a voltage of ± 320 kV.

To further appreciate the influence of the electric field on dry grass under the power line, the test arrangement was modelled in Quickfield^{TM} with a two- and a four-conductor bundle. The simulation results obtained in Quickfield^{TM} tied in well with the practical results as both results indicate that the magnitude of the ion current in dry grass under a HVDC transmission line increases with an increase in grass height and the level of applied voltage. It could be seen from the results obtained that the electric field and the ion flow of HVDC lines can lead to ignition of grass if a certain voltage is surpassed. The data contained in this dissertation will be used as a basis for further research on the dielectric characteristics of dry grass as there is little information in published literature.

Keywords: HVDC: dry grass; corona-induced current; corona-inception gradient and bush fire.

TABLE OF CONTENTS

ABBREVIATIONS

AC	Alternating Current
ASTM	American Society for Testing and Materials
CoroCam1	Corona Camera
CR	Capacitor Resistance
DC	Direct Current
HVAC	High Voltage Alternating Current
HVDC	High Voltage Direct Current
IEC	International Electro-Technical Commission
IEEE	Institute of Electrical and Electronic Engineers
PMC	Percentage of Moisture Content
RI	Radio Interference
TGA	Thermal Gravitation Analysis
UKZN	University of KwaZulu-Natal

LIST OF FIGURES

LIST OF TABLES

CHAPTER 1 INTRODUCTION

1.1 Background

An overhead transmission line still stands out as one of the most important components of today's electric power system. The fundamental purpose of the transmission system is to deliver power from generating stations to the distribution system that ultimately supplies the loads. Most of the sites suitable for power generation are located in remote areas. This necessitates long distance transmission of power over grasslands. A transmission system is essential in that it enables power utilities to exchange power for economic advantages and allow emergency assistance to be rendered whenever some generating plants are out of service. This is what is seen in the existence of power pools like the Southern African Power Pool in which eleven countries in Southern Africa have interlinked their transmission infrastructure to facilitate a reliable electricity market [1]. Both HVAC and HVDC transmission systems are found in the Southern African Power Pool.

Since, the HVAC systems are the most used and widely understood systems around the world, it would be helpful to briefly state what happens under HVAC transmission lines and then compare this with what might be happening under HVDC systems. Under HVAC systems, wood poles are used up to a voltage level of 345 kV. There have been reports of wood poles carrying transmission line conductors burning since the inception of high voltage transmission [2]. The phenomenon of wood pole catching fire is affected by such parameters as conductivity of wood surface, dryness of the wood below the surface, the shape of the metal structure attached to the wood, and the highest space potential to which the surface of the pole is exposed. Experience with HVAC systems seems to suggest that a condition for the occurrence of wood burning near hardware is that the potential on the surface of the pole at some point exceeds a space charge potential of 100 kV [2].

Pole fires have also occurred on instrumentation poles near HVAC transmission lines. There have also been reports of dead tree burning under these transmission lines [2]. Although dead trees have a very high resistance when dry, in wet weather their branch surfaces form conductive

sheaths that collect electrical charges and discharge them to the ground. Thus, the portion of dead trees that intrude inside the space potential can experience burning [2].

Transmission of power with High Voltage Direct Current technology has steadily become attractive because of improvements in technology [3]. However, it must be noted that the ratio of fair to foul weather for corona power loss is much higher for HVDC than for HVAC. The advantages of HVDC over HVAC include low losses for long distance bulk power delivery, ability for asynchronous connections, requires no transmission of VArs, and ability to efficiently offer long submarine connection.

1.2 Motivation

Worldwide, there is a constant search for means of reducing cost, improving reliability, and minimizing environmental impact of power lines. This has increased challenges in the evolution of the design methods to try and meet the challenges the power industry faces today. It is important to note that addressing these challenges at design stage is cheaper as most of the aspects are built in.

Additionally, high voltage power lines induce charges on the ground and in the environment [4-6]. For instance, Eskom operates a transmission network that stretches to approximately 28000 km on which a case study was carried out from 1993 to 2008, drawing a conclusion that 86% of the total faults were as a result of power lines interaction with nature [7]. Fire under the power line was found to be the second most prominent cause of unscheduled outages.

The desire to find ways to improve the integration of high voltage power lines into their operating environment thereby improving line performance, as shown by Eskom's case study in which a major decrease in line faults over a six year period was reported [2] led to the commencement of this research. The need to improve the power system availability while embedding power lines into the natural environment brought about the motivation in this topical area.

1.3 Objectives

1. To establish the electrical equivalent model of dry grass.

2. To establish the effects of DC corona on dry grass.
3. To establish the critical electrical field at which grass under the line can ignite.
4. To establish the combustion point of dry grass.

1.4 Research question

Corona discharge takes place on high voltage power line conductor surfaces on points where the electric field at the conductor surface is above the critical value. This leads to ionization of air in the immediate environment around the power line. The resulting ion current flows and electrifies objects under the line [8]. The measurements obtained and studies from research in [5,6,8] indicate that there is a flow of ion current on the ground of the DC lines.

Grass is one of the underlying vegetative undergrowth in the power lines and is a perennial plant which in most cases dries up in the course of the year making it a potential source of fire. So, the question is: *Can corona-induced currents from the adverse effect of the High Voltage Direct Current power lines ignite dry grass under the line?*

1.5 Hypothesis

Corona induced currents from HVDC overhead transmission lines can ignite grass under the transmission line due to the space charge and high electric fields.

1.6 Rationale

Bulk power transmission has increasingly become a topic of interest due to increased energy demand and high sensitivity on environmental issues in the world today. Overhead transmission lines operating at higher voltages have become the most economical means of transmitting large amounts of power over long distances. The lines are exposed to extreme ambient conditions such as high altitude, severe pollution, natural vegetation and uncertain weather conditions. It is imperative, therefore, that a robust and reliable transmission line design is utilized so that a safe operation of the line is granted in spite of exposure to such tough conditions.

Overhead transmission lines generate electric and magnetic fields in their vicinity, which now is of great environmental concern and a design limitation in many countries [2]. Looking at the

large number of high voltage transmission lines passing through forests and farm lands, determination and understanding of the electrical environment in the vicinity of power line in terms of ionized field parameters, space charge density, electric field intensity and current density is very essential for the assessment of environmental impact of the transmission lines on its surroundings.

Corona is a significant factor in the design of high voltage power lines because it is influenced by the key line parameters which include the diameter of the conductor, number of conductors per bundle, conductor clearance to ground and voltage level. Since corona has a large influence on the cost of designing, building and operating high voltage power lines, it is important that knowledge of its effect is fully investigated. This research will add to the already existing knowledge about the environment around the high voltage power lines. This will help in understanding and improving the evaluation of the performance of the high voltage transmission lines leading to some of the benefits that have been seen by Eskom [2].

The grass model developed will be useful in studying very critical cases that cannot be performed in practice. Therefore, the model will offer designers an effective tool. The research will highlight some of the adverse effects that power lines have on the environment which could be solved if care is taken at design stage. In fact, the data contained in this dissertation will be used as a basis for further research on the dielectric characteristics of dry grass as there is no such information in published literature.

1.7 Dissertation outline

Chapter 1 introduces the topic, 'HVDC corona-induced fire under DC power lines' by outlining the causes of fire under the transmission lines. The motivation, objectives, research question, hypothesis and rationale of this dissertation are also given. Chapter 2 looks at literature review concerning corona causes while chapter 3 presents the research methodology followed in the course of the study. Chapter 4 contains results and analysis whereas chapter 5 gives the conclusions and recommendations. Appendices A to E provide more details about how the experiments were done and results obtained.

CHAPTER 2 LITERATURE REVIEW

2.1 Introduction

Corona is a phenomenon caused by the partial electrical breakdown or ionization of the air surrounding a conductor or fitting when energized at a high voltage, whether AC or DC. Corona is a self-sustained electrical discharge that proceeds from an electron avalanche process in which neutral molecules are ionized by electron impact under the influence of the applied electric field. The ionization is localized over a portion of the distance between the electrodes [9].

Atmospheric air is composed mainly of 78% nitrogen, 21% oxygen and traces of different other elements. The electronegative nature of oxygen molecules sustains the corona discharge. Oxygen molecules easily capture free electrons and form negative ions, which aid the electron avalanche process. The avalanche process creates what is known as space charge that tends to move away from the source. Corona discharge is accompanied by visible light, audible noise, ionic current flow, energy loss, Radio Interference (RI) noise, mechanical vibrations, and chemical reactions [9-14].

Corona has some negative effects on high voltage power transmission lines that are of concern to power engineers such as power loss, audible noise, RI and TV reception interference. Nonetheless, corona still has some valuable practical uses in industrial engineering such as electrostatic precipitators, electrostatic printers, electrostatic deposition, ozone production, gas cleaning, spraying of powders, plasma chemical reactors and ionization counting [15].

2.2 Electrical discharge in air

Air serves as an insulating medium in the power system industry. It has two major advantages which are occurring in abundance and the self-restoring capability after a breakdown [9]. Impact ionization is the most important process in air discharge as can be seen from the next two paragraphs.

Taking an electrodes at high voltage in a gaseous medium induce an electric field that causes free electrons to accelerate to the anode. In the migration process, they collide with neutral air

molecules causing excitation of gas atoms and ionization of floating particles. There are a number of collisions that occur between the free electrons and air molecules along the mean free path in the direction of the electric field [9, 13]. The energy imparted during the collision is large enough to dislodge an orbiting electron, a positive ion is produced and left behind, while the new electrons together with the original electrons proceed along the field and the collision process progressively continues to happen. The effectiveness of ionization depends upon the energy that charged particles gain as they accelerate under the effect of the electric field. In a uniform electric field, the head of an avalanche is built up of electrons while the tail is clouded with positive ions as shown in Figure 2.1. This happens because electrons have higher velocities than the positive ions that might appear virtually at standstill in the time period an electron takes to reach the positive pole [5].

A lot of research has been done with regard to the investigation of mobility of positive and negative ions in dry air [4-6], [16-22]. It has been found that the mobility of ions in the drift zone is independent of the field strength when the velocity due to the field is considerably less than the average thermal velocity of air.

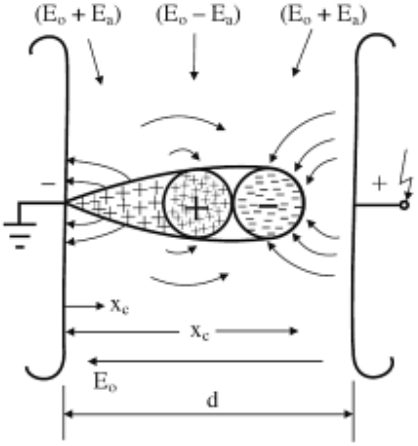

Figure 2.1: Development of an electron avalanche in a uniform electric field [9]

2.3 Mechanism of corona discharge

A gap of atmospheric air in a non-uniform electric field develops a corona discharge across a range of voltages in a small area of highly stressed electrode before the gap eventually completely breaks down. Various criteria have been developed for the onset of corona discharge, with *Streamer criteria* and *Townsend breakdown criteria* being the most common [9,14,15]. The

avalanche process in a gaseous gap is empirically expressed as shown in Equations (2.1) and (2.2) below where α is an impact ionization coefficient, η an attachment coefficient of air molecules, and γ is a coefficient representing secondary ionization.

$$\exp\left(\int \alpha' dx\right) = \frac{1}{\gamma} \tag{2.1}$$

$$\alpha' = (\alpha - \eta) \tag{2.2}$$

In non-uniform electric fields, the net coefficient ά varies as the distance, x, increases from the highly stressed electrode. The integral which gives the efficiency of secondary ionization is valid only with a positive net coefficient of ionization by electron impact. In gases, this is the process that keeps ionization in the gap.

When the electric field is very strong in the region of α, electron collision is then greater than electron attachment. The ions formed from several consecutive avalanches accumulate to form a space charge in an area of low electric field because of the slow mobility of ions. This process continuously modifies the local electric field intensity while the developed corona discharge cycle is removed from the region around highly stressed electrode. In order to properly illustrate the developments of corona the account will be looked into according to negative and positive corona modes [9].

2.4 Negative corona

On a negatively charged highly stressed electrode, cathode, electron avalanches are developed and pushed towards the anode by a continuously decreasing field [9,14,15]. Due to non-uniformity of the field distribution, an electron avalanche advancement stops in a regional surface S_o where the net ionization coefficient cancels out. However, since free electrons can move faster than ions under the applied electric field, they concentrate at the head of the avalanche, while positive ions remain in the region S_o. This leads to an alteration of the electric field and gives negative corona its modes namely; Trichel pulses, negative pulseless glow and negative streamer respectively [14].

2.5 Positive corona mode

At the positively charged highly stressed electrode, an electron avalanche is initiated on the surface S_o, a point of zero net ionization, and then grows towards the anode in an increasing nature. Electrons rapidly move toward the highly stressed positive conductor, ionizing neutral air molecules in the process [9]. The increase in charges as the electrons progress in a non-uniform electric field leads to a high electric field at the anode. Since the electron mobility is very high, this enables them to leave behind the slow drifting positive ions. When an electron avalanche occurs, excited molecules release photons that give rise to secondary avalanche processes [9,14]. Highest ionization takes place in close vicinity of the anode conductor. Due to a high electric field at the anode, low electron attachment occurs because most of the electrons are neutralized at the anode. The ionization region has a negligible thickness when compared to the gap between the electrodes.

2.6 Corona on-set voltage

When voltage is applied on a conductor to ground or between concentric cylinders, a potential is reached at which corona starts as shown in Figure 2.2. This voltage is called the critical visual corona point [2,8,9,14,15,23]. The breakdown of air under normal temperature, standard pressure and humidity, is taken as 30 kV/cm [2].

Corona on-set electric field E_c on a cylindrical smooth wire surface is given by Peek's formula [2,8,13,15] as in equation (2.3) where, r is conductor radius and H conductor height.

$$E_c = 30(1+\frac{0.301}{\sqrt{r}})r\ln\frac{H}{r} \qquad (2.3)$$

However since density of air is influenced by pressure and temperature, it is important to look at the relative density of air. The breakdown of air is affected by humidity, temperature and pressure, the Peek's formula is modified as shown in equation (2.5) while the air density δ can be obtained using equation (2.4) [24-26].

$$\delta = \frac{3.92b}{273+T} \tag{2.4}$$

Where b= pressure in cm

T = temperature in degrees

$$E_c = 30\delta(1+\frac{0.301}{\sqrt{r\delta}})r\ln\frac{H}{r} \tag{2.5}$$

The practical explanation of the occurrence of corona around a charged conductor would be that on a perfectly smooth conductor, at a gradient of 30 kV/cm, velocities of ions become sufficiently high so as to ionize other ions in air by collision. When ionic saturation is reached in air, then air starts to conduct and glows, thereby creating visual corona around the charged conductor as shown in Figure 2.2.

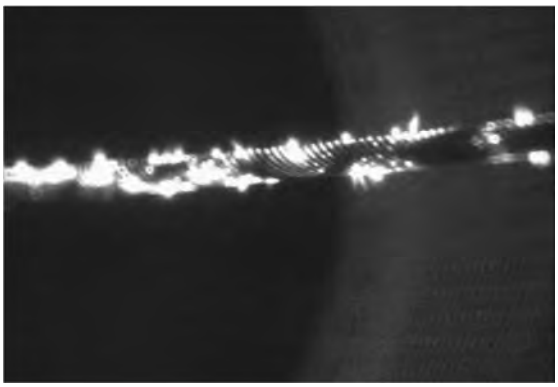

Figure 2.2 Visual Corona on Bundle wire [UKZN Lab result]

A number of laboratory tests have been done using a cage to study transmission line conductor characteristics [2,9,13,15,22,27]. According to references [9,14,28], the corona on-set voltage V_o for a smooth conductor-to-plane configuration is given as in equation (2.6).

$$V_o = E_c r\ln(2H/r) \tag{2.6}$$

In which $H >> r$ normally, and the crical electric field E_c is calculated as already given in equation (2.3).

2.7 Factors influencing corona

Corona on high voltage transmission lines occurs due to the ionization of air surrounding conductors. This is because the conductor surface electric field becomes greater than the critical break down electric field E_c. Occurrence of corona is influenced by a number of variable factors as outlined below.

2.7.1 Conductor

Conductor size affects the corona on-set voltage by influencing voltage gradient on the surface of the conductor. Increasing conductor size raises the corona on-set voltage as shown in Equations (2.3) through (2.6). Conductor surface voltage gradient has an inverse relationship with conductor size [15,29-33].

Conductor surface condition creates regions of uneven electric field distribution. Roughness of conductor lowers the onset voltage. Surface irregularity [34,35] is influenced by stranding, water droplets, ice, insects and snow. Reference [36] shows the effect of pollution deposit on a bundled conductor surface. Stranding of a conductor increases surface irregularity [32] as the field at the tip of each strand is enhanced by 40% as compared to a smooth conductor having the same diameter. The corona on-set voltage changes around the periphery of each strand by 10% when compared to a smooth conductor.

Increasing the spacing between the conductors reduces the surface voltage gradient which raises the corona on-set voltage. In [33] and [37] it was found that there exists an optimum sub-conductor spacing. Bundled conductors reduce corona effects as the effective diameter is higher. The inverse relationship of conductor surface voltage gradient with conductor diameter was established by Whitehead in 1910 and this theory still helps us to understand the kind of conductor sizes required for a particular voltage level in modern day overhead transmission lines [14].

2.7.3 Atmosphere

The on-set voltage is also affected by weather as stated in [37,38]. Breakdown voltage of air is directly proportional to the density of the atmospheric air present in between the power conductors. Increasing temperature increases the ions kinetic energy as shown in [39] in which the load current influences on corona by causing temperature rise was investigated. In the discussion of [39], it is reported that with temperature as the dominant factor influencing mobility of the positive ions, it was found that mobility increases with electric field and decreases with temperature. For the negative ions, it was reported that the mobility increases with temperature but decreases with increasing electric field.

Humidity and dust increases the presence of particles in natural air, which in turn, increases the number of ions present around the conductor. These particles increase the space charge resulting in a lower on-set voltage. However, the increased ions are slower and this reduces the corona-induced current in the end [4,6,24,40,41].

Wind extends the region of ion flow, and affects space charge velocity, ion current and electric field [4,37,40,41]. Wind flowing perpendicular to the line gives higher effect on the corona current distribution at ground level mainly on bipolar lines. Since wind removes ions from the ion cloud that forms around the highly stressed conductors to the opposite polarity field, this disturbs the ion balance causing the conductor to produce more ions in an attempt to restore the equilibrium. This mean that increase in wind velocity increases the ion movement causing an increase in corona losses [2]

2.7.4 Line configuration

Corona performance is affected by the field intensity at the conductor surface which is inversely proportion to the radius, the conductor height above the ground and the line voltage. A set of equations used to determine corona is given in published literature [9] for different symmetrical configurations from which a general standard form can be developed that applies to all symmetrical configurations [12,21,35].

In [37], vertical and horizontal configurations of bipolar DC transmission lines are investigated and results compared in terms of electric field and current density measured at ground level. This outlines how different configurations can affect corona.

2.8 Environment under the power line

HVDC transmission systems have numerous advantages but impose a lot of design challenges to engineers with regards to increased corona and the subsequent space charge. Space charge is composed of ions and charged particles [3]. Thus, corona and the electric fields are of particular importance.

Under the HVDC power lines, the direction of the electric field does not change with time, resulting in the space between the electrodes being filled up with ions with a polarity similar to the polarity of the conductor. The electric field and wind act on the space charges to produce ionic current in space as the charged particles and electrons are moved by electric field and wind [4-6,33,37]. Wind extends the region of ionic current flow beyond the right of way required for HVDC transmission lines [5]. The extension could be up to several hundred meters from the conductors, depending on the wind speeds.

On the contrary, the space charge generated by HVAC transmission lines is confined to a small volume immediately surrounding the conductors [12,20,21,37,42]. The space charge is constrained near the conductors and oscillates with the electric field. Therefore its effect is negligible on the overall field distribution.

The accumulation of ions under the HVDC power line can result in the electrification of objects under the line. These occurrences are both technically and environmentally unacceptable [2,4,6,9].

Experimental results show that there is a clear difference in the coupling mechanisms under positive and negative polarity. It tends to indicate that the coupling/induction is more significant under negative polarity [11]. Electric field and current density profiles under the transmission line are strongly influenced by line configuration, magnitude of line voltage, wind and humidity. It is extremely difficult to carry out stable short time measurement for a practical line because of

unpredictable wind and weather conditions. Electric field strength on ground level is mostly influenced by space charge that is produced by corona. Away from the Right Of Way, it is wind speed that accounts for the ionic current flow because the electric field has little effect. Since it reduces with distance from the conductor center line [2,4,5,23,37,40,43].

Unipolar DC transmission lines have ions of only one polarity drifting in space because of the unidirectional electric field between the conductors and ground. Mathematical models for the representation of the interaction between the electric field and ionic currents in the unipolar DC transmission line, ignoring wind influence, are done by taking simplified assumptions which then reduce the system to the following non-linear differential equations [2,12,20,21,30,44,45] in (2.7) for Poisson equation and (2.8) for Laplace equation where V is voltage, E electric field, ρ Poisson's factor and ε electric constant.

$$\nabla.E = -\rho V / \varepsilon \tag{2.7}$$

$$\nabla^2.V = 0 \tag{2.8}$$

Mobility μ of ions is as given in equation (2.9) where V is voltage and E electric field.

$$\mu = \frac{V}{E} \tag{2.9}$$

Current Density **J** is calculated using equation (2.10) where p is charge density, μ mobility, and E electric field.

$$J = \rho\mu E \tag{2.10}$$

The concentration of ions, n, in ions /cm^3, where e is electron charge is given as in equation.

$$n = \frac{J}{eE\mu} \tag{2.11}$$

Current Continuity is as given in equation (2.12) where the parameters have already been defined above.

$$\nabla.J = 0 \tag{2.12}$$

The total current required is then evaluated using equation (2.13) below.

$$\int \vec{J} d\vec{A} = \vec{I} \tag{2.13}$$

However, with wind speed, w, taken into account, as is the case in most practical transmission lines, the ion current density equation changes to equation (2.14).

$$J = \rho(\mu E \pm w) \tag{2.14}$$

On bipolar lines, corona occurs simultaneously on both positive and negative poles [29,31,38,46]. The space between the conductors is filled with a cloud of both positive and negative ions which drift towards their opposing pole leading to ion recombination.

This phenomenon accounts for a higher corona loss in bipolar dc transmission lines when compared with monopole lines. Calculation of mutual interaction of the electric field and ionic currents in the bipolar DC transmission line with no wind conditions are done using nonlinear partial differential equations (2.15) through (2.19) outlined below. These equations are well defined and used in [31,38,46] for positive and negative ions.

$$\nabla . J^{+} = -\left(\tau \rho^{+} \rho^{-}\right) / e \tag{2.15}$$

$$\nabla . J^{-} = -\left(\tau \rho^{-} \rho^{+}\right) / e \tag{2.16}$$

$$\nabla . E = \left(\rho^{+} + \rho^{-}\right) / \varepsilon \tag{2.17}$$

$$j^{+} = \left(-\mu^{+} \rho^{+} E\right) \tag{2.18}$$

$$j^{-} = \left(-\mu^{-} \rho^{-} E\right) \tag{2.19}$$

However, most of the practical situations require an account for wind speed, *W*, to be made. Therefore, the equations (2.18) and (2.19) are respectively modified to equations (2.20) and (2.21) as used for a bipolar dc line.

$$j^{+} = \left(\rho^{+}(-\mu^{+} E + W)\right) \tag{2.20}$$

$$j^- = \left(\rho^-(-\mu^- E + W)\right) \tag{2.21}$$

The ion flow characteristics in the presence of wind are important for assessing the dispersion range of ions from HVDC transmission lines. It has experimentally been proven that the presence of wind affects the corona current and ion current density measured on the ground [2,4,11,37]. The density of the space charge in both bipolar and monopolar configurations depends on the intensity of corona generation on the pole [28] and [29] while corona is significantly affected by the prevailing atmospheric conditions.

Under no wind conditions as shown in equations (2.18) and (2.19), space charge moves along flux lines of the electric field. The inter-electrode electric field is highest under the no wind conditions. With wind, ions experience mechanical force in addition to already existing electrical forces which increase their mobility. Both wind speed and its direction determine the distribution of space charges. Consequently, the forced movement imposed on ions by wind makes it possible to have negative ions existing under the positive pole in certain instances.

2.8.2 Corona power loss

Corona power loss on monopolar and bipolar DC transmission lines has been calculated mainly using various methods based on Finite Element or Charge Simulation Techniques. The movement of space charge around the conductor is the source of corona power loss [2]. Corona loss varies with applied voltage measured for different heights under HVDC lines for both bipolar and monopole. Corona loss is higher for a bipolar line than a monopole line. Corona loss decreases as the distance away from the transmission lines increases [13,14,47]. The point of highest ion flow is directly under the conductor and this is the point of measurement in this dissertation.

2.9 Properties of dielectric materials

Dielectrics are materials that are polarized upon subjection to an electric field. When a dielectric material is placed in an electric field, electrons do not flow through the material like in a conductor because they are inhibited by an interior restraining force between the positive and

negative charged centers [48-51]. With the external field applied charged particles, a force is exerted on the positively charged nucleus and the negatively charged electrons to produce a displacement. This will slightly shift them from their equilibrium positions causing dielectric polarization.

However, displacement equilibrium is obtained when the applied forces are balanced by the internal attractive Coulomb force of the couplets [49,50]. The formed electron dipole has positive charges aligned towards the electric field and negative charges moved in the opposite direction as shown in figure 2.2 below. This creates an internal electric field which reduces the overall field within the dielectric medium. Materials formed from weakly bonded molecules will have polarization and also reorientation of molecules so that their symmetry axis aligns to the field. Dielectric materials are used in electrical industries as insulators and for making capacitors.

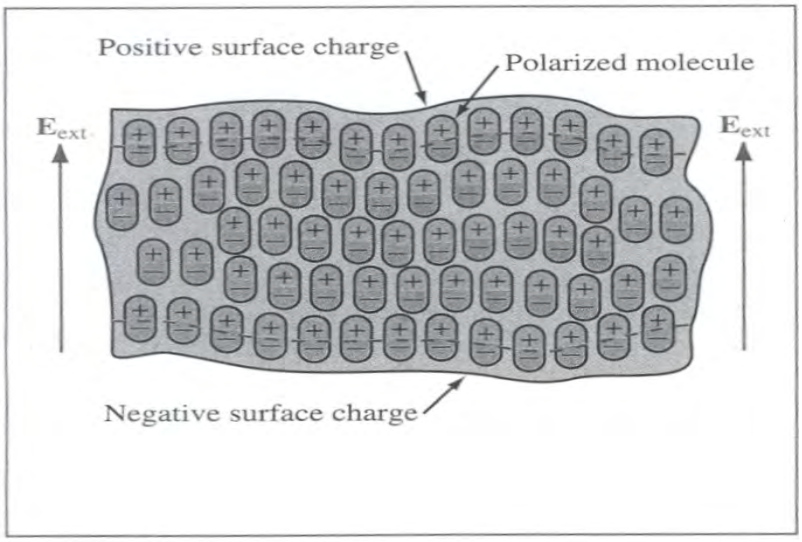

Figure 2.3: Alignment of charges in a dielectric material [49]

The response of an insulating medium to a time dependent electric field is determined by the complex permittivity ε, which at a given frequency and temperature, is the intrinsic property of the material. This is expressed by equation (2.22).

$$\varepsilon = \varepsilon_r + j\varepsilon^{"} \tag{2.22}$$

Permittivity signifies the measure of the ability of the medium to dispose its charges so as to oppose the applied field [49-53]. This is also a material property that governs the charge storage and the displacement of current density from electric field

Figure 2.4 is used to explain the losses in an insulator. It can be noted that in an ideal capacitor I_c will lead I_R by 90^0 as shown in figure 2.5 which shows the phase diagram of the currents of a practical capacitor in which the capacitive current (I_c) is the imaginary part and the resistive current (I_R) is the loss component. In practice, I_c will lead I_R by an angle less than 90^0 from which a vector analysis reveals that the tangent of an angle between (I_c) and (I_R) is tan δ, which defines the dissipation factor. This is the ratio of an insulating material's resistance to its capacitive reactance at a specified frequency.

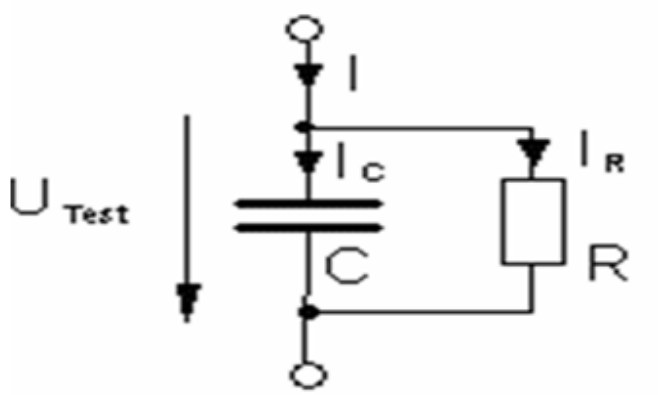

Figure 2.4 Capacitor equivalent circuit [34]

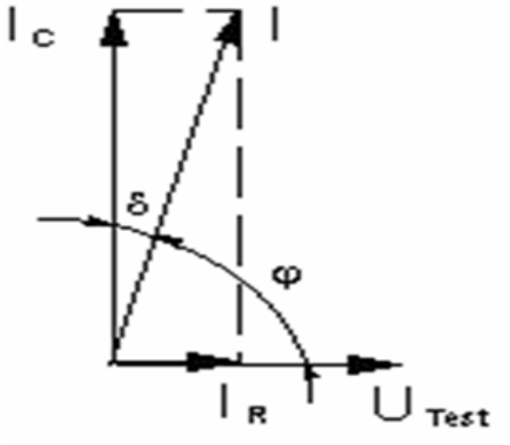

Figure 2.5 Practical capacitance vector diagram [34]

Furthermore, if we take a dielectric material in the electric field and let E to be the electric field applied on the electrode and J as the terminal current per unit electrode area, then the terminal current *i* is as given in equation (2.23).

$$i = \oint_s J da \tag{2.23}$$

The component of J due to conduction is as given in equation (2.24).

$$J_c = E\sigma \tag{2.24}$$

The displacement current from surface charge is as given in equations (2.25) and (2.26).

$$J_d = \frac{d(E\varepsilon)}{dt} \tag{2.25}$$

$$J = J_c + J_d \tag{2.26}$$

However, if the permittivity of the material is constant, then equations (2.27) to (2.29) become the results with the parameters that have already been defined above.

$$J_d = E\dot{\omega} \tag{2.27}$$

$$J = iE\omega(\varepsilon + \frac{\sigma}{i\omega}) \tag{2.28}$$

$$\varepsilon^* = (\varepsilon' + j\varepsilon'') \tag{2.29}$$

2.9.1 Properties of wood

As observed in chapter 1, there are reports of wood under HVAC overhead transmission lines burning. However, since a number of studies have been done on wood already and it is helpful to look at its properties and see how these might relate to those of grass and help in forming the structure work of this study. Wood has a complex, yet ordered microstructure with porosities ranging from 50 to 80 percent by volume [54]. Wood consists of cellulose, lignin and hemicelluloses. Cellulose chains are highly ordered and partially crystalline. These chains are

bound together by the hemicelluloses to form micro fibrils. The micro fibrils and amorphous lignin combine to form the primary cell wall structure [55]. The main cells in wood are parallel to the longitudinal direction (growth direction) in the tree.

Wood is grouped into two categories, hard and soft wood. Hardwood microstructure consists of smaller cells with large-diameter vessels which transport water. Softwood microstructure consists of a more ordered arrangement with larger and longer cells than those of hardwoods. Both microstructures have smaller pores running in the radial direction [55].

In the study of dielectric characteristics of woods, the perturbation and free space techniques have been used widely [53,55,56]. The factors which can affect the dielectric properties of a porous material such as wood are material-related properties of volume porosity, pore size, pore distribution and absorbed water content. Porosity causes a decrease in the dielectric permittivity, since air has a dielectric permittivity close to 1. The pore distribution and shape controls the mixing rules used to combine the permittivity of air and the material [55-58].

There are also measurement-related factors such as temperature and frequency, which affect the dielectric permittivity of wood through the relaxation mechanisms of the material [59]. However, it is shown [57] that the dielectric permittivity is higher at low frequency. Humidity affects water content in a hygroscopic material, which in turn increases the dielectric permittivity according to [55-58] because water has a higher dielectric permittivity of 80.

Cellulose materials are highly hygroscopic. This is one of the main difficulties in the testing of the dielectric permittivity of material with this composition. The presence of moisture has a large effect on the specific inductive capacity and this also subsequently affects the conductance [55,58]. The nature of these effects on wood is well illustrated as shown in [57] which shows how the capacitance increases and the resistance decreases with absorption of moisture. The results indicate that the dielectric increases with rising moisture content as explained by Kol. in the study of *Thermal and Dielectric Properties of Pine Wood*.

The orientation of the electric field with respect to the structure is affected by the type of wood. The electrode configuration affects how the dielectric permittivity is calculated [55,57] Dielectric

measurements as a function of frequency also provide a measure of the energy dissipation in the material [50,58]

2.9.2 Corona-induced fires

When an electric field is applied to a dielectric material, (grass in this case), conduction current, however small it may be, flows through the material. This current, heats up the specimen and the temperature rises. The heat generated is transferred to the surrounding medium by conduction through the solid dielectric and by radiation from its outer surfaces. Equilibrium is reached when the heat used to raise the temperature of the dielectric, plus the heat radiated out, equals the heat generated. When a certain critical voltage is reached, the heat generated may be more and this can lead to burning of grass. If wooden poles and dead trees can burn under HVAC lines, then going by the geometry of grass, it makes sense that dry grass will catch fire due to high electric fields and space charge under a HVDC transmission line [34].

CHAPTER 3 RESEARCH METHODOLOGY

3.1 Introduction

This chapter presents the investigation of the influence of corona-induced ion currents by the HVDC transmission lines on the ignition of dry grass under the lines in the right of way. An experimental set-up to measure the ion currents flowing in dry grass under the HVDC lines due to electric field and space charge was established. To further appreciate the influence of the electric field on dry grass under the power line, the test arrangement was modelled in Quickfield^{TM} with a two and a four conductor bundles.

3.2 Research methodology and assumptions taken

Having analysed results from the research in [4-6,21-31] which conclusively puts up an accepted descriptive phenomenon of the electric field under the DC Power lines, and taking a theoretical model that assumes grass as a practical capacitor C_g as shown in Figure 3.1 below, the dielectric characteristics of grass can thus be analysed [47-52].

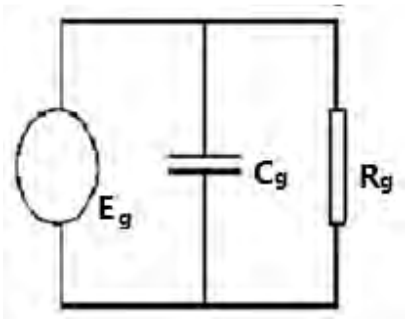

Figure 3.1 Electrical Equivalent Circuit of Grass under the power Line [47]

The ion current I_g due to the space potential E_g under the line flows through the grass resistance R_g. The power P is then generated by the current through the resistance of grass as shown in equation (3.1) below, and this gives rise to the production of heat that can cause burning of grass.

$$P=I_g^2R_g \tag{3.1}$$

Dry grass with a potential to grow to a considerable height above the ground was identified as a sample. The result in this experiment was subjected to the local conditions of KwaZulu-Natal province in terms of climate and vegetation. There has been some unexplained bush fires under the Cahora-Bassa HVDC line that have happened from time to time. Therefore, the grassland of Kwazulu-Natal province was studied using the articulations from [60].

Five grass samples were identified that meet the relative heights suitable for testing. These samples were identified as Hyperrhenia filipendula, stenotaphrum secundatum, Hyparrhenia Hirta, Cymbopongon Validus and Hyperrhenia Aucta & H Rufa. All the grass gathered had inflorescence for easier identification. Only the grass type that had not been exposed to nature for a long time had to be picked. This reduced the variations in the results by bringing consistency into the vegetative state of the dry grass collected.

Grass is composed of a cellulose material as outlined in [54-58] which makes it highly hygroscopic when exposed to uncontrolled environments. This means that its moisture content would vary considerably. The collected grass was kept in a controlled environment to achieve consistency in the moisture content. This meant a measurable fixed amount of moisture content had to be maintained which reduced discrepancy in the results.

Dry grass being made out of cellulose like wood [57,58] is an insulating material. Therefore, all the samples with known moisture content were subjected to an electrical test to establish their electrical equivalent model as per test procedures in [54,55]. Since there are no known dielectric properties for grass in literature, several tests were performed and then the data subjected to statistical analysis to come up with normalised values from several sampled data. There was no reference data for the ignition temperature of grass. Therefore, the digital combustion material analysing equipment [57,58] was used in this dissertation.

An experimental test to investigate the effect of corona on dry grass under the HVDC power line using an indoor test line was performed. The indoor test line was used so as to eliminate the variation in weather whose effect requires a much longer time of testing to analyse. Grass was bunched into a fixed radius so that only variation in grass heights was tested while maintaining the same cross-section area. Repeated tests were done and checked for consistency in the results.

The major assumption taken in the experiments was that grass was a one cylindrical solid component so as to have meaningful analysis by holding grass into a regular shaped bundle. The theory of the environment under a transmission line states the boundary conditions of the electric field as varying from the minimum at ground level to the maximum field on the conductor. This made taking grass height to be a variable parameter in this experiment an important aspect.

Finally, the variation of air conductivity with the electric field was studied by performing a measurement experiment of the same so as to appreciate how conductance of air is affected by the field which was required for the simulation.

3.3 Grass sample selection

The grass habitat that was found to be of particular interest in this research was the Elephant grass as it is commonly referred to. The Hyperrhenia Aucta & H Rufa grass type was identified because of the species height dominance and a location preference that matched the environment under the power lines. Hyperrhenia Aucta & H Rufa is a tall grass that often occupies well watered lands and, when dry, has been subjected to frequent burning. It is particularly abundant in areas where soils have been previously disturbed due to some developments like roads construction and power line routing. This grass type is often known to have a characteristic of invading and eventually dominating other species especially in areas where grazing is less likely [60].

The grass type is distinct as it appears as a robust perennial plant with stems that can grow to heights of 280 cm high, usually un-branched or scantly branched. Thus, this is the grass type that was subjected to numerous tests in the corona-induced fire investigations.

3.3.1 Grass collection and storage

Dry Hyperrhenia Aucta & H Rufa grass was gathered from the bushes around Durban and then stored in a specially designed wooden house. The wooden house is shown in Figure 3.2 on the following page. The house composed of wooden sleepers arranged horizontally so as to enable well ventilated environment. A heater was installed for temperature control inside the house. This allowed the room ambient temperature conditions to be modulated. The inside of the

wooden house is as shown in Figure 3.3. Since, the collection of grass was done during a period of high humidity in Durban which was from November to December being a raining season of the year. This meant that the collected grass had absorbed a lot of moisture being a highly hygroscopic material.

Studies [55,57,58] have shown that wet material with cellulose has a higher conductivity of electricity due to the absorbed moisture mixed with the mineral elements left in the body structure of dry grass. Electric field studies [61,62] have proved that a conducting surface always develops an equal electric field distribution. It was therefore found not ideal to study the wet grass. In view of this, all the collected grass had to have its moisture content reduced by storing it in the wooden house where moisture conditioning was carried out.

The temperature in the house was initially kept at 48 ^{0}C with a low humidity so as to keep the air dry and increase the absorption of moisture from the grass. This allowed the grass to release excess moisture thereby reducing the water content in dry grass to an acceptable level of 11% and below. It was found necessary to reduce the moisture content to this level because most of the bush fires under the HVDC line have been observed to occur during the dry season of the year.

Figure 3.2 Wooden house used for environmental conditioning of grass

Figure 3.3 Inside the Conditioning House

The grass was stored in the conditioning room for five days during which moisture tests were done daily until when no noticeable changes were obtained in the weight percentage of water content. The room temperature was maintained constant by the heat generated by the 20 incandescent lamps of 100 Watts each installed in the house. The room temperature inside the house was then kept at 38 ^{0}C. A gas fired open Bunsen burner was additionally used during periods of rain to keep the room dry.

3.3.2 Testing moisture content in grass samples

The moisture content in grass was determined by removing the grass moisture using an industrial oven with temperature control functions that enabled to set the temperature at 105 ^{0}C. Bunches of grass samples were weighed prior to being put in the oven and then dried until a constant weight was attained. The difference in the weights, between the initial weight W_1 and the final constant weight W_2 was the moisture content in the grass which was expressed as the percentage of the initial weight as shown in equation (3.2) where PMC is percentage of moisture content. The results are shown in Tables A1.2 to A1.5 in section A1.1 of Appendix A.

$$PMC = \frac{W_1 - W_2}{W_1} \tag{3.2}$$

3.4 Experimental Set-up

The electrical characteristics of the dry grass were determined using the tan delta equipment explained in [64] and the test cell shown in figure 3.4 below. The electrical conductivity of air was determined using a two-stage Walton-Cockroft generator and the test cell. The arrangement of the HVDC test line used is as shown in figure 3.5. The parameters for the test line are shown in tables 3.1 through 3.3. Measurements of ion currents were done as indicated in figures 3.6 and 3.7 then then the test line was modelled in Quickfield^{TM} software.

3.4.1 Dielectric characteristics of grass

Direct measurements are used mainly on power frequencies and low temperatures. This was used in this dissertation. The grass samples were molded into regular shapes that depended on the test cells. The Capacitor Resistance (CR) Meter [51,63] was used to measure the dielectric properties of grass. For loose materials like grass, a dielectric test cell consisting of a fixture of two adjustable plates into which the sample was installed for evaluation of its electrical properties was used. By connected to an automatic CR meter, the capacitance (C) was measured [64]

Guidelines on the testing of wood [55,57,58] were followed for the tests on grass. Previous wood tests provided valuable information. The testing was done according to the guidelines of the International Electro-technical Commission (IEC) and the American Society for Testing and Materials (ASTM) [63-65]. These references outline the details of testing methods and measurement techniques of dielectric constants with a focus on the fundamentals and principles for solid insulators.

The guide for cutting grass samples into small regular pieces which could easily fit in the test cell and then compressed for tight packing is as shown in Figure 3.5.The test chamber was weighed without grass and then with compressed grass. After each test, the test chamber was carefully cleaned and dried.

Hydraulic compression was used with a loading of 20 kg to ensure tight and compact packing so that the chances of air introducing errors were minimized. In each test sequence, the voltage was

raised slowly from 2 kV to 7 kV in six definite steps. During each test cycle pressure, temperature and humidity were measured.

Figure 3.4 Grass compacted in a test cell

The capacitance for grass was measured as, C_{xm} and conductance as $G_{xm,}$ using the CR meter. Tests were then repeated with air in the cell and then capacitance and conductance for air were measured and noted as C_a and G_a respectively.

The dielectric constant for grass was obtained by dividing capacitance of grass C_{xm} with capacitance of air C_a as shown in equation (3.3).

$$\varepsilon'_r = \frac{C_{xm}}{C_a} \qquad (3.3)$$

It is important to know that the permittivity obtained for grass is lower than the actual because there is always some air between the electrodes and the sample. Section A1.2 of Appendix A contains the detailed procedure of how the permittivity and conductance of air was determined.

To validate the method used for determining the permittivity of grass, the permittivity of transformer oil was determined using the same apparatus. This approach was used because so as to be sure of the permittivity value obtained and check the methodology used. Since the permittivity for Transformer oil is well known. The approach for the validation is given in section A1.3 of Appendix A.

3.4.2 Electrical conductivity of air

A varying voltage from a two-stage Walton-Cockcroft generator supplied the test voltage for the current conduction test of the natural air at room temperature, pressure and humidity in a uniform field measured between two fixed parallel plates. These tests were performed in an indoor HVDC laboratory at Westville Campus of UKZN. During the test, increasing voltages were measured with the corresponding conductance as indicated on the tan delta instrument. The tests were repeated five times to check the consistency in the values taken. These tests were done so as to appreciate what goes on in the air (Figure A1.3 in section A1.2 of Appendix A) when the electric field is present.

3.4.3 HVDC test line

The HVDC test line in the HVDC laboratory is a mono pole line with a single span. The test line is suspended between two steel anchor towers mounted on wooden slabs with a distance of 7.55 m apart as shown in the side view of Figure 3.5. The line has a middle span height of 2.4 m and shielded by a single earth wire mounted at 3.1 m above the ground. The initial test configuration had four conductors in a bundle with a sub-conductor radius of 1.4 cm and spacing distance of 1.8 cm.

The test line was energized by a power supply consisting of a two-stage Walton-Cockcroft generator supplied from two cascaded transformers each with a ratio of 0.23/100 kV with a cascaded output of 550 kV ac. The transformer ac output is rectified by the Walton-Cockcroft generator to energize the test line to a voltage of ±500 kV maximum and current of 7.5 mA.

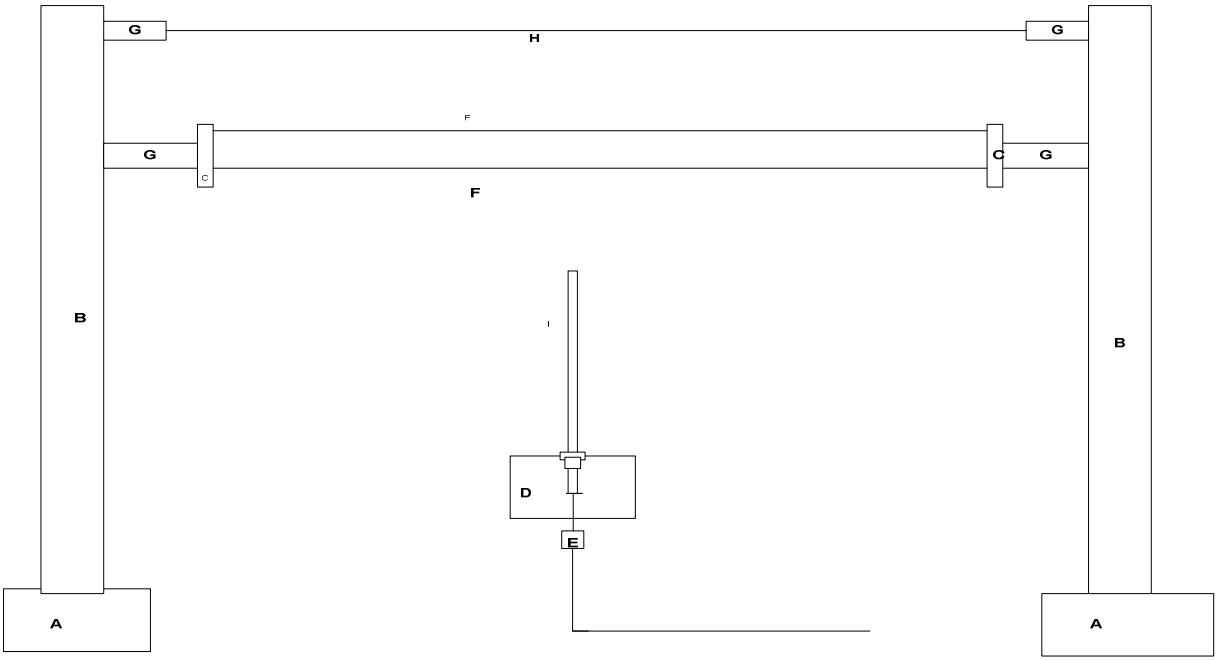

Figure 3.5 Test line arrangement diagram

However, the available test voltage range is ± 320 kV due to safety clearances in the laboratory. The specifications of the power supply and test line are summarized in Tables 3.1 through 3.3.

Table 3.1 HVDC test line components

A	Wooden Block
B	Steel Structure
C	Metal Plate
D	Perspex Sample holder
E	Shunt Resistor
F	Conductor
G	Insulator
H	Earth wire
I	Grass

The following were the other equipment used: 500 kV DC Test Kit, Pico-meter, Thermal Temperature Sensor Camera, Corona Camera (CoroCam1), Field meter, and Hygrometer.

Table 3.2 Power source circuit parameters

Parameter	Value
C1	150 kV, 100 nF
C2	300 kV, 50 nF
C3	300 kV, 50 nF
C4	300 kV, 50 nF
D1	300kV, 20 mA
D2	300 kV, 20 mA
D3	300 kV, 20 mA
D4	300 kV, 20 mA
R_m	300 kV , 2x 600 MΩ
R'_m	560 Ω
Rg	10 kΩ
Voltage Divider	20 kΩ
T1	0.23/100 kV
T2	0.23/100 kV

Table 3.3 HVDC test line parameters.

No. of sub-conductors	Diameter [cm]	Spacing [cm]	Conductor height [cm]	Earth wire height [cm]	Grass radius [mm]	Grass heights [cm]
4	2.3	18	230	310	10	40-220

The procedure adhered to during the tests was as follows:

1. Using a negatively charged test line with four conductors in a bundle configuration and a sub-conductor radius of 1.4 cm, a bunch of dry grass from sample A, cut to 40 cm height was placed under the test line.

2. The sample was then subjected to an increasing voltage in steps of 20 kV over the range of 0 to 320 kV DC.
3. At each voltage ramp, corona-induced current was measured and the grass sample surface was scanned using a thermal scanner for any localized sudden temperature changes and results recorded. CoroCam1 was used to capture any corona activity.
4. The test cycle was then repeated for each grass height. The grass heights tested were 40 cm, 80 cm, 120 cm, 160 cm, 180 cm, 200 cm and 220 cm. The test was performed without changing the line configuration and sub-conductor radius.

3.4.4 Corona-induced ion current measurement

The ion current measurement was done by directly connecting an HV probe from a shunt resistor attached to the copper base plate in the sample holder to a digital multi-meter fluke, model 187, and then to ground as shown in Figure 3.6. Since the base plate was not directly earthed, measurements of corona-induced ion currents were possible.

Although the test was done indoors, temperature, humidity, and pressure were constantly measured before and after each test as a precaution to ensure that there were no major changes because corona loses are significantly influenced by weather [5,30,42]. Sudden variation could negatively impact on the results.

3.5 Simulation methodology

The simulation was done by first developing the electrical equivalent model of dry grass, then the second part was to develop a Quickfield^{TM} test line model and the last part was the setting up of test conditions. The results were then compared with the experimental results. In the simulation the relative permittivity of grass that was used was 3.6 and the conductance was 0.0078×10^{-6} S. This data was obtained from the normalized values in appendix A1.2 after carrying out statistical analysis on the data using the model in figure 3.1 to represent grass. The simulation done was a two-dimensional finite element analysis.

3.5.1 Specific issues addressed

1. Varying the number of conductors in a bundle

2. Varying grass heights

The HVDC overhead transmission line was modelled as shown in figure 3.8 below.

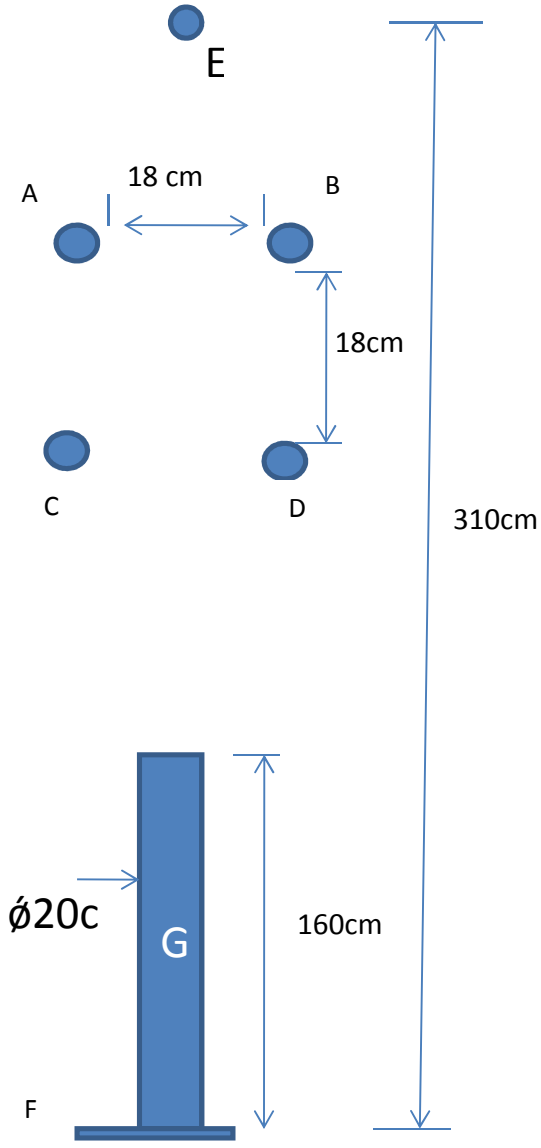

Figure 3.6 Cross section view of the HVDC test line at UKZN Westville HVDC laboratory

In Figure 3.6, A, B, C, and D, are the four wires part of the conductor bundle, E is the earth wire, G grass, and F copper plate. Quickfield^{TM}, being an electromagnetic field analysis software based on the finite element method, was then used to solve the partial differential equations for a monopole line as represented by equations (2.7), (2.8) and (2.12).

Dirichlet boundary conditions were used in the model by providing the electrostatic potential V(r) on the conductor surface and taking a grounded plate to be at 0 V [20,66]. With the mathematical model presented, it was possible to simulate and evaluate the electric field for different heights of grass. The density of the finite elements was made higher in the critical regions of the dielectric where higher accuracy was required.

3.5.2 Simulations performed

The following were the actual steps followed in the simulations:

1. A negatively charged test line with a configuration of four conductors in a bundle and a sub-conductor radius of 1.4 cm was used.
2. Grass for sample A, with a permittivity of 3.61 and a height of 40 cm along the y-axis, was placed between the line and the ground plate.
3. The sample was then subjected to an increasing voltage in steps of 20 kV over the range 0 to 320 kV DC.
4. The evaluated corona-induced ion current and electric field were then plotted against the applied line voltage.
5. The simulation cycle was then repeated for each grass height in sample A. The used heights were 40 cm, 80 cm, 120 cm, 160 cm, 180 cm, 200 cm and 220 cm.
6. The number of conductors in a bundle for the test line configuration was then changed from 4 to 2 while maintaining the same sub-conductor radius of 1.4 cm. Steps 2 to 5 above were then repeated.
7. The number of conductors in a bundle for the test line configuration was then changed from 2 to 1 while maintaining the same radius of 1.4 cm. Steps 2 to 5 above were then repeated.
8. The simulation cycle was then repeated as outlined in steps 2 to 7 above for the positive pole and same sub-conductor radius and results recorded.

CHAPTER 4 RESULTS AND ANALYSIS

4.1 Introduction

The results in this section show that corona induced currents from HVDC lines can indeed ignite grass under the transmission line due to space charge and high electric fields. The permittivity and conductance of grass were also determined as indicated in Appendix A1.2, and the test used to determine these two parameters was validated by determining the permittivity for Transformer oil as explained in Appendix A1.3.

4.2 Thermal gravitation analysis (TGA) results for dry grass

The thermal gravitation analysis shown in Figure 4.1 indicates that grass ignites at 80 ^{o}C which can be noted in the sudden change in the rate of change in weight and heat flow. The progressive curve shows that grass then burns to carbon which then re-ignites to burn to ashes at 350 ^{o}C as indicated by the sudden change in rate of weight change.

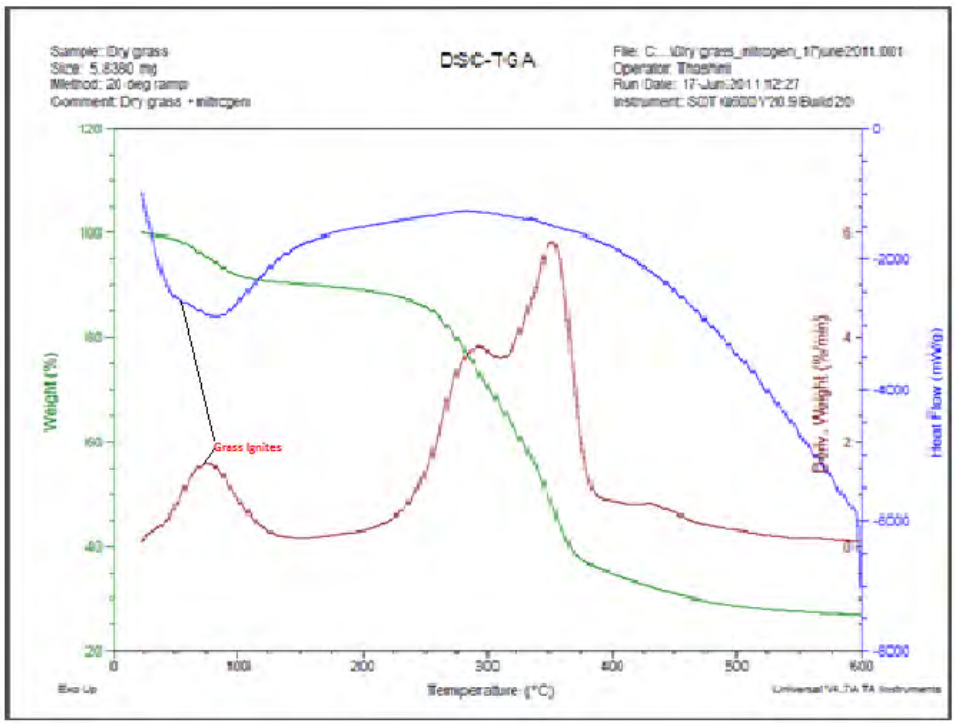

Figure 4.1 Combustion of dry grass in nitrogen –TGA results

In order to prevent combustion the sample was analyzed in nitrogen to remove moisture and volatiles up to 600 ^{o}C, and then allowed to cool to 400 ^{o}C. Following which the nitrogen was replaced by air and the sample heated from 10 ^{o}C to 800 ^{o}C until it turned into ash. The three curves in Figure 4.1 are;

- The green curve is the TGA curve - percentage weight vs temperature
- The brown curve is the derivative curve - derivative percentage weight vs temperature
- The blue curve is the heat flow

However, in the laboratory, during the pratical test of grass under the test line, the highest temperature caputured was 71.8 ^{0}C before grass ignited. It was difficult to determine the actual ignition temperature using the thermal scan as the combustion was spontaneous and fire had to be extinguished before it could spread and cause damage under the test line.

4.3 Corona-induced ignition of dry grass under the test line

Figure 4.2 Thermal scan on 150 cm grass under the HVDC test line

Figure 4.2 above shows the ignition point (71.8 ^{0}C) of grass as reported in section 4.2 above. This was captured in the laboratory. The grass of height 150 cm under the HVDC transmission line with four wire conductor bundle that got burnt (figure 4.3) at the applied voltage of 320 kV and 5.4 µA corona-induced ion current. The grass was effectively 90 cm below the conductor bundle. This measurement is obtained by subtracting grass height from the conductor height which was measured at 240 cm, if we remove the grass height , this gives us the effective

measure of the grass from the conductor bundle. Grass, like all insulated objects under a HVDC transmission line, are charged by corona-generated ions through a process called ion flow electrification. Since dry grass is a dielectric material, it means theoretically it does not have any practical ability to conduct electric current as outlined in the assumption that insulators do not have any losses.

The practical position is that a leakage current exists which is defined as dielectric loss. These losses act as a thermal source under high-voltage conditions. Dry grass being a practical dielectric material is modelled to comprise a capacitor in parallel with a resistor as shown in figure 3.1. A reasonable potential is held across the resistor on which heat is generated by the current that flows through it.

Applying this theory to dry grass, it can reasonably be agreed that with suitable ambient conditions and moisture content attained, there exist possibilities that grass can ignite as shown in figure 4.3 below.

The resistance of a bunch of dry grass is not uniform in all practical sense. There are some regions with higher resistance that can cause high voltage concentration. The high resistance regions generate heat from corona-induced ion current. These areas develop a localized arcing which gradually develops to a thermal runaway and fire eventually. This fact can be observed from the results on the grass under the HVDC test line which showed that only certain localized portions of the grass got burnt as shown in figure 4.3.

Figure 4.3 Burnt grass bunch with height of 150 cm under posistive corona.

The grass was not burnt at the tip where there was visible corona streamer effect as shown in Figure 4.4. The portions that got burnt are at the base where grass made contact with the grounded copper plate and in the middle of the grass stalk. This meant that the combustion of grass was due to the corona-induced ion current flowing in and around the dry grass. Thermal imaging also showed the gradual temperature rise on the grass samples as the corona-induced current increased as is shown in Figure 4.2.

Figure 4.4 Positive corona on 150 cm dry grass under the HVDC test line

It should be noted that the observed thermal scan in figure 4.2, which shows that the grass did not heat up uniformly hence it could not all ignite at the same time but had some region getting hotter than others.

4.4 V- I Corona-induced current on dry grass under HVDC test line

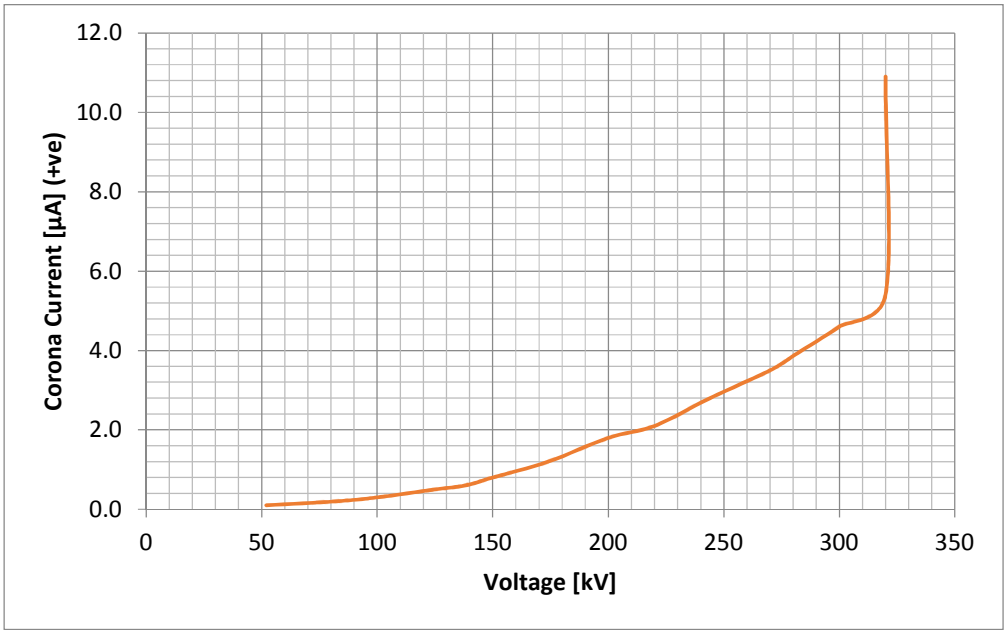

Figure 4.5 I-V characteristic of 150 cm grass under the postive pole 4 Wire Bundle (HVDC test line)

Figure 4.5 shows how applied voltage varies with corona-induced ion current flowing in dry grass of height 150 cm under a high voltage overhead transmission line. It is evident that corona-induced current in dry grass increases with increasing voltage magnitude of the transmission line as observed in figure 4.5, until the grass ignited at 320 kV.

Empirical calculations using the standard form equations outlined in [9] have been used below to simplify the conductor radius and evaluate the experimental results. The maximum conductor gradient for a monopole configuration of a test line at which the grass ignited was calculated as follows:

s = 17 cm; $r^{'}$ = 1.4 cm; H = 90 cm; Applied Voltage V= 320 kV

For four wire conductor bundle the maximum conductor field is given by:

$$E_m = \frac{V\left(1+\frac{4\sqrt{3}r}{s}\right)}{4rLn\left(\frac{H}{\sqrt[4]{(\sqrt{2})rs^3}}\right)} \quad (4.1)$$

The equation (5.18c) in [9] was corrected by replacing the 3r with 4r in the denominator. This correction was done after working out the equations and comparing the results with the computation done by the authors in [9]. The maximum conductor electric field E_m at which the grass ignited at the conductor voltage of 320 kV is given by equation (4.2).

$$E_m = 36.895 kV/cm \quad (4.2)$$

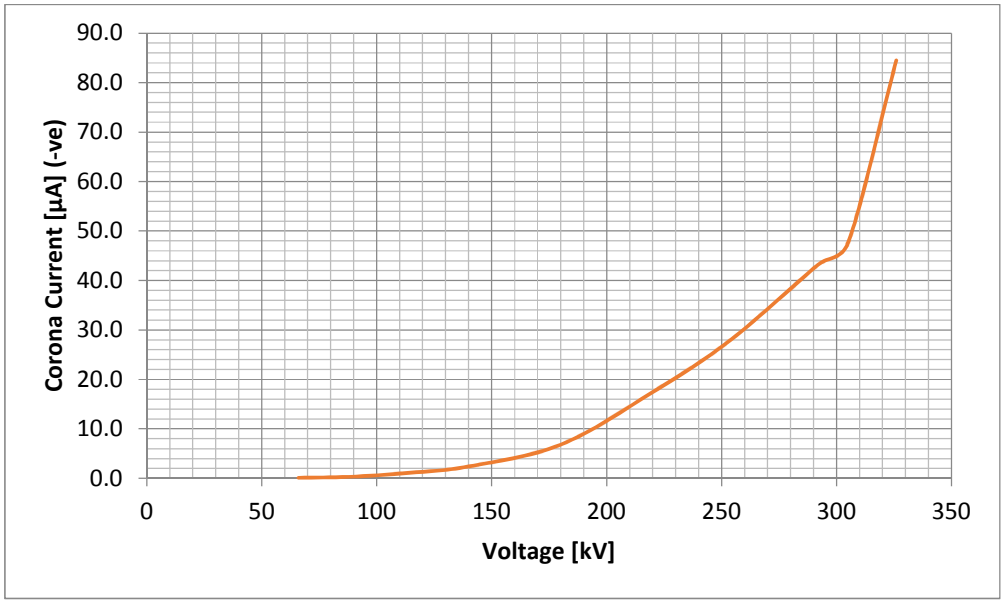

Figure 4.6 I-V characteristic of 96 cm grass under the postive pole 2 Wire Bundle (HVDC test line)

It was further noted that with reduction in conductor bundle, there was a reduction in the grass height to 96 cm under the two wire conductor bundle at which the grass got burnt with the applied voltage of 304 kV and 47.6 µA corona-induced ion current as shown in Figure 4.6.This showed a significant reduction in the conductor voltage and an increase in the induced current. The grass was effectively 144 cm below the conductor bundle.This measurement is obtained by subtracting grass height from the conductor height which was measured as 240 cm. If we remove the grass height, this gives us the effective measure of the grass from the conductor bundle.

Taking the two-wire conductor configuration into account, the maximum conductor field is given by equation (4.3):

$$E_m = \frac{V\left(1+\frac{2r}{s}\right)}{2rLn\left(\frac{H}{\sqrt{rs}}\right)} \quad (4.3)$$

Thus, the maximum conductor electric field E_m at which the grass ignited at the conductor voltage of 304 kV is given by the following calculation in equation (4.4):

$$E_m = 15.86 kV/cm \quad (4.4)$$

4.5 Corona-induced Ionic Currents In Relation To Conductor Voltage

The characteristic of corona induced ionic current on dry grass under the HVDC power line was established for different conductor configuration and using different polarity for varying grass height. For each configuration the results are shown in appendix D. However Figure 4.7 and Figure 4.8 have been taken for analysis from the negative pole (test line) with four wire conductor bundle for the 110 cm grass height and simular measurements were done for a 47cm grass height under the four wire conductor bundle as shown.

The results obtained did match very well to the ones obtained by Sunaga Y et al in their paper that showed that the electric fields and the ion current on the grounded insulated objects under a HVDC line [6] varies to the square of the applied voltage. The plots were additionally found to be similar to those obtained in [20,30,66]. This theoreticaly means an insulated object like grass in this case will consolidate charge from the ionic flow that exist under the power line which will then result into a corona ion current that leaks to ground as all practical insulators have a resistance. This current leakage will increase with the increase in the applied conductor voltage following a second order quadratic function which is in agreement with what Peek found in [29] in which the corona loses were found to be obeying a second order quadratic law .

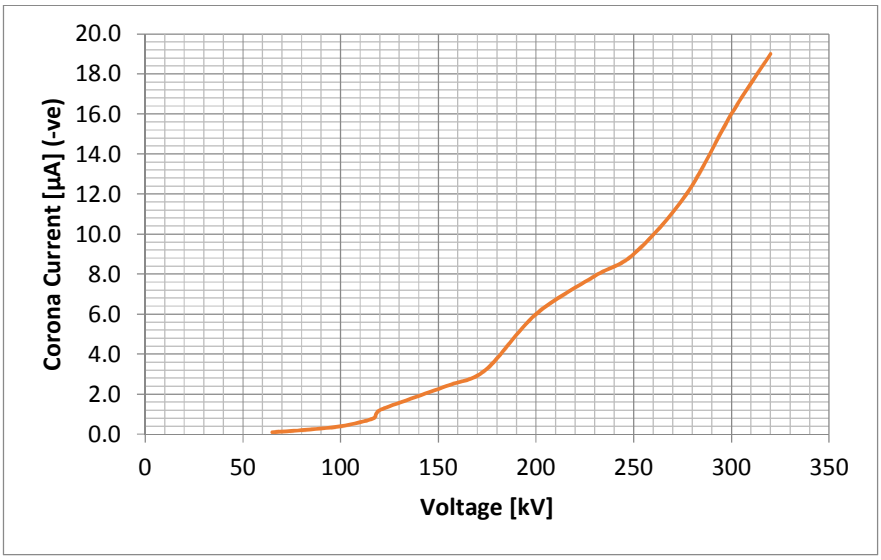

Figure 4.7 I-V characteristic of 110 cm grass under the postive pole 4 Wire Bundle (HVDC test line)

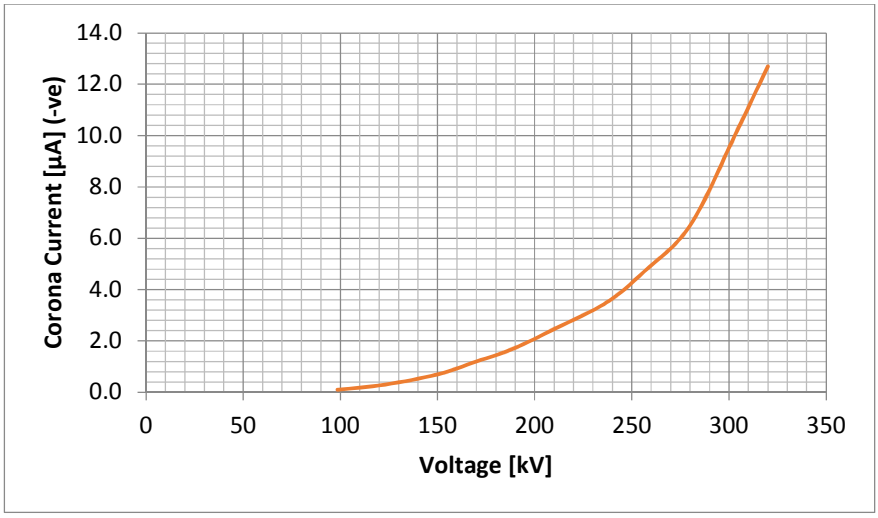

Figure 4.8 I-V characteristic of 47 cm grass under the postive pole 4 Wire Bundle (HVDC test line)

4.6 Corona-induced currents with different grass heights

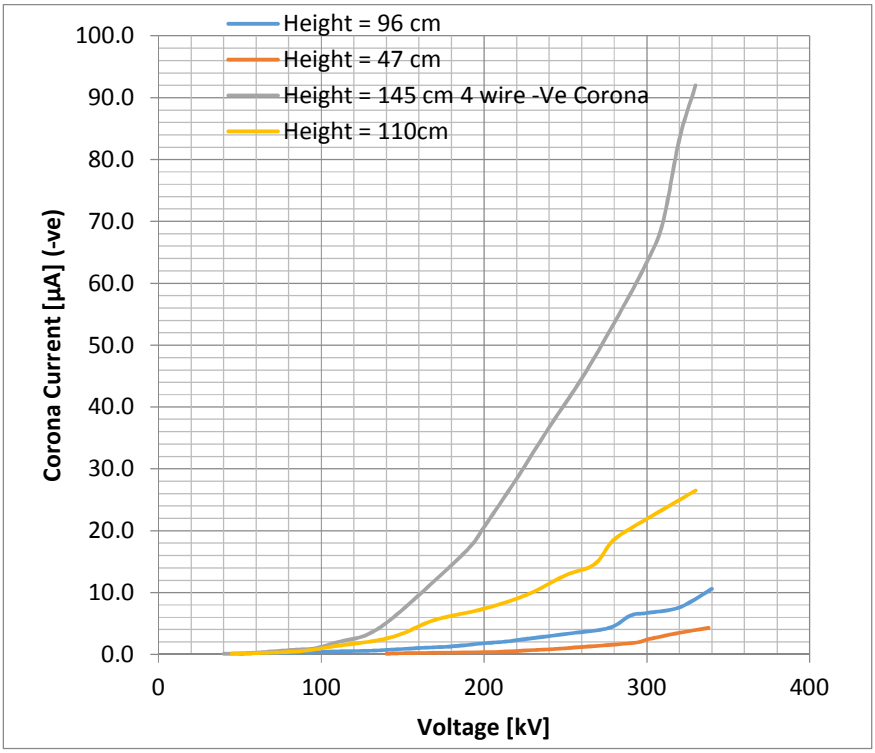

Figure 4.9 I-V characteristic for varying grass heights

In order to analyse the effect of varying grass height, different current plots from different grass heights with same conductor configuration and polarity in the case above, a four wire conductor bundle and negative polarity were plotted on the same graph, the results shown in Figure 4.9 above indicate that the magnitude of the corona-induced ion currents increases with an increase in grass height. This ties in well with theory from which, it is known that the electric field under a DC power line increases with height above the ground. This is also confirmed in measurements carried out in [6,37]. This also indicates that the closer you get to the charged conductors the higher the induced charge. What can be noted is that for an insulated object under the HVDC line, the induced ion current is influenced by the electric field that develops between the object

and the charged conductors with respect to ground as elaborated by varying heights plotted in Figure 4.9.

4.7 Positive and Negative corona-induced currents grass heights

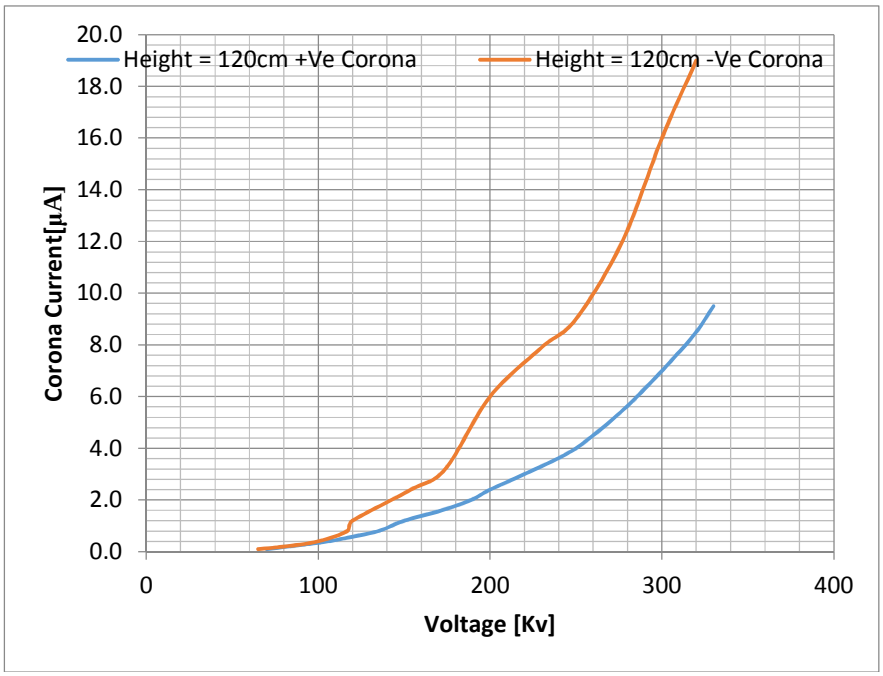

Figure4.10 I-V characteristic for positive and negative corona for grass height of 120 cm

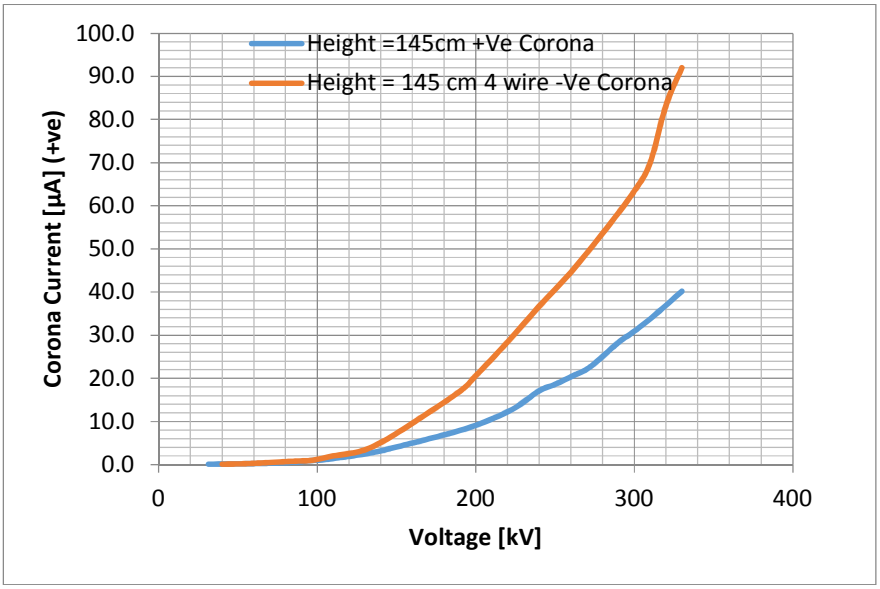

Figure 4.11 I-V characteristic for positive and negative corona for grass height of 145 cm

In order to analyse the effect of polarity in the electric field coupling on dry grass under the HVDC power line, measurements from grass of the same height with matching configuration but different polarity were taken and plotted on the same graphs as shown in the results in Figures 4.11 and 4.12 above. The results showed that the absolute values of corona-induced ion currents in grass increase with the increasing height of grass for both the positive and the negative corona effects.This could evidently be observed from the two graphs that ion currents for the grass height of 145 cm are higher than those at a grass height of 120 cm. However the most standing out observation is that negative corona-induced currents on grass at same height are greater than those of positive corona-induced current for the same applied voltage.

The results obtained are a close match with the trend obtained in [5,26,28]. The difference is attributed to the electron mobility. Corona forms at a much lower voltage under the negative polarity than the positive because of this phenomenon which attribute to the building up of more space charge and increased ion flow on the negative pole this can further be observed from the two graphs in figure 4.11 and 4.12 where there is more induced current on the grass under the negative pole.

4.8 Corona-induced currents for different sub-conductor configurations

In order to analyse the effect of conductor configuration on corona induced ionic current same measurements from two equivalent grass height using different conductor configuration were taken and plotted on the same graph as shown in figure 4.12. The results in figure 4.12, shows the corona-induced currents in dry grass for a height of 145 cm under a two-conductor bundle and a four-conductor bundle overhead test line. The results here show that the corona-induced ion current measured under a four-wire conductor configuration is lower than that measured under a two-wire conductor configuration. This confirms the importance of increasing conductor-bundle configuration for high voltage overhead lines.

To further appreciate how corona is affected by conductor gradient and level of voltage, a simulation of corona on a two-conductor bundle and a four-conductor bundle was done using Quickfield^{TM} from which the bright spots depicting electric field stress on the conductor

indicating corona development for the two different conductor arrangements. Comparing figures 4.12, 4.13 and 4.14 it can be seen that the two wire conductor bundle has significantly greater electric field stress than in the four wire conductor bundle. Figure 4.12 indicated that there is a significant difference in currents between the two configurations. Similar observations were made in experiments carried out in [6,20].

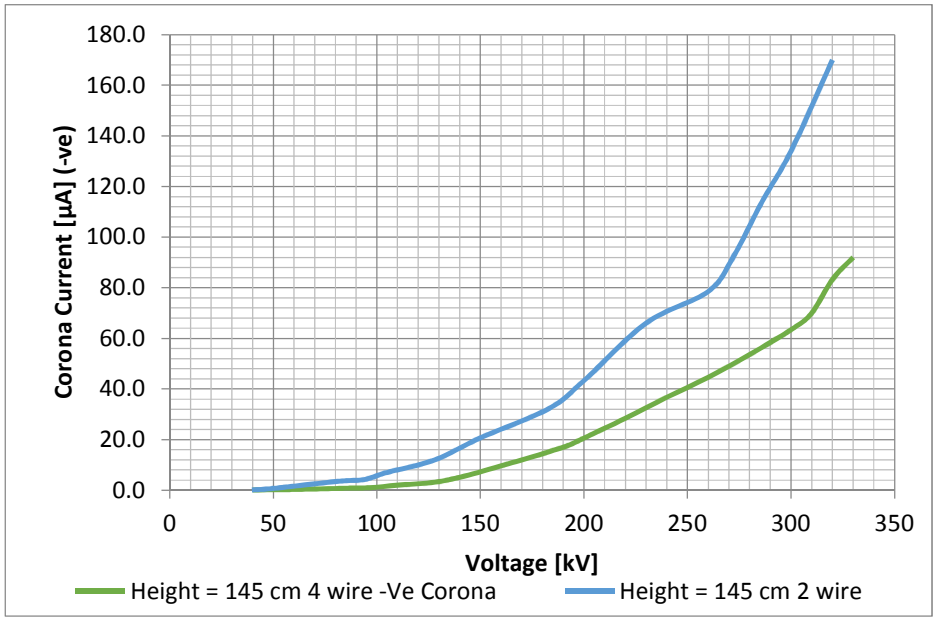

Figure 4.12 I-V characteristic for two wire and four wire

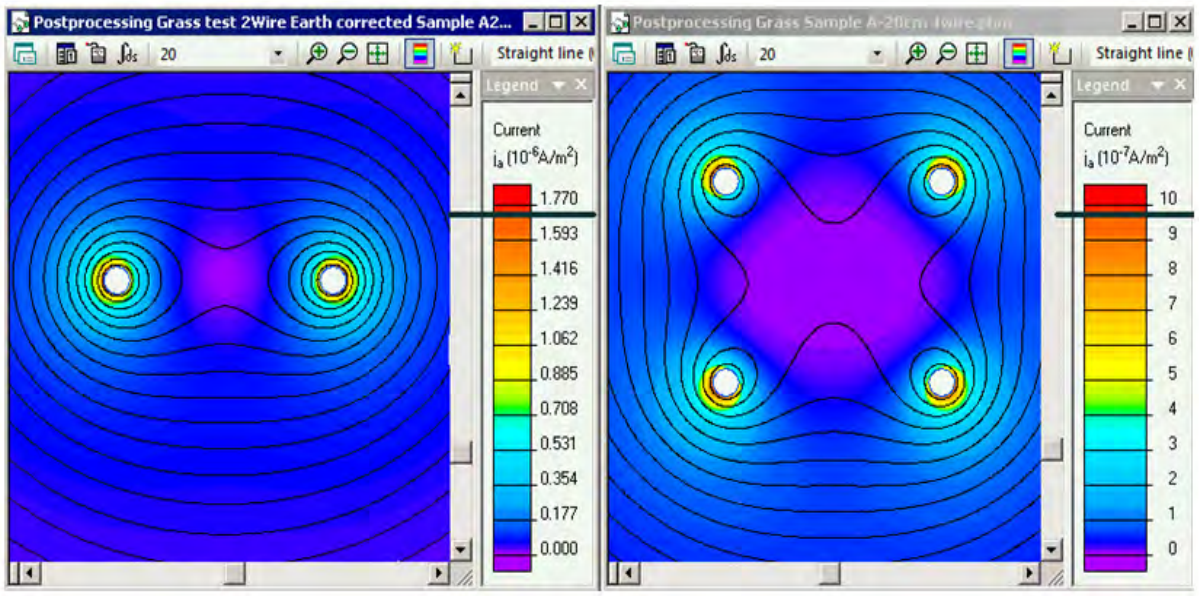

Figure 4.13 Simulation of Corona for a 2-wire bundle and a 4-wire Bundle at different scales

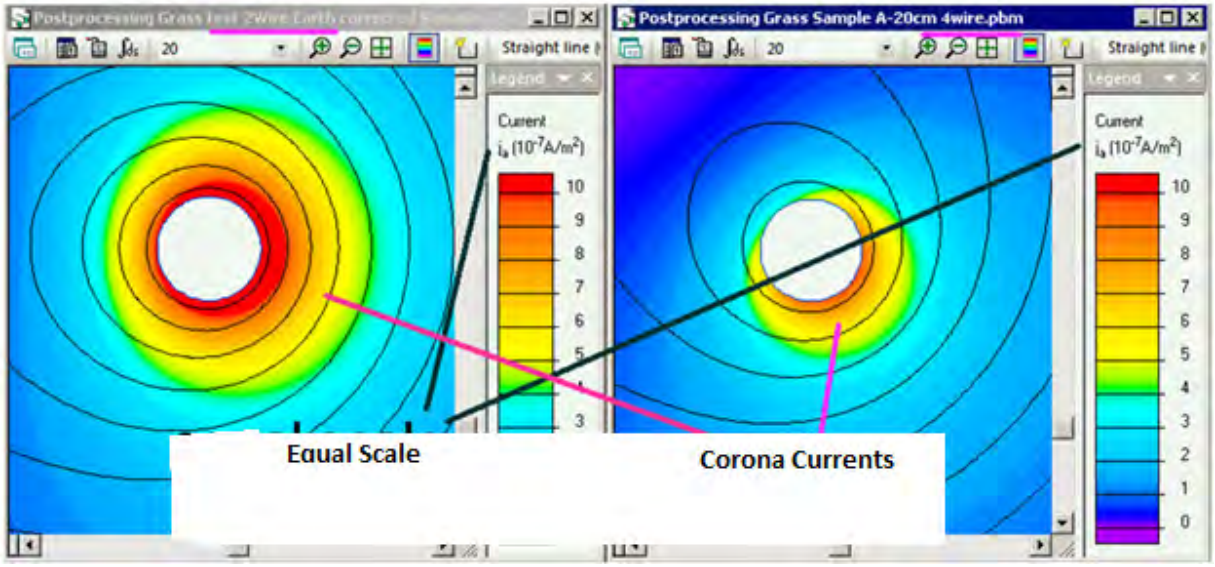

Figure 4.14 Simulation of a 2 wire conductor bundle (left) and a 4 wire conductor bundle (right)

This observation can be attributed to the fact that increasing the number of sub-conductors increases the effective conductor radius thereby reducing the electric field on the surface of the conductor. This means increasing conductor size reduces the surface gradient because of reduction in the rate of the electric field with lateral distance. This means electric field on larger conductors can support longer streamers. These observations tie in well with theory. In fact, the

experimental results (Figure 4.11and 4.12) and the simulated results (Figures 4.13 and 4.14) are both in agreement with a number of research findings on a practical transmission line as shown in [9]. These results in the three graphs indicate that the magnitude of the ion current in dry grass under a HVDC transmission line increases with an increase in grass height and the level of applied voltage.

This characteristic was further reviewed by the results from the empirical calculation as shown in Appendix C which indicated that the conductor maximum peripheral field drops with an increase in the number of sub-conductors from 21.35 kV/cm to 18.1 kV/cm for a change from a two-wire conductor to a four-wire. This was done by taking same grass height and applying same conductor voltage on the two different conductor configuration then carrying out a mathematic calculation as explained in [9]. The results indicate that the effects of the number of sub-conductors indeed compare well with the simulation results shown in figures 4.13 and 4.14. The modeling results compare well with the measured currents in figure 4.11 and 4.12 thereby amplifying the finding that corona activities increase with reduction in conductor size.

4.9 Simulated corona-induced current on grass

Grass was simulated with the normalized parameters as indicated in appendix B using a two dimensional finite element software, Quickfield^{TM}, the I-V characteristic results obtained were found to be consistent with the practical measurements as shown in Figures 4.7 and 4.8. This was in agreement with the results obtained in the works done in [6,8,11-13]. The results show a quadratic increment of induced corona ion current with increase in the applied conductor voltage. This can be seen in figures 4.15 and 4.16 in which the current for 20 cm and 40 cm grass bundles respectively were modelled in Quickfield^{TM} and plotted.

However in the model grass was assumed to be a single block substance which is not the case in reality. Grass in the natural inhabitant consist of loose steams that had to be bunched together to form a single sample that was then subjected to a practical test. It is not possible to compact loose steams of grass without trapping some pockets of air. This accounted for the difference in the magnitude of the current flows between the measured and simulated when comparing figures 4.15 and 4.16 to the ones above.

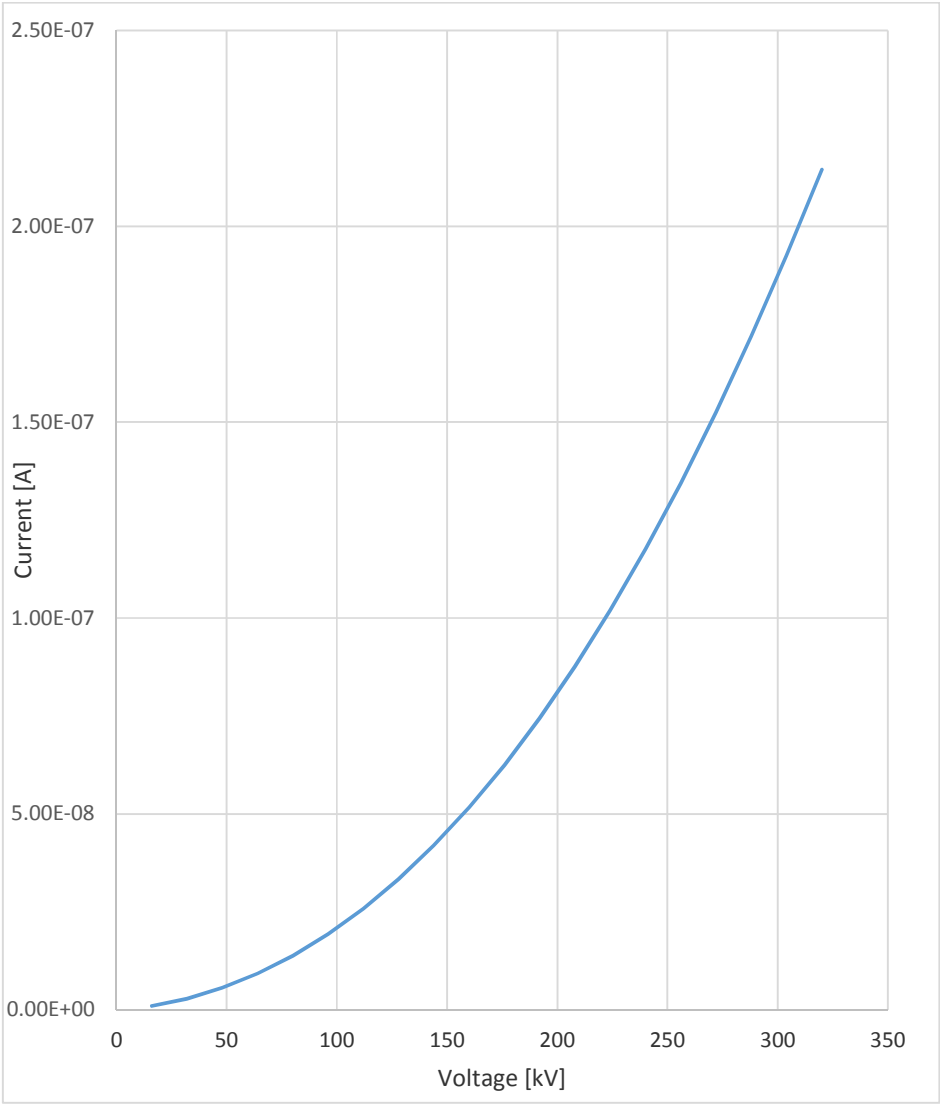

Figure 4.15 Simulation of I-V characteristic for grass height of 20 cm under a HVDC two wire conductor bundle

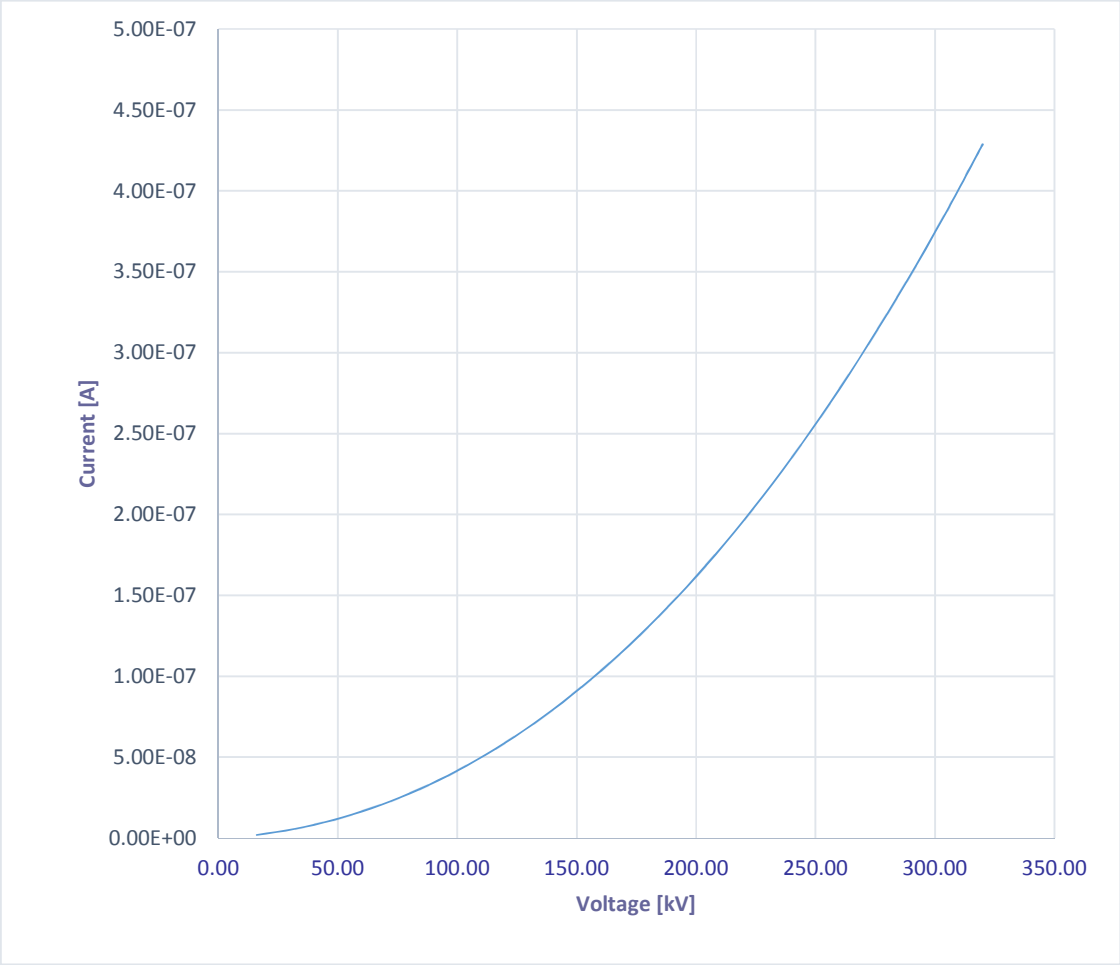

Figure 4.16 Simulation of I-V characteristic for grass height of 40 cm.

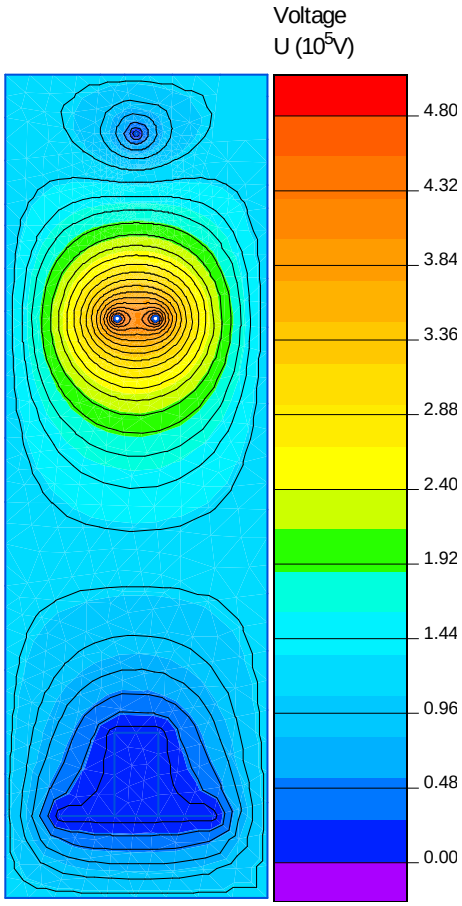

Figure 4.17 Simulation of corona-induced voltage on grass height of 20 cm

Figure 4.17 shows the equipotential lines for the simulation of 20 cm grass under the two conductor bundles in Quickfield™. This shows that grass is a dielectric material can hold electrical charge although there is a small resistive current leakage leading to a heat generation.

CHAPTER 5 CONCLUSION AND RECOMMENDATION

This dissertation has looked at how corona electric field strength can give rise to burning of dry grass under overhead power lines. From the results, it can be concluded that the electric field and the ion flow under HVDC lines can ignite dry grass when the conductor gradient is greater than 15.86 kV/cm for a two wire conductor bundle and 36.895 kV/cm for a four wire conductor bundle.

It has also shown that the magnitude of the corona-induced ion current in dry grass under a HVDC transmission line increases with an increase in grass height. Negative corona-induced current under a power line is found to be greater than the positive corona-induced current. This is because corona forms at a lower voltage under negative polarity than positive polarity and this is attributed to the building up of more space charge and increased ion flow under a negative pole. It should furthermore be noted that the electric field at ground level is more enhanced under a negative pole than under the positive pole.

During the study, it was realized that there is little published data on the characteristics of dry grass when subjected to the effect of the electric field strength. Hence, by applying the general principles of the electromagnetic induction of the environment under the power transmission lines that dry grass was experimented on to see how it burns due to corona-induced current flowing in dry grass. Thus, it is important that more research on the phenomenon of corona-induced bush fires under HVDC power transmission lines is undertaken so that clear guidelines on minimizing this effect are provided after looking reviewing effects of factors that influences the combustion of grass.

The grass habitat that was found to be of particular interest in this research was the elephant grass as it is commonly referred to. However, its scientific term is the Hyperrhenia Aucta & H Rufa grass type because of the species height dominance and locational preferences. From the various grass types tested, only this grass type produced consistent electrical test result on which statistical methods were applied as shown in Appendix B to analyze. For future study, it is also important that the density of grass is taken into account in experiments as a variable to establish

its effect. Future studies could also look at the effect of variable moisture content in grass in relation to ignition of grass.

It should be noted that the main objectives established at the outset of this dissertation have been achieved. One factor which has stood out in this research is that the generation of ion concentrations near HVDC lines can cause excessive induced voltages on adjacent insulated objects like dry grass and dry trees underneath the line.

It can be concluded that when an electric field is applied to a dielectric (grass in this case), conduction current, however small it may be, still flows through the material. It is this current that heats up the specimen and that causes the temperature rises. The heat generated is transferred to the surrounding medium by conduction through the solid dielectric and by radiation from its outer surfaces. Equilibrium is reached when the heat used to raise the temperature of the dielectric, plus the heat radiated out, equals the heat generated. When this critical voltage is reached, the heat generated may be more and this can lead to burning of grass.

In fact, at a critical voltage the ion concentrations under HVDC lines above ambient levels become significant, and no wonder even wooden poles and dead trees can burn under HVAC lines. Going by the geometry of grass, it makes sense that dry grass will catch fire due to high electric fields and space charge under a HVDC transmission line. Thus, wood poles, bushes, and trees in the immediate surroundings of high voltage DC or AC lines can experience corona, a result of high intensity electric fields.

For transmission lines, it is thus important to take into account the overhead conductor height above ground as the close we get to the conductor the greater the electric field. An economic optimum conductor spacing should always be sought for when designing transmission lines in order to avoid the adverse effects of the electric field.

REFERENCES

1. Maketa A., Southern African Power Pool Planning and Prospecting for Renewable Energy, 2013 International Renewable Energy Agency.
2. *EPRI AC Transmission Lines Reference Book-200 kV and Above, Third Edition*. EPRI, Palo Alto, CA: 2005. 1011974.
3. Bahrman M. P., "HVDC transmission Overview", IEEE Explore Nov 20, 2008.
4. Charter P. J, Johnson G. B., "Space charge measurement downwind From Monopolar 500 kV HVDC Test Line", IEEE Transaction On Power Delivery, Vol.3, No 4, October 1988.
5. Hara M., Hayashi N., Shiotsuki K., Akazaki M., "Influence of Wind and Conductor Potential On Distribution of Electric Field And Ionic Current Density At Ground Level In DC High Voltage Lines To Plane Geometry," IEEE Transaction On Power Apparatus And System, Vol.Pas-101, No 4, April 1982.
6. Sunga Y., Amano Y. , Sugimoto T., "Electric field And Ion Current At The Ground Voltage Of Charged Objects Under HVDC Lines," IEEE Transaction On Power Apparatus And System, Vol.Pas-101, No 4, April 1981.
7. Britten A. C., Burgers A. A., Vosloo H. F., "Susceptibility of 400kV Transmission Lines to Bird Streamers and Bush Fires," Energize Dec 2011.
8. Sarma M. P., Jainischewsky W. J., "Corona Loss Characteristic Of Practical HVDC Transmission Lines Part 2: Bipolar Lines," IEEE Transaction On Power Apparatus And System, Vol. PAS 89, No5/6, May/June 1970.
9. Slam M. A., Anis H., Morshedy A. E., Radwan R., *High Voltage engineering Theory and practice,* CRC Press Tylor and Francis Group 2000.
10. Schmidt G., Fiegl B. kolbeck S., " HVDC Transmission and The Environment," Power Engineering Journal October 1996.
11. Govender D., Ijumba N. M., Britten A. C., Sibilant G. C., "Study of the Electrical Environment below HVDC Transmission lines," Proceedings of the 16th International Symposium on High Voltage Engineering, SAIEE, Innes House, Johannesburg, 2009.
12. Yu M, Kuffel E., "A New Algorithm for Evaluating The Field associated With HVDC Power Transmission Lines in the Presence of Corona and Strong Wind," IEEE Transaction On Power Apparatus And System, Vol.29, No 2, April 1993.

13. Sarma M. P, Jansischewskj W., "DC corona on Smooth Conductors in air," IEE Proc, BVol.116, No1, January 1969.
14. Grigsby L. L., *Electrical Power Engineering Hand Book,* CRC press, IEEE 2001.
15. Rafiroiu D.,. Suarasan I, Morar R., "Inception Of Corona Discharge in Typical Electrical Configurations For Electrostatic Process Application," IEEE 1999.
16. Richards H. E, *Essentials of Modern Chemistry*, Rinehart press California 1975.
17. Atkins P. W., *Physical Chemistry*, Oxford University Press 1987.
18. Steven S. Zumdhal, Susan A. Zumdhal, Chemistry, *Houghton Mifflin Company,* 2007.
19. T. Taukuma, T. Kwamoto, "A Very Stable Method For Ion Flow Field Of HVDC Transmission Lines," IEEE Transaction On Power Delivery Vol.PWRD-2, .No.1, January 1987.
20. Abdel-Slam M., Abdel Saltter, Farahally M., "Monopolar Corona on Bundle Conductors," IEEE Transaction On Power Apparatus and system Vol. PAS-101, No 10, October 1982.
21. Maruvada P. S., "Corona Generated Space Charge Environment In The Vicinity Of HVDC Transmission Lines."
22. Lattarulo F., DiLecce F., "Experimental Analysis Of DC Corona On Unipolar Transmission Lines," IEE Proceeding Vol. 137, Pt C No. 1, January 1990.
23. Lowke J. J., Alessandro F. D., "Onset Corona Fields and Electrical Breakdown Criteria," 2003, J.Physic D: Applied Phys.36 2673.
24. Gray B. Johnson; " Degree of Corona Saturation of HVDC transmission Lines ;" IEEE Transaction On Power Delivery Vol.4 .No.2 , April 1990.
25. . Aboelsaad M. M, Shafai L., Rashan M., "Numerical Assessment of Unipolar Corona Ionised Field Quantities Using The Finite Element Method," IEEE Transaction On Power Apparatus And System, Vol. 136, No2, April 1989.
26. Sawanda Y, Subga Y, "Method of Calculating Ionized Field of HVDC Transmission Line And Analysis Of Space Charge effect On RI," IEEE Transaction on Power Apparatus and System, Vol.PAS-99, No.2, March/April 1980.
27. Trinh N. G., Maruvada P. S., Pioier B., "A Comparative Study of The Corona Performance of Conductor Bundles For 1200 kV Transmission Lines."
28. Mokwape J. L, *A Study of HVDC Transmission Line Audible Noise and Corona Loss in an indoor Corona Cage,* UKZN, Durban, South Africa 2007.

29. Peek F. W. Jr, *Dielectric Phenomena In High Voltage Engineering*, Lightning Source UK Ltd.
30. Komac-Shi, "Calculation Of Ionic Flow Field Of HVDC Transmission Lines By Finite Method," IEEE Transaction On Power Apparatus And System Vol. PAS-100, No2, December, 1981.
31. Maruvada P. S.,. Dallaire R. D,. Norios-Elye O. C, Thio C. V., Goodman J. S., "Environmental Effects Of the Nelson River HVDC Transmission Lines RI, AN, Electric Field Induced Voltage And Ionic Current Distribution Test," IEEE Transaction On Power Apparatus And System, Vol. PAS 101, No4, April 1982.
32. Satter S. A., "Corona Current and Field Profile under Neath Vertical Bipolar HVDC Lines With bundle Conductor," IEEE Transaction on Electrical Insulation, Vol 27, No 2, April 1992.
33. Nakano Y., Sunaga Y., "Availability of Corona Cage For Prediction Of Radio Interference Generation From HVDC Transmission Lines," IEEE Transaction On Power Delivery Vol.5, No 3, April 1990.
34. Naidu M. S., Kamaraju V., "High Voltage Engineering." Second edition, McGraw-Hill, N. Y., 1996.
35. Yang, J. Lu, Y. Lei. "Calculation Method for The Electric Filed Under Double Circuit HVDC Transmission," IEEE Transaction On Power Delivery Vol.-23, No.4, October 2008.
36. Suda T., Hirayama Y., Sunga Y., "Aging Effect Of Conductor Surface Conditions On Corona Characteristic," IEEE Transaction On Power Delivery Vol.3, No.4 ,October 1988.
37. Comber M. G., Johnson G. B., "HVDC Field And Ion Effect Research At Project UHV Results Of electric Field And Ion Current Measurements," IEEE Transaction On Power Apparatus And System, Vol.Pas-101, No 4, April 1982.
38. Lu T., Feng H., Zhao Z., Cui X., " Analysis of the Electric Field and ion current Density under Ultra-High voltage Direct Current Transmission Line Based on Finite Element Method," IEEE Transaction on Magnetics, Vol 43, No 4, April 2007.
39. Pedrow P. D.,. Qin B. L, Wang Q. Y., " Influence of load Current On Bipolar DC Corona," IEEE Transaction On Power Delivery, Vol.8, No.3, July 1993.

40. Fatokuma F. O., Jayaratne E. R., Morawska. L, Rachman R., Birtwhistle D, Mengeersen K, "Characterization Of The Atmospheric Electrical Environment Near a Corona Ion Emitting Source," Elsevier 2008.
41. Abdel-Slam M., Abdel Saltter, Farahally M., "Finite Element Solution Of Monopolar Corona Equations," IEEE Transaction on Electrical Insulation Vol. EI-18, No 2, April 11 1983.
42. Kostyushko V. A., Kryslov A. V., Nikiforov E. P., Savchenko O. V., Solomonik E. A. , Zhelezko Yu, "Power Losses In electrical Networks Depending On weather Conditions," Power Technology and Engineering, Vol 39, No1, 2005.
43. Hamouz Z. A., " Finite Element Computation Of Corona Around Monopolar Transmission Lines," Elsevier Science 1989, Electric Power system Research 48.
44. Benamar B., Favre E., Donnot A., Rigo M. O., "Finite Element Solution For Ionized Fields In DC Electrostatic Precipitator," Proceedings of COMSOL Users Conference 2007.
45. Abdel Alam M., Abdel-Sattar S., "Calculation of Corona V-I Characteristic Of Monopolar Bundles Using The Charge Simulation Method," IEEE Transaction On Electrical Insulation, Vol 24, No.4, August 1989.
46. . Sarma M. P, Jainischewskyj W., " Corona Loss Characteristic Of Practical HVDC Transmission Lines Part 2; Bipolar Lines," IEEE Transaction On Power Apparatus And System, Vol. PAS 89, No5/6, May/June 1970.
47. Deno D. W., " Calculating Electric Effect Of Over-Head Transmission Lines," IEEE Power Engineering Society 1973.
48. Yu X., Liu B., wang X., "Prediction of the dielectric dissipation factor tanδ of polymers with an ANN model bassed on DFT calculation," ELSEVIER Reactive & Functional Polymers 68, 2008
49. Ulaby F. T , *Applied Electromagnetics*, Pearson Prentice Hall,2004.
50. Kao, Kwan Chi, *Dielectric phenomena in solids: with emphasis on physical concepts of electronic processes*, Elsevier, Inc. 2004
51. Wadhwa C. L. , *High Voltage Engineering*, New Age International, New Delhi, 2007.
52. Melih Inal, " Determination of dielectric properties of insulator materials by the ANFIS: A comparative study," Elsevier Journal Of Material Processing Technology 195- 2008.

53. Venkatesh M. S. and V. Raghavan G. S., "Overview Of Dielectric Properties Measuring Techniques," Canadian Biosystem Engineering, Vol 47, 2005.
54. Hakansson E. , Amiet A. Kaynak A., "Dielectric Characterization Of Conducting Textile using free Space transmission Measurements: Accuracy and Methods For improvement," Elsevier Science Direct , synthetic Metals 157, 2007.
55. Duchow K. J.,. Gerhardt R. A, "Dielectric Characteristic Of Wood and Wood Infiltration With Ceramic Precursors," Elsevier Material Science and Engineering C4, 1996. pp 125-135.
56. William L. J, *USA Department Of Agriculture Forest Product Laboratory General Technical Report FPL-GTR 6 Electric Moisture Meter For Wood*, Rev. June 1988.
57. Hamiyet Sahin Kol, "Thermal and Dielectric Properties of Pine Wood in Transverse Direction," BioResource 4-1663-1669, 2009.
58. Ishida Y., Yoshino M., "Dielectric Studies On Cellulose Fibers," Journal Of applied Polymer Science, Vol 1, issue No 2, 1959.
59. Honda T., Fukuoka M., Yoshuzawa S., Kanamoto T., "The Effect of Moisture On The Dielectric Relaxation In Wood," Journal Of applied Polymer Science, Vol 27, 1982.
60. Booysen P. D.,. Bransby D. I,. Tainton N. M, *Common Veld and Pasture Grass of Natal* , Shuter &Shooter Peitermaritzburg, 1976 South Africa.
61. Richard Fitzpatrick Maxwell's *Equations And The Principles Of Electromagnetism,* Infinity Science Press LLC, Massachusetts, 2008.
62. Humphries Jr, *Finite-elements Methods For Electromagnetics*, CRC Press USA, 1997.
63. Todd M. G., Shi F.G., " Validation Of Novel Dielectric Constant Simulation Model And The Determination Of Its Physical Parameters," Elsevier Science Microelectronics Journal 33 (2002), pp 627-632.
64. Haefely Test AG, Operating Instructions, Haefely Test AG, 2820 Automated C, L and Tan delta measuring bridge, Version 1.9.
65. British Standard 2067-1953, *Determination of Power Factor and Permittivity Of Insulating Materials.*
66. Wintle H. J., "Unipolar Wire to Plane Corona A definitive Computation," IEEE Transaction on Electrical Insulation, Vol 27, No 2, April 1992.
67. Groeneveld R, Meeden G, "Measuring Skewness and Kurtosis," The Statistician 33 (1984), Institute of Statisticians.

68. Evans M., Hasting N., Peacock B. *Statistical Distributions*, John Wiley and Sons INCO, New York,1993.
69. ANSI/IEEE Std 101-1987 IEEE Guide for the statistical Analysis of Thermal Life Test Data.
70. Walpole R. E., Myers R. H., Myers S. L. and Ye K., *Probability and Statistics for Engineers and Scientists*, Prentice Hall, 8th edition, 2006.
71. Lovric M., *International Encyclopedia of Statistical Science*, Springer, Berlin,2011.
72. Barlow R. J. *Guide to the use of statistical Methods in physical Sciences*, John Wiley, Sussex, 1989.

APPENDIX A

DETERMINATION OF GRASS PARAMETERS

A1.1 Determination of grass weight

Two samples, A and B as shown in Table A1.1 below, were used for dry grass in the investigations. Sample A gave consistent results that could easily be analyzed by using statistical methods in Appendix B. However, sample B grass gave results of various magnitudes such that it was not easy to analyze them using statistical methods. Whence, the results gathered on sample B experiments are not included in this thesis. The results on sample A could be relied on because they tied in well with theory.

Table A1.1 Grass identification

Sample	Group
A	Hyparrhenia aucta & h. rufa
B	Other grass types

After no change in weight test, five successive weight measurements were noted as shown in Tables A1.2 to A1.4. This indicated that there was no further moisture content in the grass samples in the oven.

Table A1.2 Grass weight Test 1

	Weight before heating (grams)	Weight after 3 hrs heating (grams)	Weight after 6 hrs heating (grams)
Glass Beaker	151.2008	151.2008	151.2008
Grass + Beaker	158.7053	157.8511	157.8511
Grass only	7.5045	6.6503	6.6503
Water	0.8542		
Water content [%]	11.383		

Table A1.3 Grass weight Test 2

	Weight before heating (grams)	Weight after 3 hrs heating (grams)	Weight after 6 hrs heating (grams)
Glass Beaker	151.2008	151.2008	151.2008
Grass + Beaker	158.0676	157.3145	157.3145
Grass only	6.8668	6.1137	6.1137
Water	0.7531		
Water content [%]	10.967		

Table A1.4 Grass weight Test 3

	Weight before heating (grams)	**Weight after 3 hrs heating (grams)**	**Weight after 6 hrs heating (grams)**
Glass Beaker	151.2008	151.2008	151.2008
Grass + Beaker	157.6137	156.8904	156.8904
Grass only	6.4129	5.6896	5.6896
Water	0.7233		
Water content [%]	11.279		

Table A1.5 Grass weight Test 4

	Weight before heating (grams)	**Weight after 3 hrs heating (grams)**	**Weight after 6 hrs heating (grams)**
Glass Beaker	151.2008	151.2008	151.2008
Grass + Beaker	157.7147	156.9964	156.9964
Grass only	6.5139	5.7956	5.7956
Water	0.7183		
Water content [%]	11.027		

A1.2 Determination of relative permittivity and conductance for grass

The skewness, calculated using equation (B 1.7), for the normal distribution function obtained in Figure A1.1 for relative permittivity in sample A is -0.294. This falls within the standard error ±0.7746 calculated using equation (B 1.6). Further analysis of individual sample tests revealed that each mean was near the consolidated mean, apart from sample test no. 3 which produced a permittivity mean of 2.5336, considerably lower than the real permittivity mean of 3.6078. This is because grass, though of the same species, the soil where it grows may affect its chemical composition. This explains why different batches displayed varying results. The individual standard deviation of the samples was also found to be consistent and could fairly be compared to the real standard deviation of the consolidated sample data which is 0.5623 for permittivity. This meant that the samples were treated uniformly and the absorbed errors were also uniformly distributed. The covariance of individual test results showed that there was no significant change in the permittivity and conductance within the voltage test range. This signified that the test sample did not get burnt by the applied voltage range of 2 kV to 7 kV.

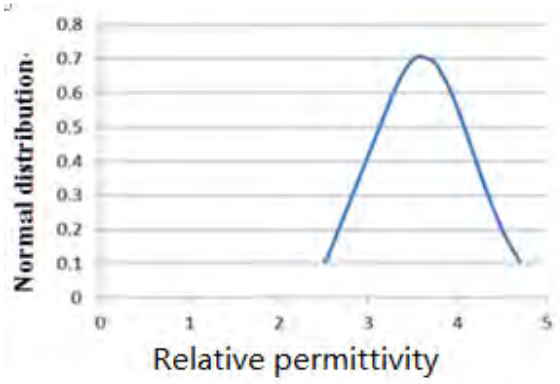

Figure A1.1 Normal distribution curve for Relative Permittivity-Sample A

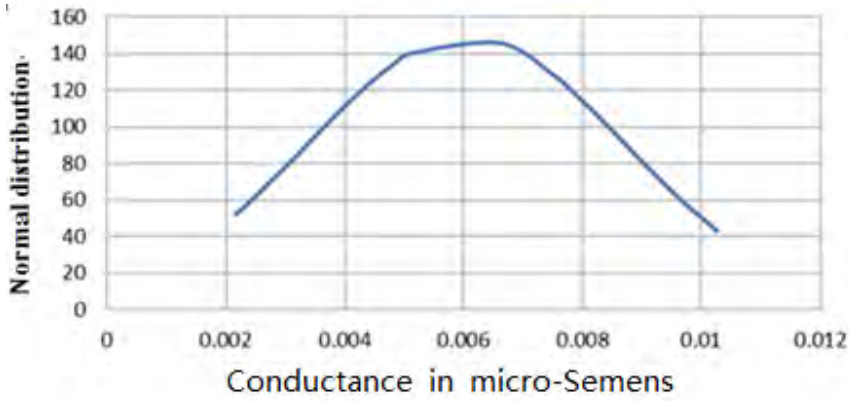

Figure A1.2 Normal distribution curve for Conductance-Sample A

The distribution curve for conductance was positively skewed with a statistic skewness of 0.8419 which was found to be outside the standard error of ±0.7746. This skewness (Figure A1.2) was attributed to significant variations in conductance for sequence tests cycles 1 and 2 which resulted in some wider gap in data distribution as shown in Appendix C. The distribution curve shows that there are comparatively fewer data points above a mean of 0.00707 µS for conductance. This conductance was for the volume of grass in the test cell. However, there is need to investigate the effect of grass density in future research. Further investigation could not be conducted in this area, but for the test in this experiment, the same density was maintained for all the grass tested by weighing the grass bunch and then checking the density from the volume.

The normal distribution assumes random errors are distributed normally along the curve [67,68]. However, this assumption breaks down in cases of multiple sources of errors that are correlated. Furthermore, when the errors are not truly randomly distributed, then the assumption's validity is

questioned. In this test, the error distribution is normally distributed shown by the closeness in magnitudes between sample tests.

The standard error of the mean, which is the standard deviation of errors in the sample with respect to the real mean, is given by equation (B1.6) and calculations are shown below:

For Permittivity, standard error= $((0.5623)/(39)^{1/2})= 0.09$

For Conductance, standard error= $((0.00407)/(39)^{1/2})= 0.00065$

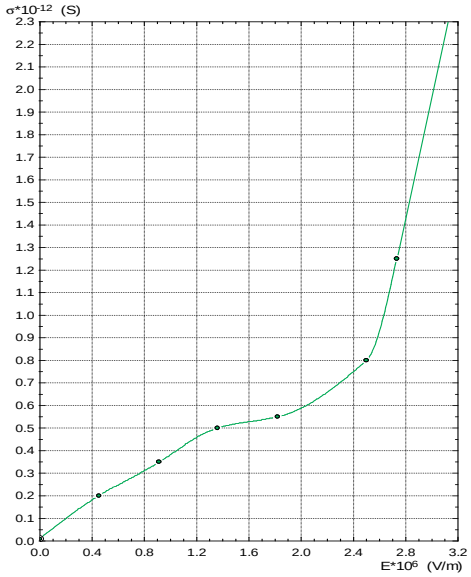

Figure A1.3 Variation of conductivity of air Vs applied electric field

Figure A1.3 clearly shows that conductivity of air does increase with the increasing electric field. This observation is consistent with theory [9].

A1.3 Validation of grass permittivity test using new Transformer oil test as control

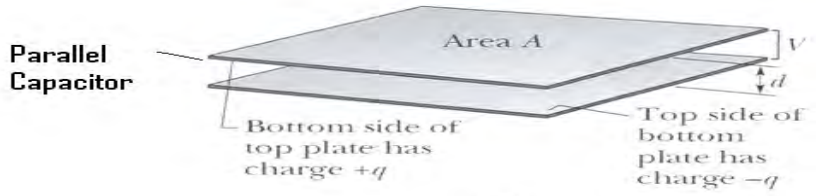

Figure A1.4 Parallel capacitor configuration

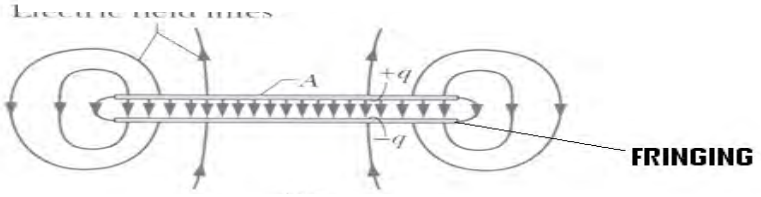

Figure A1.5 Parallel capacitor fringing of electric fields

Oil was tested as a control for the test of grass permittivity. The test cell used had a rectangular shaped parallel plate capacitor configuration as shown in Figure A1.4. This test was performed as outlined in section A1.2 of this dissertation for the test of grass permittivity and conductance with same equipment and test conditions maintained. A permittivity mean of 2.395 and conductance mean of 0.0137 were obtained from 6 tests. The distribution function was not plotted because of a leak as this particular test chamber was not designed to contain liquids. Therefore, only a few sample tests could be performed with this chamber.

The covariance of individual test results showed that there was no significant change in permittivity or conductance within the voltage test range which was an indication that the samples were tested within their dielectric strength capability.

The testing of new transformer oil was used to validate the methodology used in testing the permittivity and conductance of grass since oil is an insulating liquid widely used and has a permittivity that has been measured and established universally as ranging from 2.2 to 2.3. The values obtained compared very well with the theoretical values for oil with a marginal error of 4%. This meant that the method used to test grass samples can be technically acceptable with negligible errors. The percentage error in the test was attributed to the fringing at the electrode

ends as shown in figure A1.5. This chamber did not have guard rings installed and the gap between electrodes was noted to be larger than 35 mm.

APPENDIX B

STATISTICAL ANALYSIS OF GRASS

B1 Statistical methods

A larger number of data was collected from several tests so that a precise estimate could be established from the tests performed per grass sample. It was therefore found inevitable to use statistical methods to analyze the results. Statistics are able to show patterns which human eyes and brain can easily comprehend. Graphical statistical data analysis shows the features which are hidden when the data is in numerical form [67-72]. With this tool it is possible to:

1. Show the possible errors in the data.
2. Show the features of the dataset, e.g. symmetry, skew, scatter.
3. Test for a normal distribution.

From the statistical analysis only one grass sample produced acceptable results, this was the Hyperrhenia Aucta & H Rufa.

Karl Gauss is credited for the recognition of the normal curve of errors and also Pierre-Simon de Laplace for discovering the normal distribution. The normal curve is referred to as the Gaussian distribution [71,72].

A Statistic is referred to as any function of random variables in a random sample. In normal distribution, there are some special mathematical properties which form the basis of many statistical tests. Although no real datasets follow the normal distribution exactly, many kinds of data follow a distribution that is approximately Gaussian. A normal distribution can be defined by two parameters, the mean and the standard deviation. By definition, normal frequency distributions are continuous but not all datasets follow normal distributions.

The mean is used to define the central location in a set of normally distributed data. In a normal data set, the median, mode, and mean are nearly equal. The area under the curve equals all of the observations or measurements. The normal distribution is given by equation (3.15).

The Normal Distribution is used to know the data population in which the probabilities of obtaining different random samples from within the distributed data set is the basis for statistical testing [67-70].

B 1.1 Mean

This is a numerical average of a given data sample evaluated using equation (B1.1) below.

$$\overline{X} = \sum_{i=1}^{N} \frac{X_i}{N} \qquad \text{(B 1.1)}$$

B 1.2 Standard deviation

This is a measure of variability. Large variability in a data set produces relatively large values of *(x — x)2* and thus a large sample variance. This indicates the level of dispersion of data about the mean. The quantity (N — 1) is called the degree of freedom associated with the variance estimate. It is evaluated using equation (B1.2).

$$\sigma = \sqrt{\frac{1}{(N-1)} \sum_{i=1}^{N} (x_i - \overline{x})^2} \qquad \text{(B 1.2)}$$

B 1.3 Variance

The average squared deviation from the mean, a measure of the spread of data, is:

$$V = \sigma^2 \qquad \text{(B 1.3)}$$

B 1.4 Covariance

Level of inter-dependence of the two variables in a statistical sample. If there is no inter-relation, the covariance is zero. The formula is as shown in equation (B1.4).

$$CoV = \frac{1}{N} \sum (x_i - \overline{x})(y_i - \overline{y}) \qquad \text{(B 1.4)}$$

B 1.5 Normal Distribution

Characteristics of normal distribution have an unveiled bell curve with most values near the middle datum or average of the sample. Very few values near the upper and lower extremes fit the formula of a normal distribution frequency analysis of data given as in equation (B 1.5).

$$frequency\ \ of\ X_i = Y_i$$

$$Y_i = \frac{1}{\sigma\sqrt{2\pi}}(e)^{-\left[\frac{(X_i-\mu)^2}{2\sigma^2}\right]} \qquad \text{(B 1.5)}$$

B 1.6 Standard Error

This is measured using equation (B 1.6).

$$SE = \frac{\sigma}{\sqrt{n}} \qquad \text{(B 1.6)}$$

B 1.7 Skewness

This is a measure of describing deviation from normal distribution using the third moment of the mean. It is either skewed to the left (negative skew), or skewed to the right (positive skew). The measure of skewness is given as in equation (B 1.7).

$$k_3 = \frac{n\sum(X_i - \bar{X})}{(n-1)(n-2)}$$

$$g1 = \frac{k_3}{s^3} estimate\ of\ \gamma, \qquad \text{(B 1.7)}$$

If $\gamma 1 < 0$, then distribution is skewed to the left

If $\gamma 1 = 0$, then distribution is normal

If $\gamma 1 > 0$, then distribution is skewed to the right.

APPENDIX C

DETERMINATION OF CONDUCTOR SURFACE GRADIENT

Empirical calculations using the standard form equations outlined in [9] have been adopted below to amplify the conductor radius and compare the results to the pattern that was obtained experimentally and from the simulation. Taking equation (2.6), $V_o = E_c r \ln(2H/r)$, where H is the height above ground or distance between poles and r is the conductor radius, and for bundle conductors, $r' = GMR$, where GMR is Geometrical Mean Radius of a bundled conductor and s is the sub bundle radius: The conductor gradient for a monopole configuration of a test line is calculated as follows:

s = 17 cm, r' = 1.4 cm, H = 240 cm, Applied Voltage V= 200 kV

$$E_m = \frac{V\left(1+\frac{2r}{s}\right)}{2rLn\left(\frac{H}{\sqrt{rs}}\right)} \qquad \text{(C1.1)}$$

The maximum Conductor Electric field E_m at 200 kV will be:

$$E_m = 21.35 kV/cm \qquad \text{(C1.2)}$$

For four wire conductor bundle the maximum conductor field is given by:

$$E_m = \frac{V\left(1+\frac{4\sqrt{3}r}{s}\right)}{4rLn\left(\frac{H}{\sqrt[4]{(\sqrt{2})rs^3}}\right)} \qquad \text{(C1.3)}$$

This equation was corrected by replacing the 3r with 4r in the denominator as written in [9]. This was done after working out the equations and comparing the results with the computation done by the authors in [9]. The maximum conductor electric field E_m at 200 kV is:

$$E_m = 18.104 kV/cm \qquad \text{(C1.4)}$$

APPENDIX D

I-V Characteristics Measured

D1 Positive Polarity with Two Wire Conductor Bundle

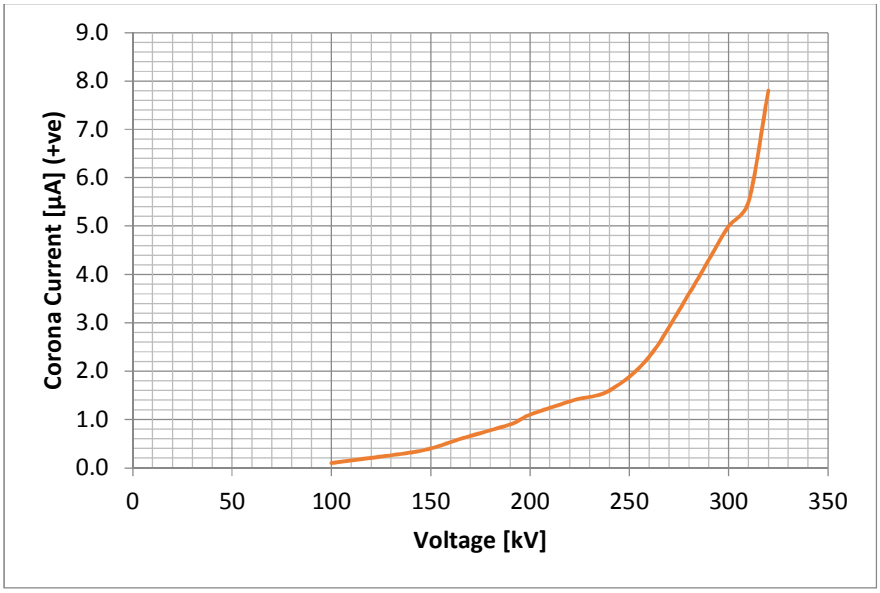

Figure D1.1: I-V Characteristic for 47 cm Grass Height Under 2 Wire Positive Pole

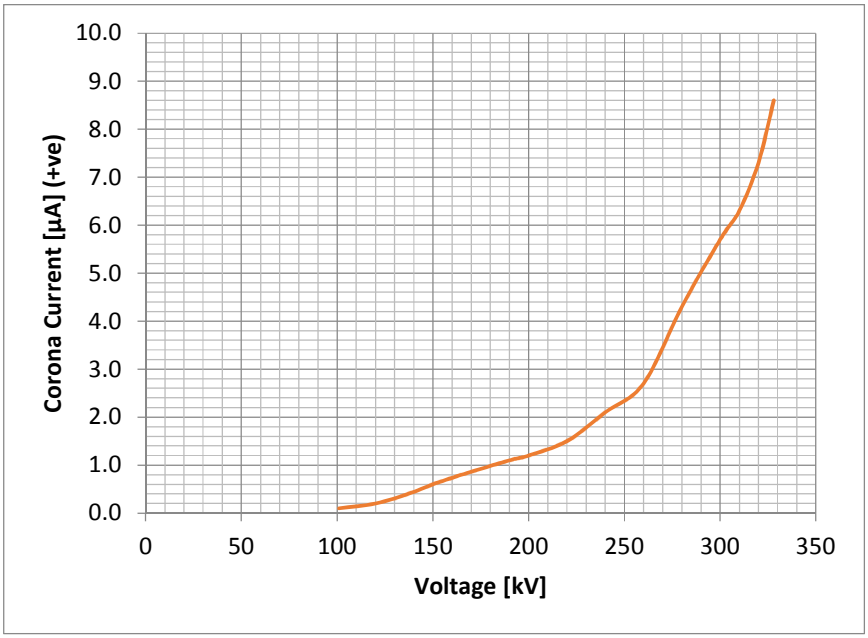

Figure D1.2: I-V Characteristic for 43 cm Grass Height Under 2 Wire Positive Pole

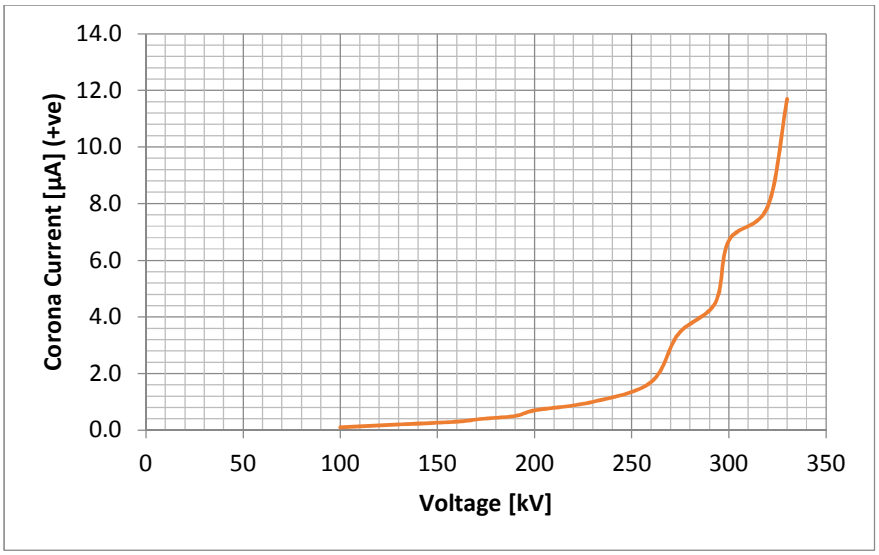

Figure D1.3: I-V Characteristic for 63 cm Grass Height Under 2 Wire Positive Pole

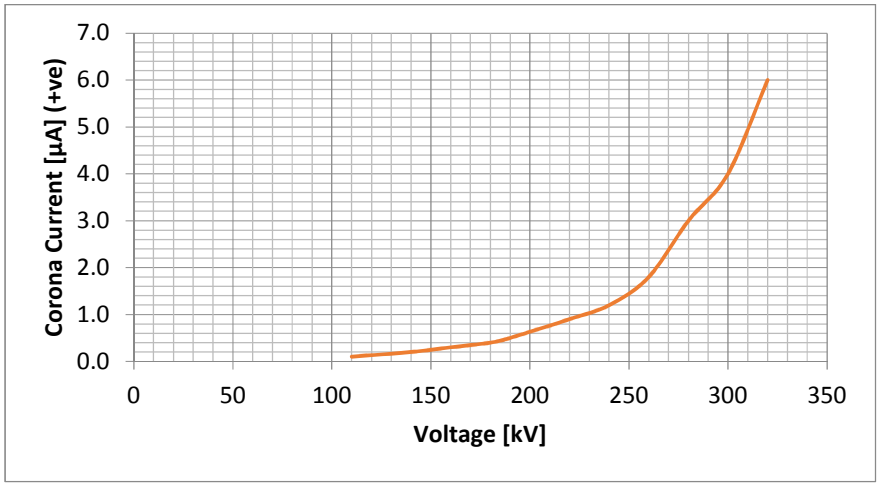

Figure D1.4: I-V Characteristic for 63 cm Grass Height Under 2 Wire Positive Pole

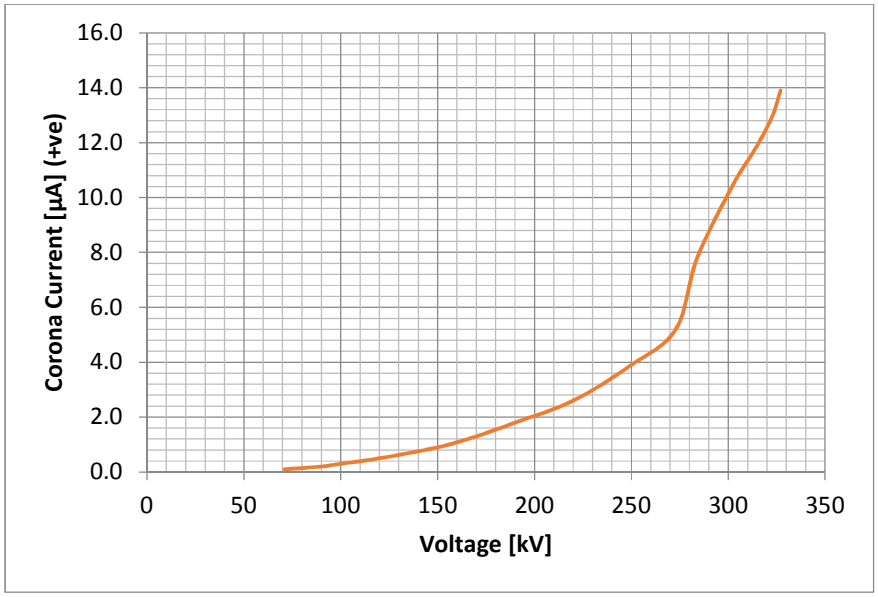

Figure D1.5: I-V Characteristic for 96 cm Grass Height Under 2 Wire Positive Pole

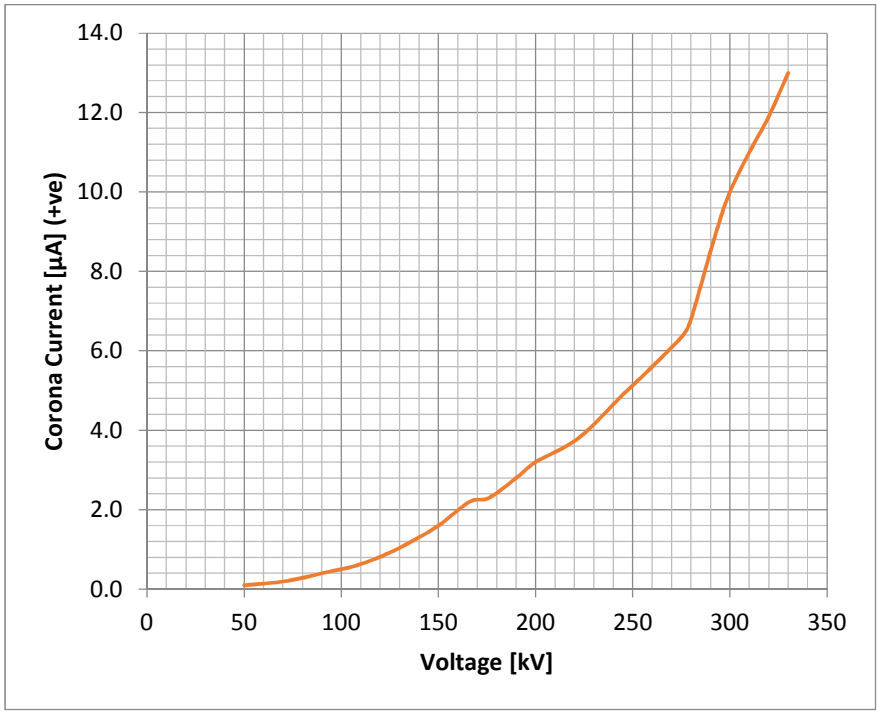

Figure D1.6: I-V Characteristic for 110 cm Grass Height Under 2 Wire Positive Pole

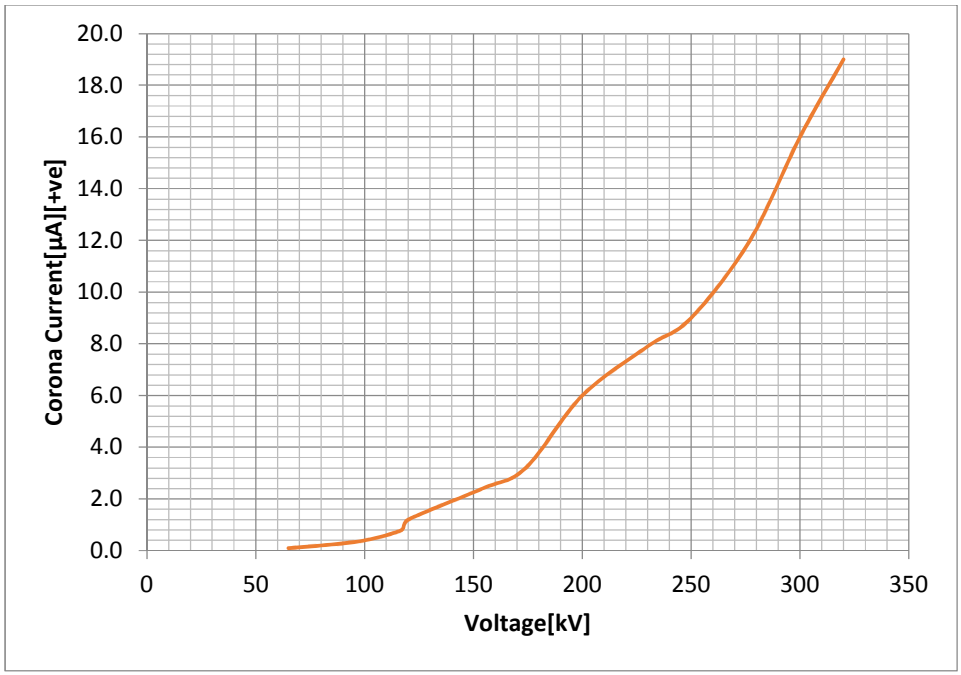

Figure D1.7: I-V Characteristic for 120 cm Grass Height Under 2 Wire Positive Pole

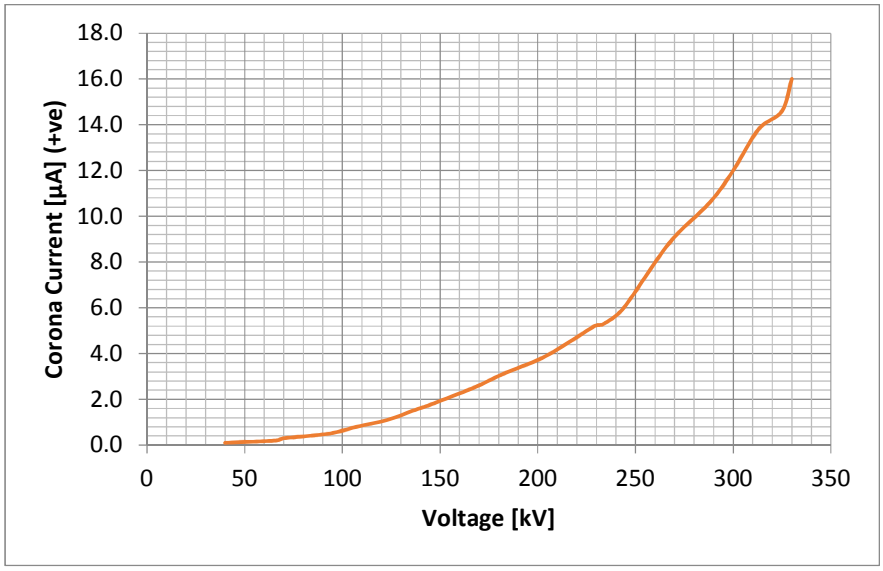

Figure D1.8: I-V Characteristic for 135 cm Grass Height Under 2 Wire Positive Pole

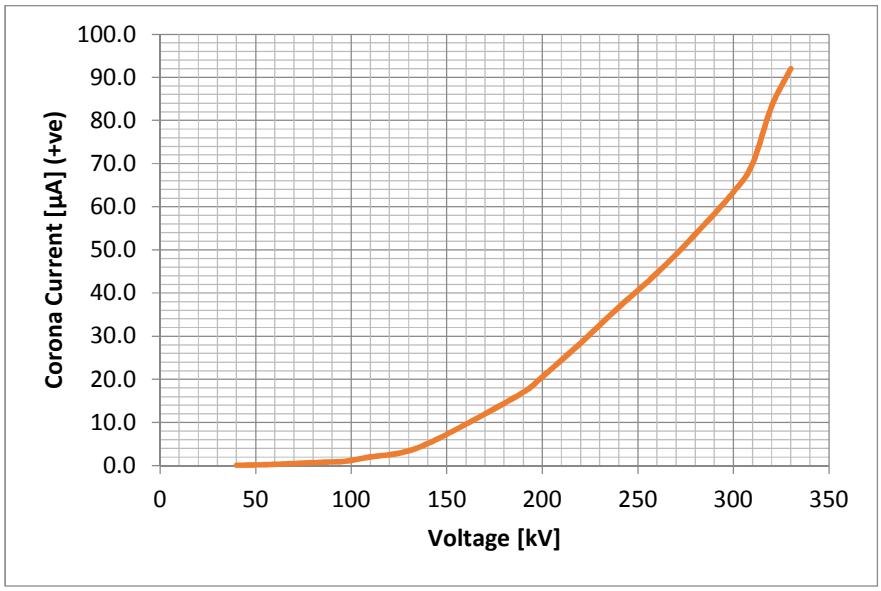

Figure D1.9: I-V Characteristic for 145 cm Grass Height Under 2 Wire Positive Pole

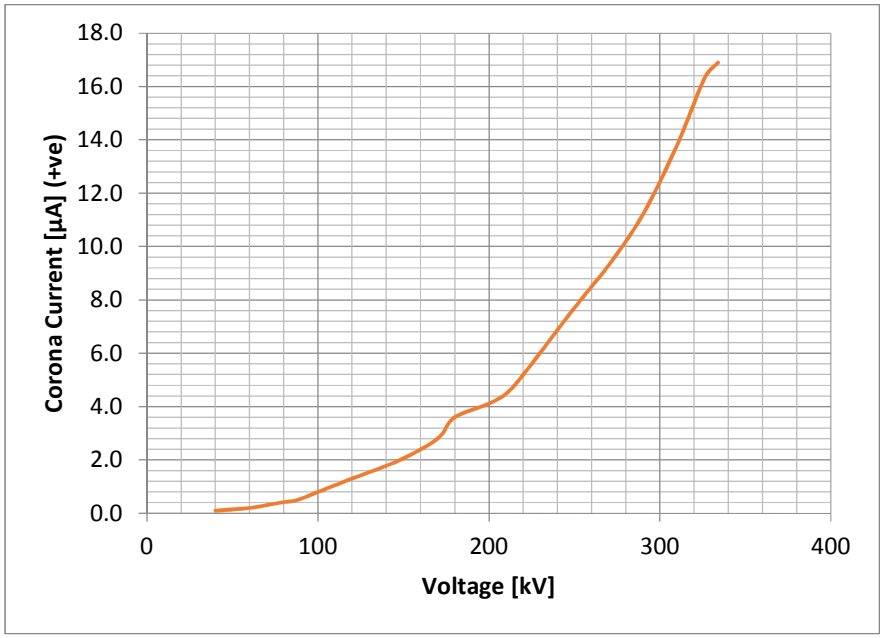

Figure D1.10: I-V Characteristic for 151 cm Grass Height Under 2 Wire Positive Pole

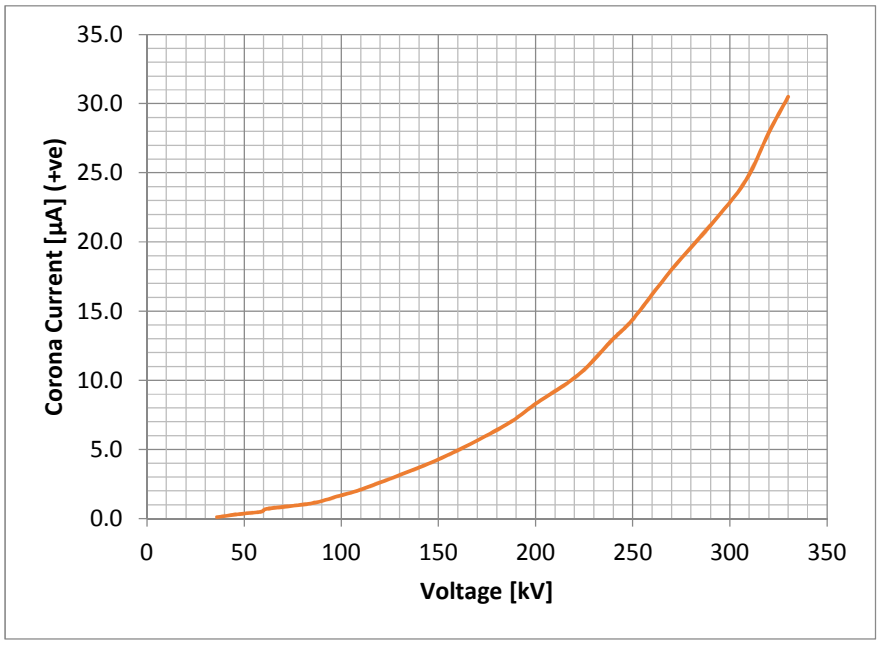

Figure D1.11: I-V Characteristic for 165 cm Grass Height Under 2 Wire Positive Pole

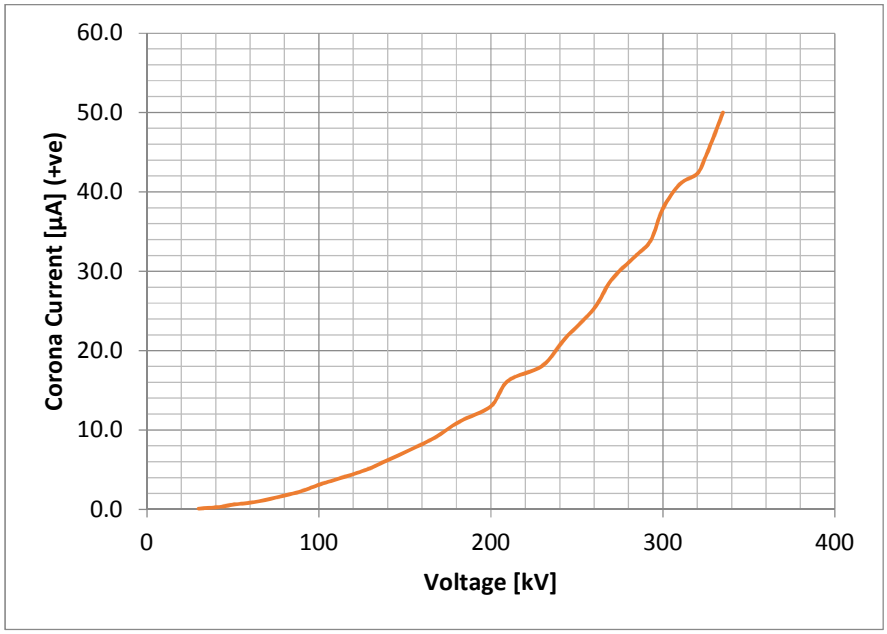

Figure D1.12: I-V Characteristic for 170 cm Grass Height Under 2 Wire Positive Pole

D 2 Negative Polarity with Two Wire Conductor Bundle

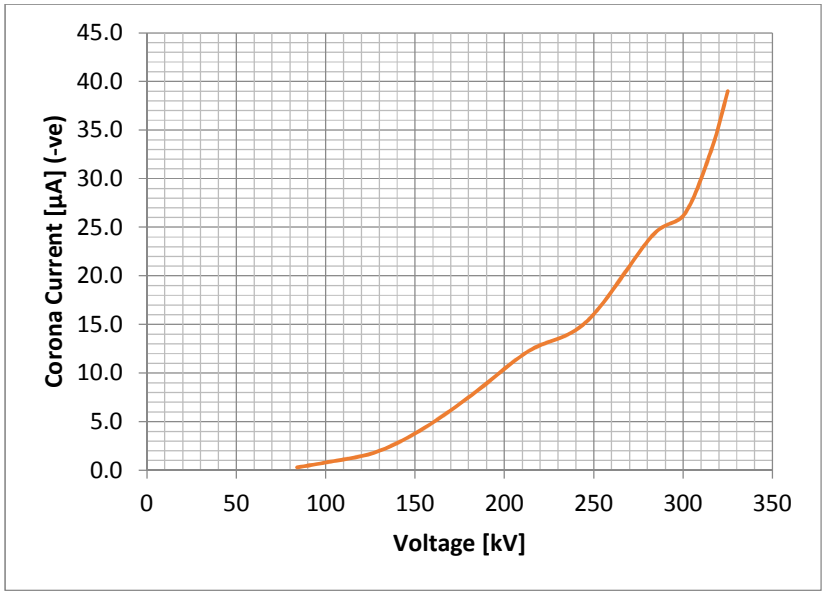

Figure D2.1: I-V Characteristic for 47 cm Grass Height Under 2 Wire Negative Pole

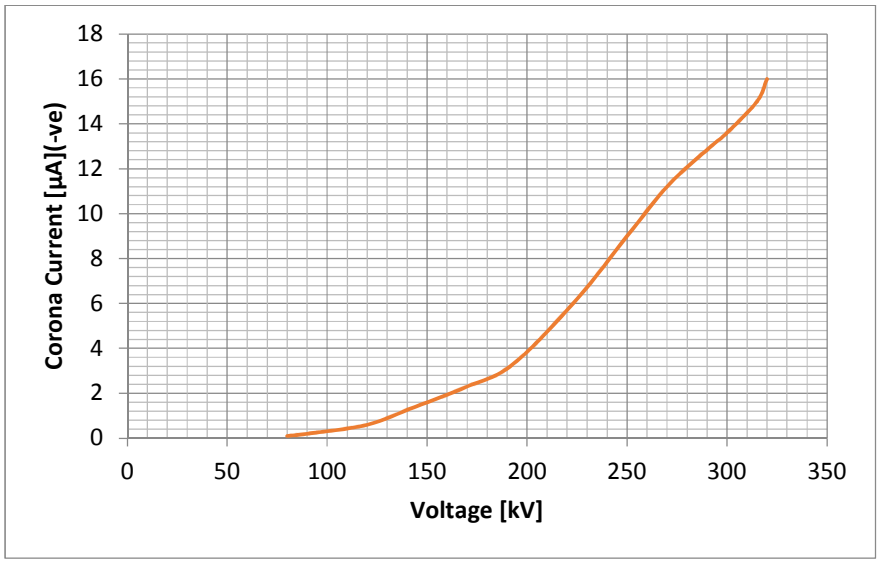

Figure D2.2: I-V Characteristic for 60 cm Grass Height Under 2 Wire Negative Pole

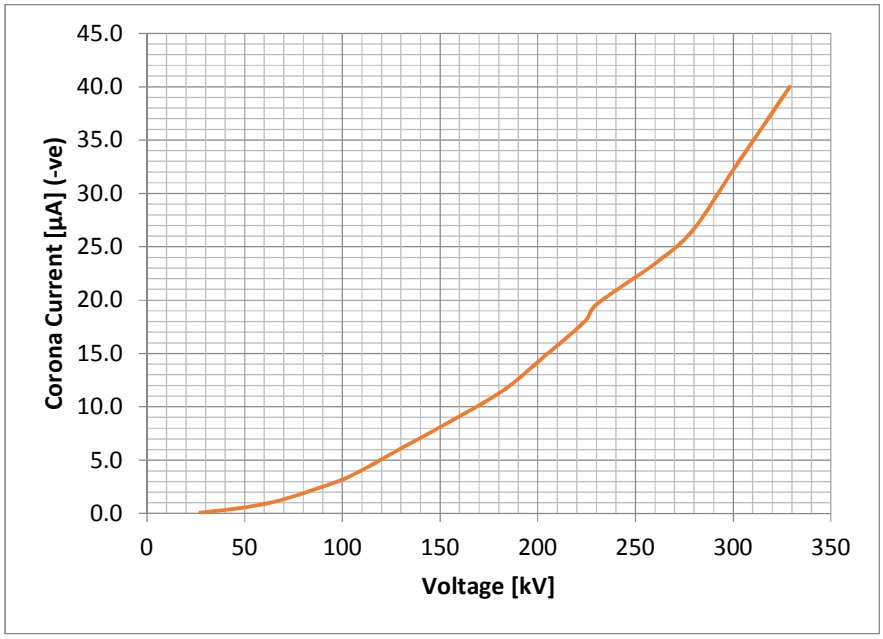

Figure D2.3: I-V Characteristic for 80 cm Grass Height Under 2 Wire Negative Pole

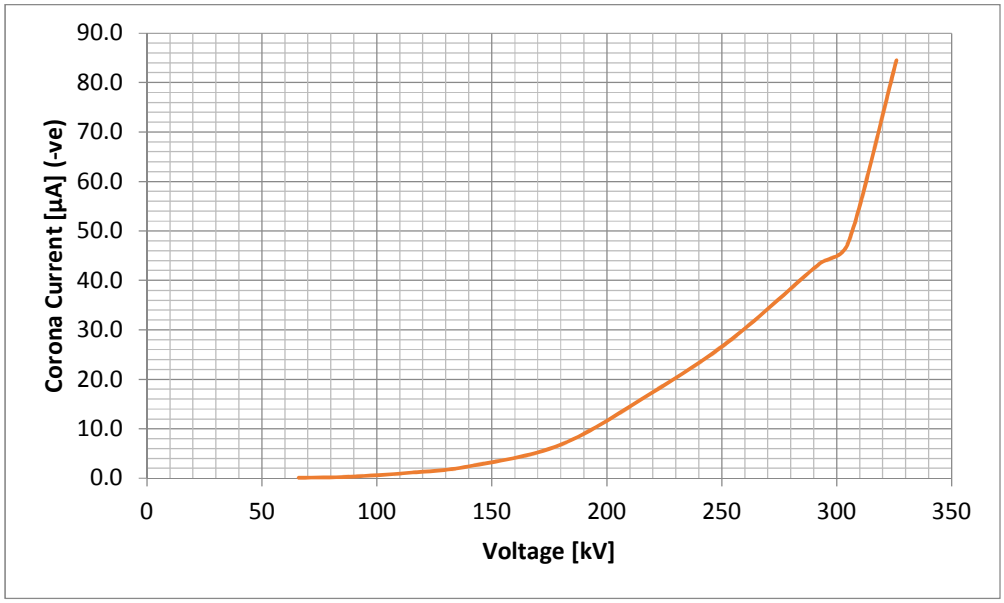

Figure D2.4: I-V Characteristic For 96 cm Grass Height Under 2 Wire Negative Pole

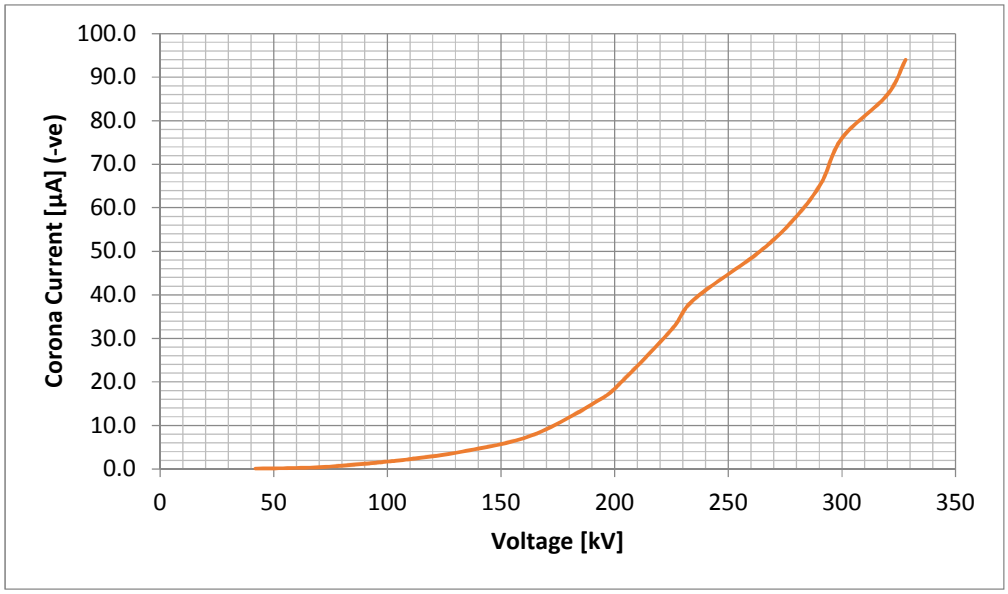

Figure D2.5: I-V Characteristic For 96 cm Grass Height Under 2 Wire Negative Pole

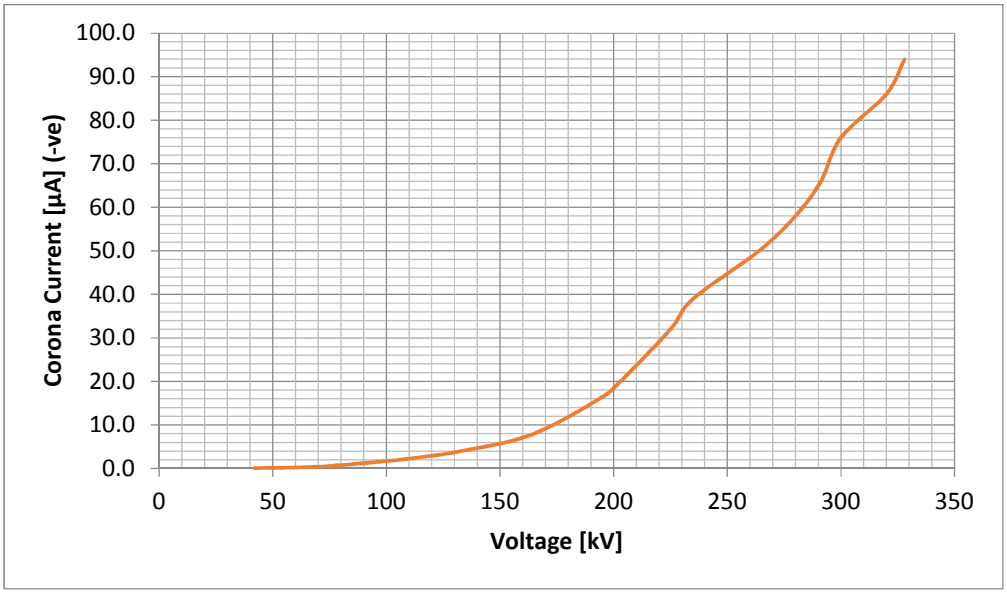

Figure D2.6 I-V Characteristic For 110 cm Grass Height Under 2 Wire Negative Pole

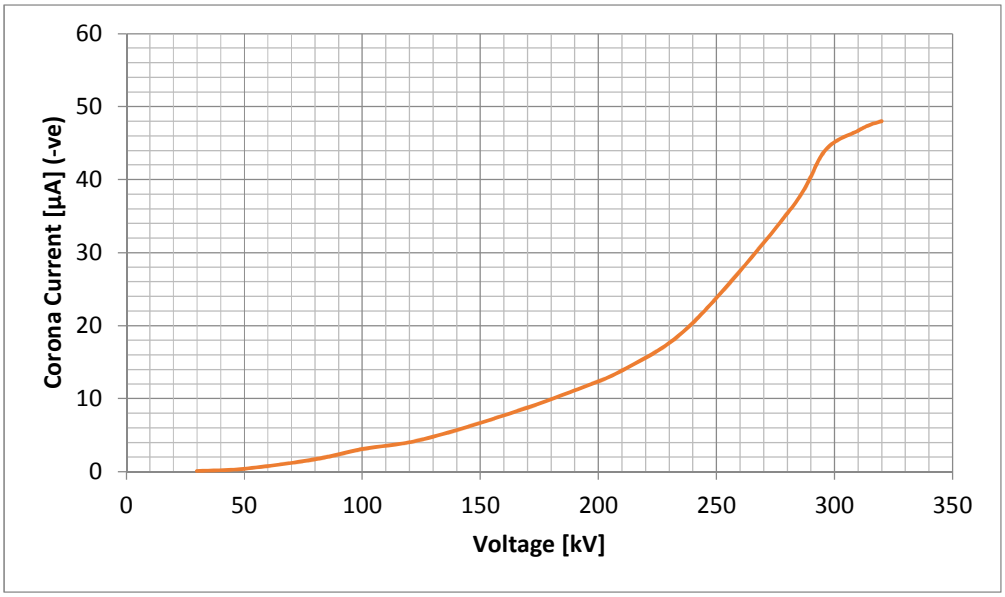

Figure D2.7: I-V Characteristic For 120 cm Grass Height Under 2 Wire Negative Pole

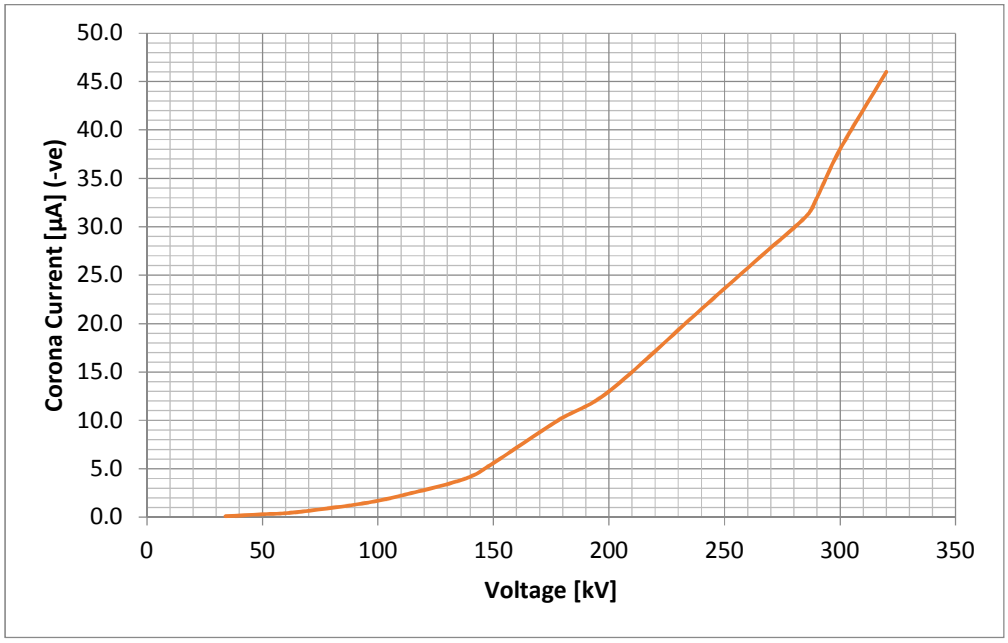

Figure D2.8: I-V Characteristic For 130 cm Grass Height Under 2 Wire Negative Pole

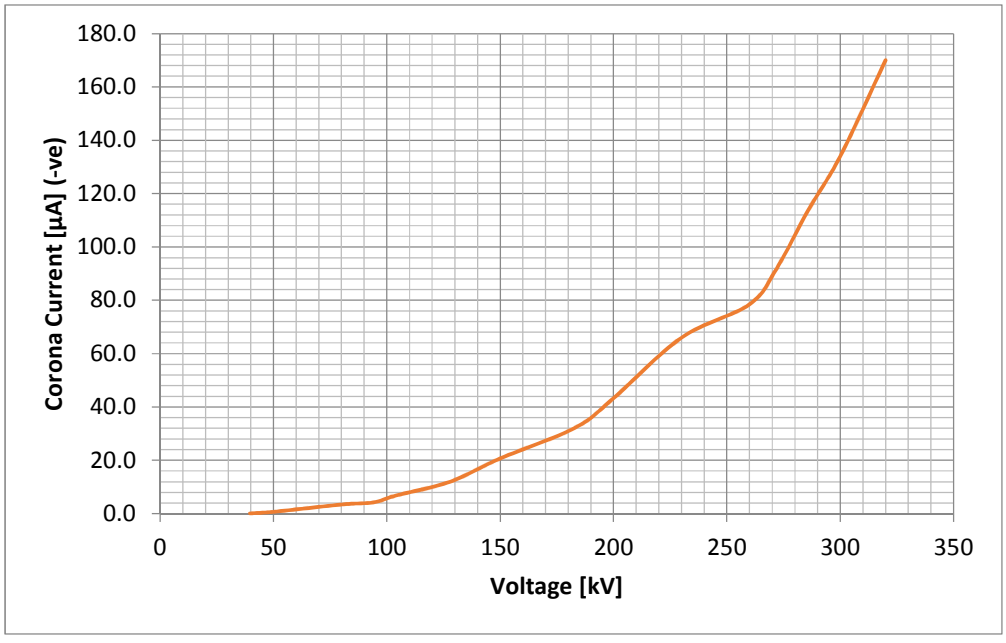

Figure D2.9: I-V Characteristic For 145 cm Grass Height Under 2 Wire Negative Pole

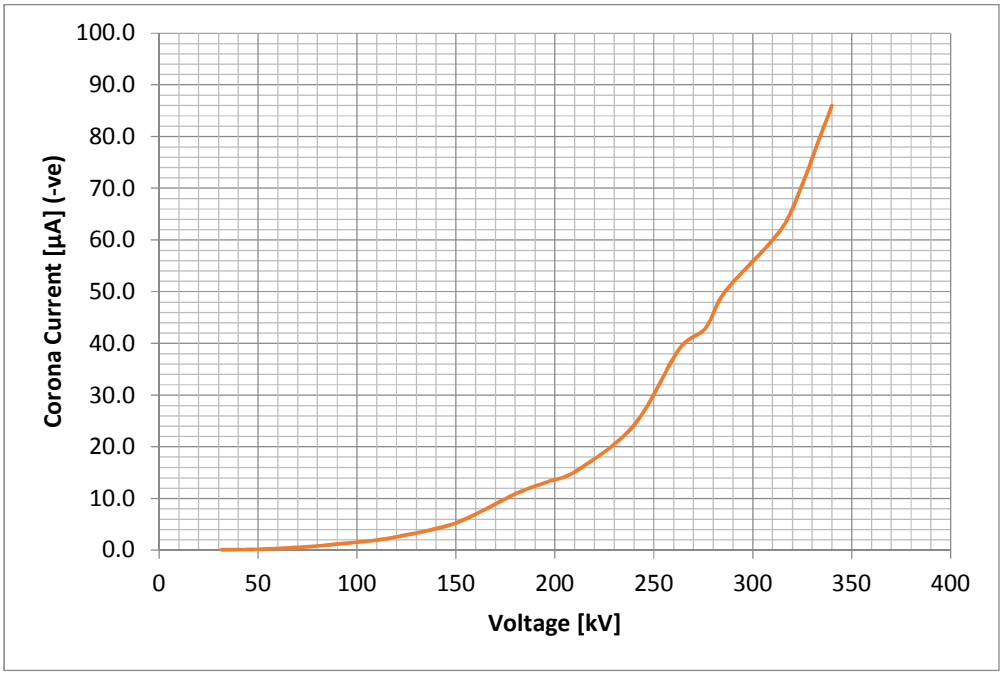

Figure D2.10: I-V Characteristic For 150 cm Grass Height Under 2 Wire Negative Pole

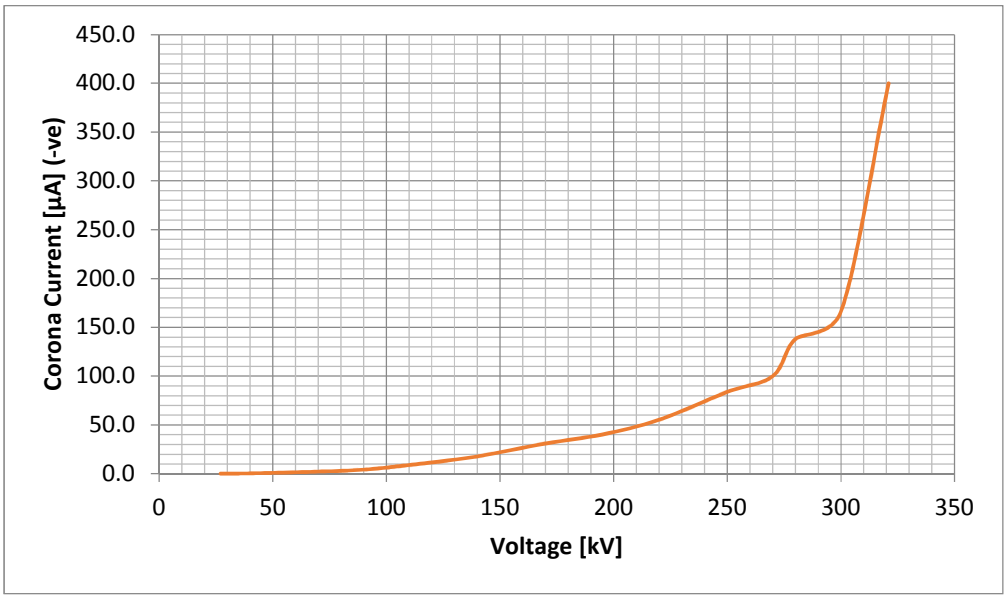

Figure D2.11: I-V Characteristic For 165 cm Grass Height Under 2 Wire Negative Pole

D3 Negative Polarity with Four Wire Conductor Bundle

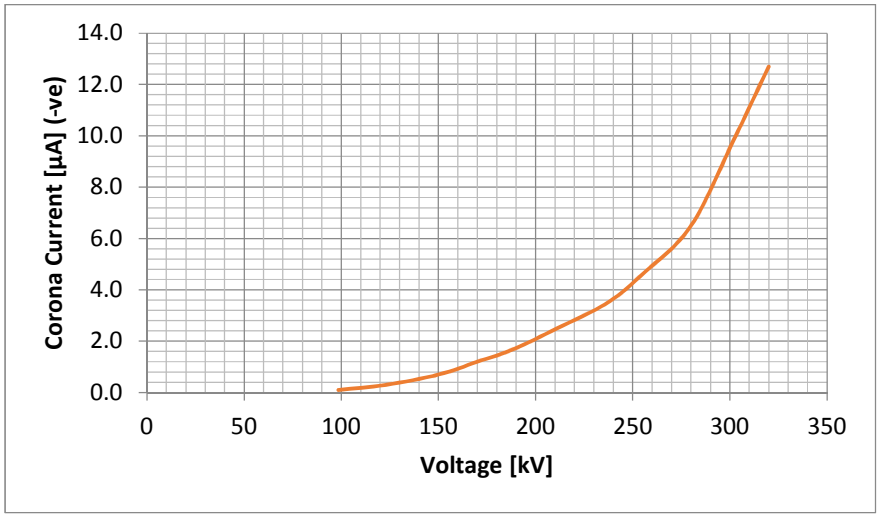

Figure D3.1: I-V Characteristic For 47 cm Grass Height Under 4 Wire Negative Pole

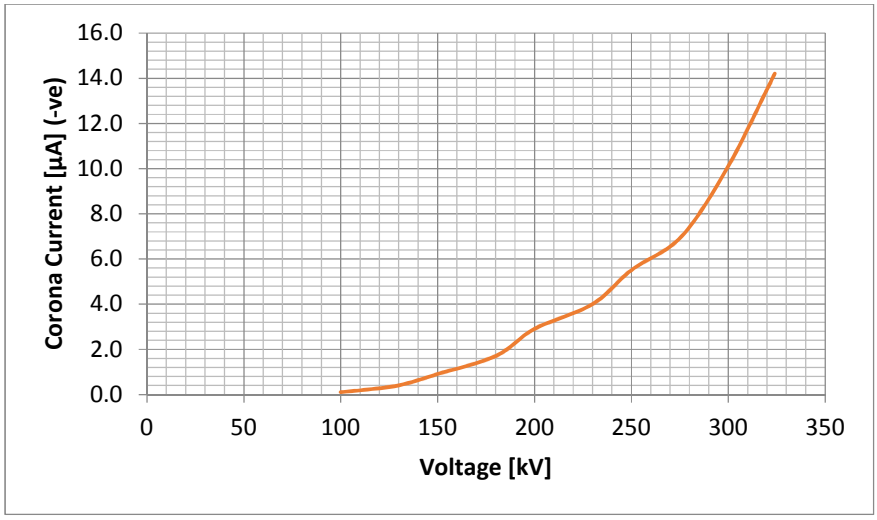

Figure D3.2: I-V Characteristic For 63 cm Grass Height Under 4 Wire Negative Pole

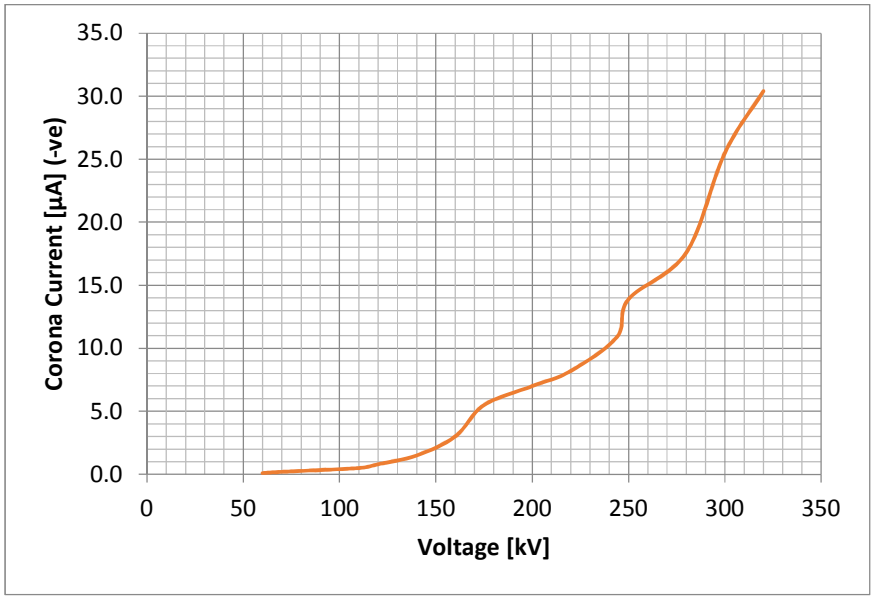

Figure D3.3: I-V Characteristic For 96 cm Grass Height Under 4 Wire Negative Pole

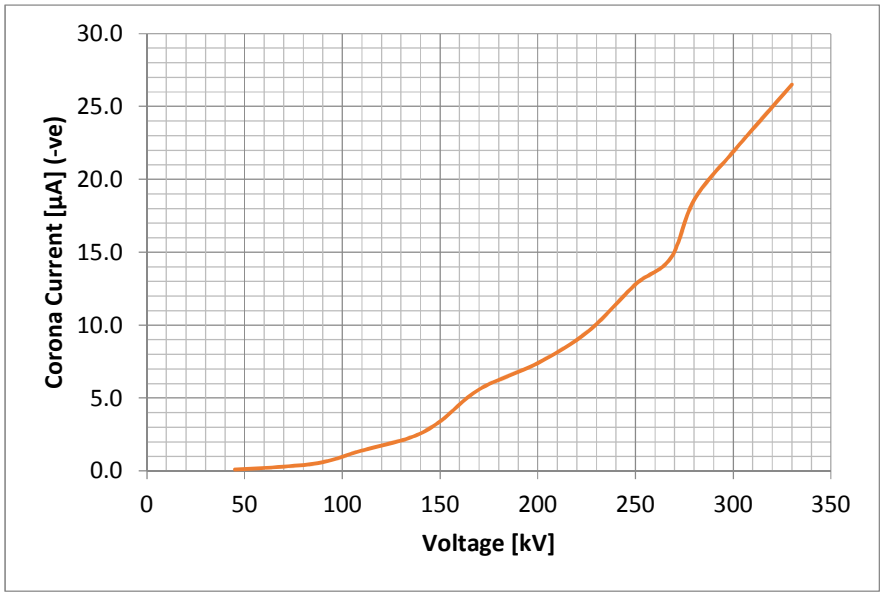

Figure D3.4: I-V Characteristic For 110 cm Grass Height Under 4 Wire Negative Pole

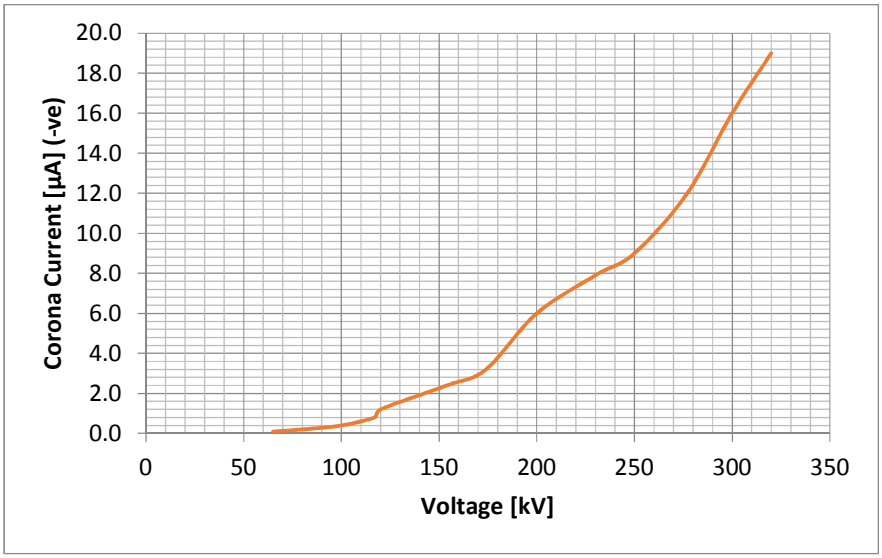

Figure D3.5: I-V Characteristic For 110 cm Grass Height Under 4 Wire Negative Pole

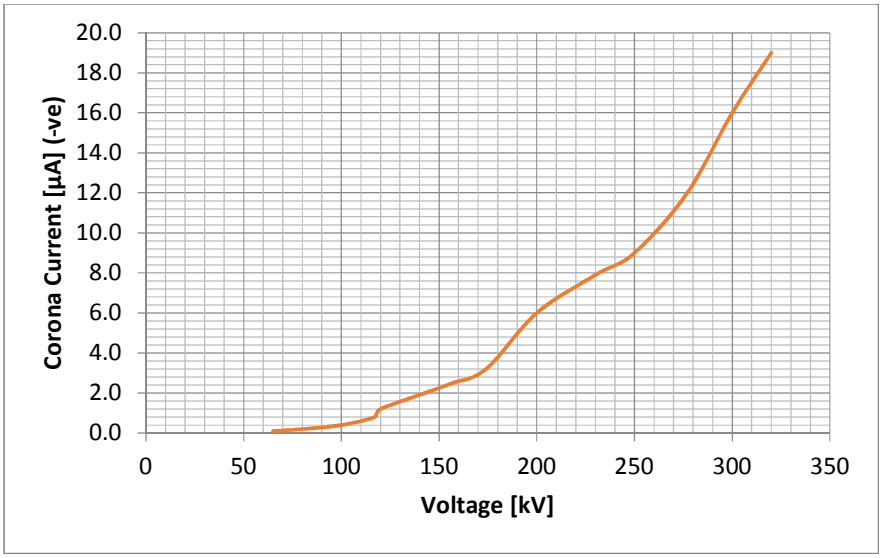

Figure D3.6: I-V Characteristic For 120 cm Grass Height Under 4 Wire Negative Pole

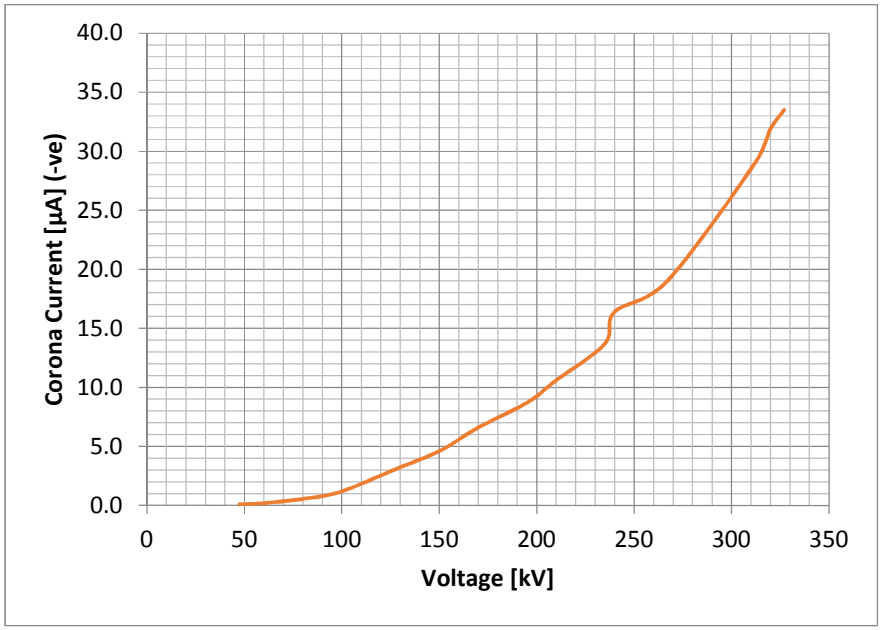

Figure D3.7: I-V Characteristic For 135 cm Grass Height Under 4 Wire Negative Pole

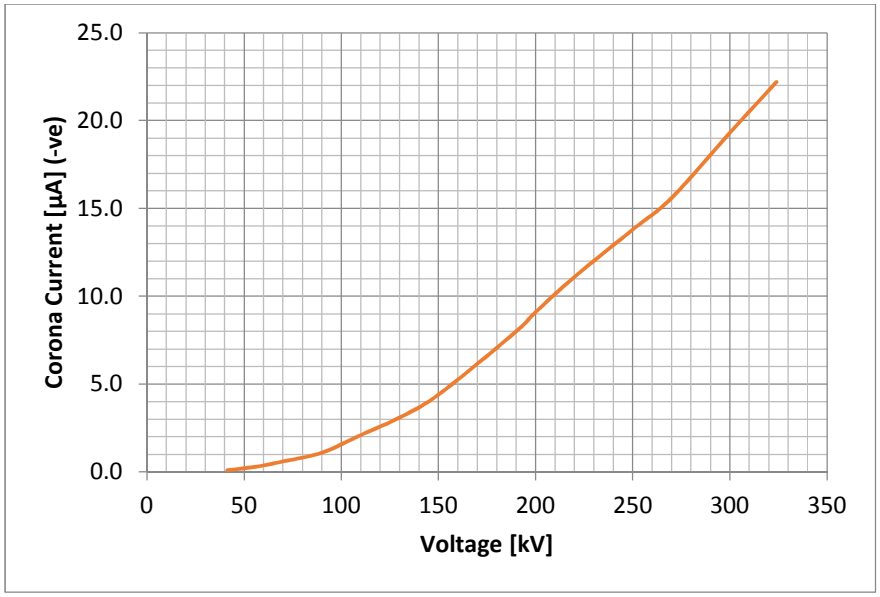

Figure D3.8: I-V Characteristic For 148 cm Grass Height Under 4 Wire Negative Pole

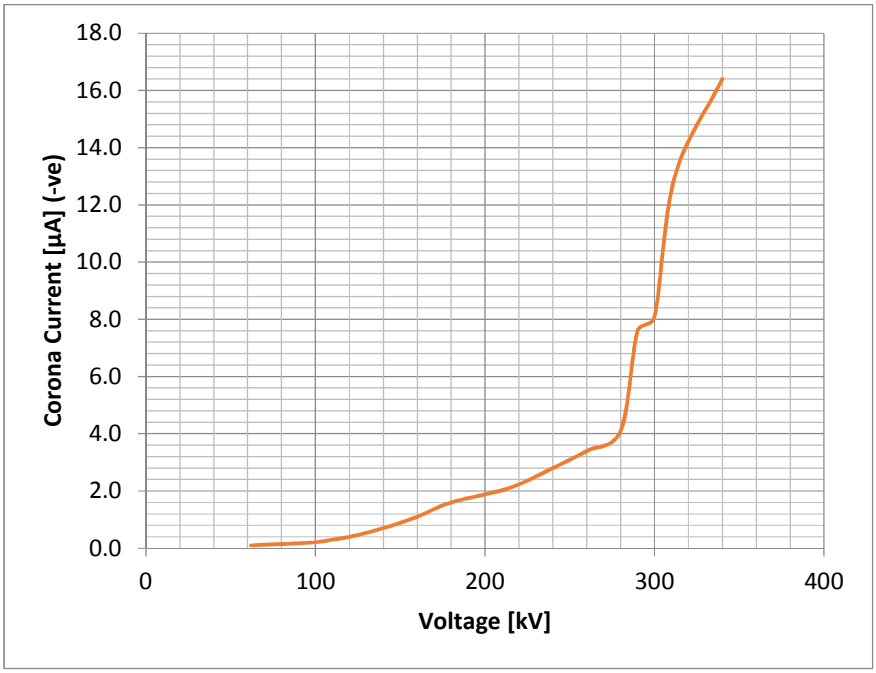

Figure D3.9: I-V Characteristic For 151 cm Grass Height Under 4 Wire Negative Pole

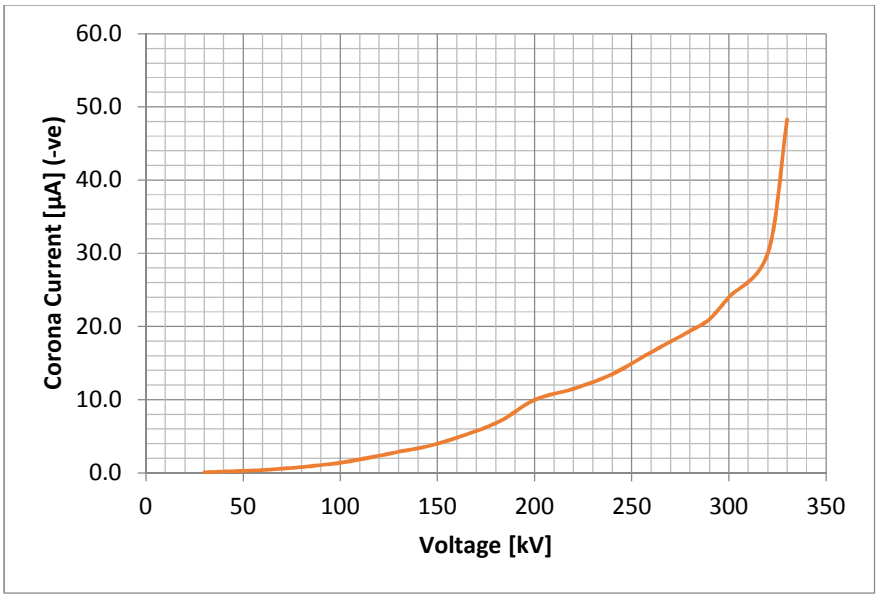

Figure D3.10: I-V Characteristic For165 cm Grass Height Under 4 Wire Negative Pole

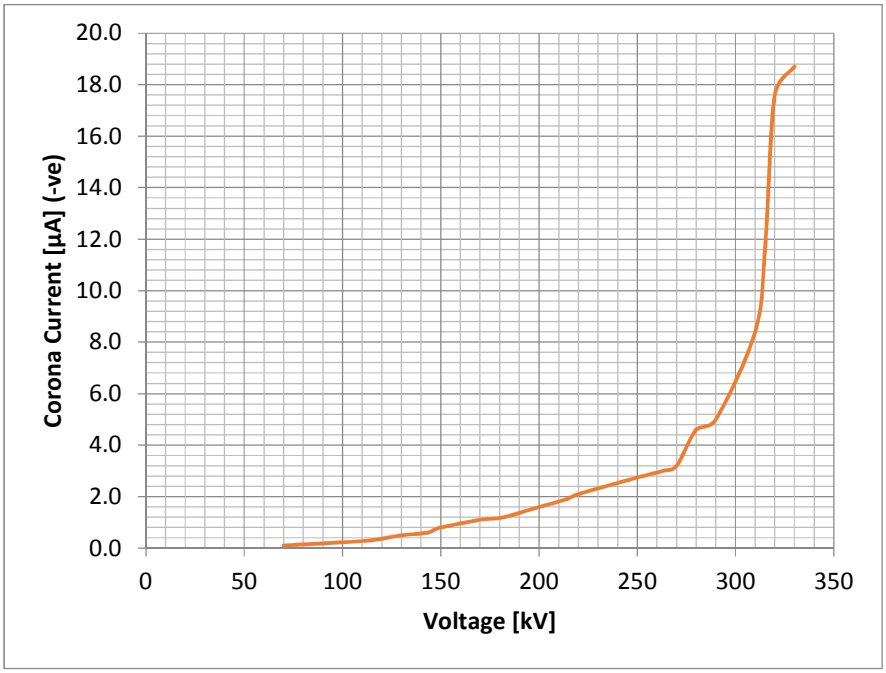

Figure D3.11: I-V Characteristic For150 cm Grass Height Under 4 Wire Negative Pole

D4 Positive Polarity with Four Wire Conductor Bundle

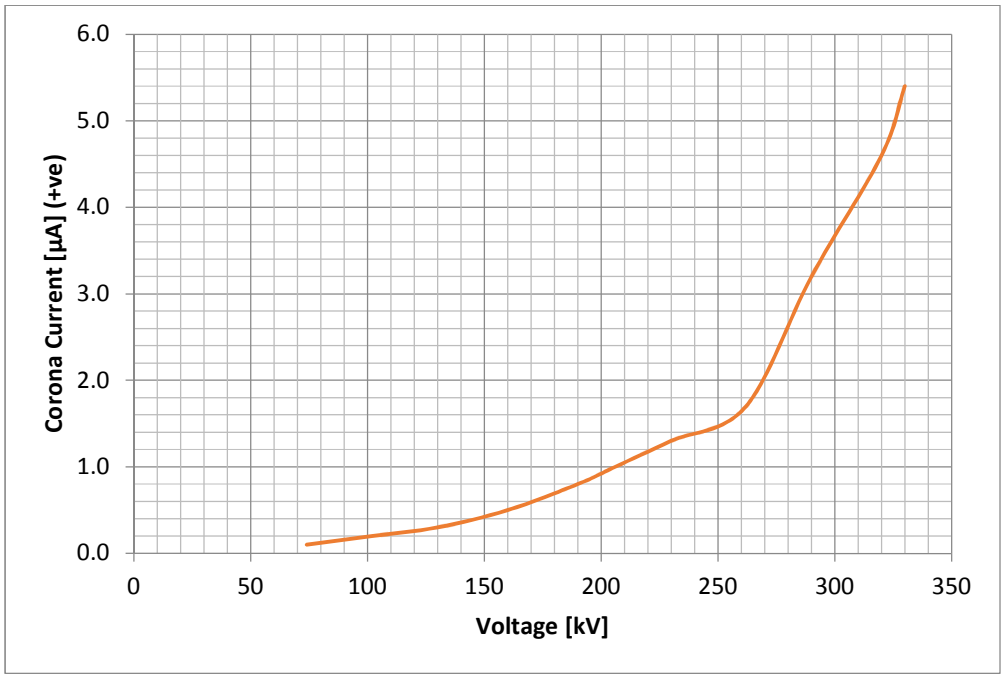

Figure D4.1: I-V Characteristic For 45 cm Grass Height Under 4 Wire Positive Pole

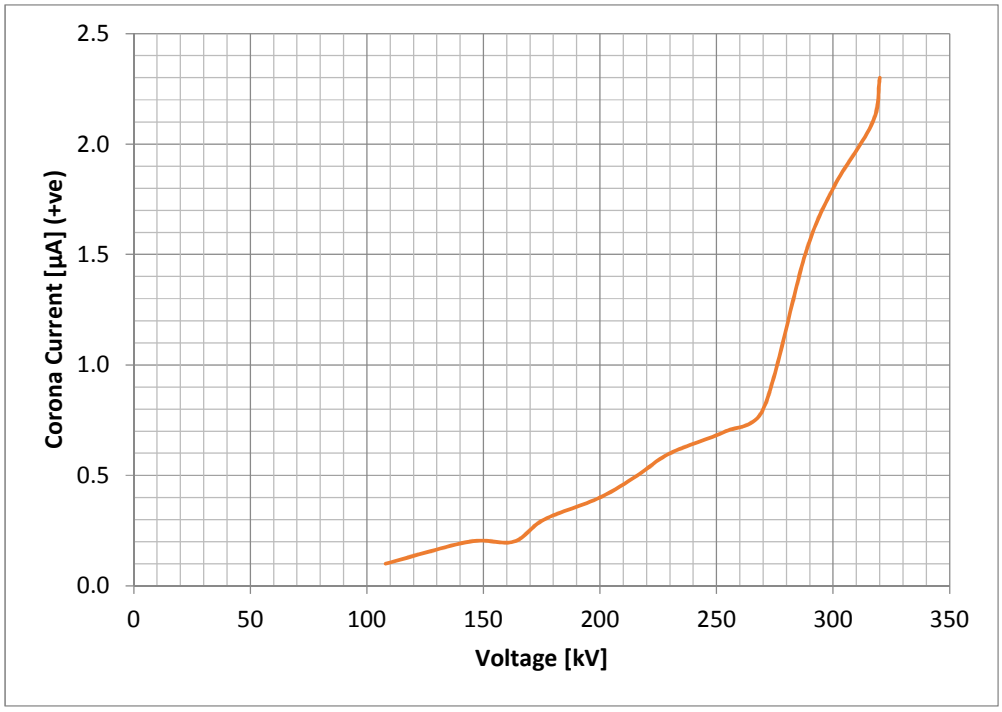

Figure D4.2: I-V Characteristic For 47 cm Grass Height Under 4 Wire Positive Pole

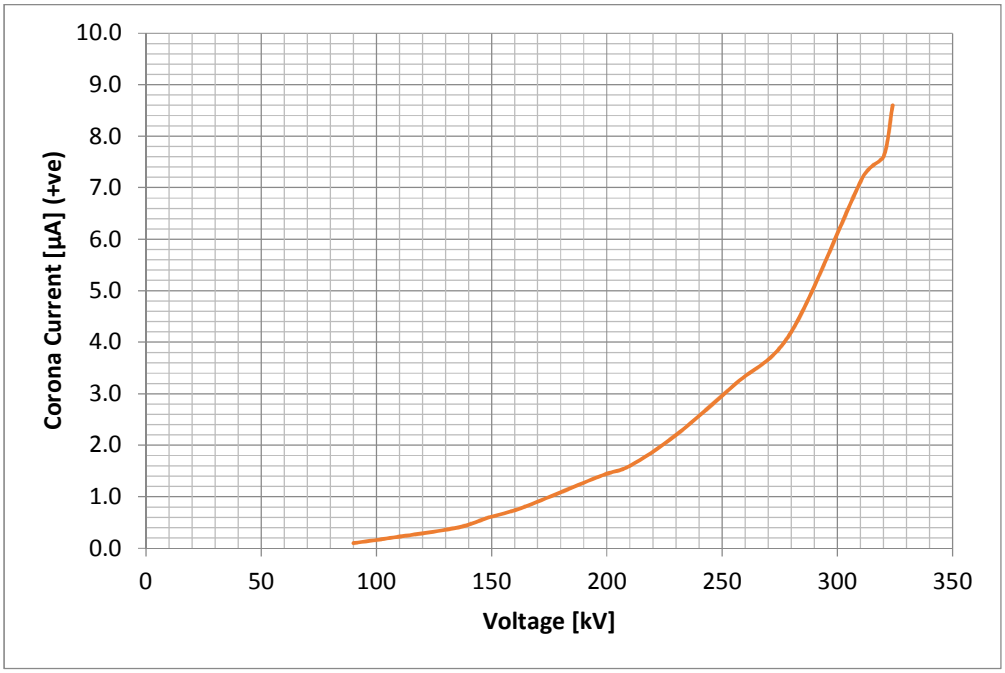

Figure D4.3: I-V Characteristic For 63 cm Grass Height Under 4 Wire Positive Pole

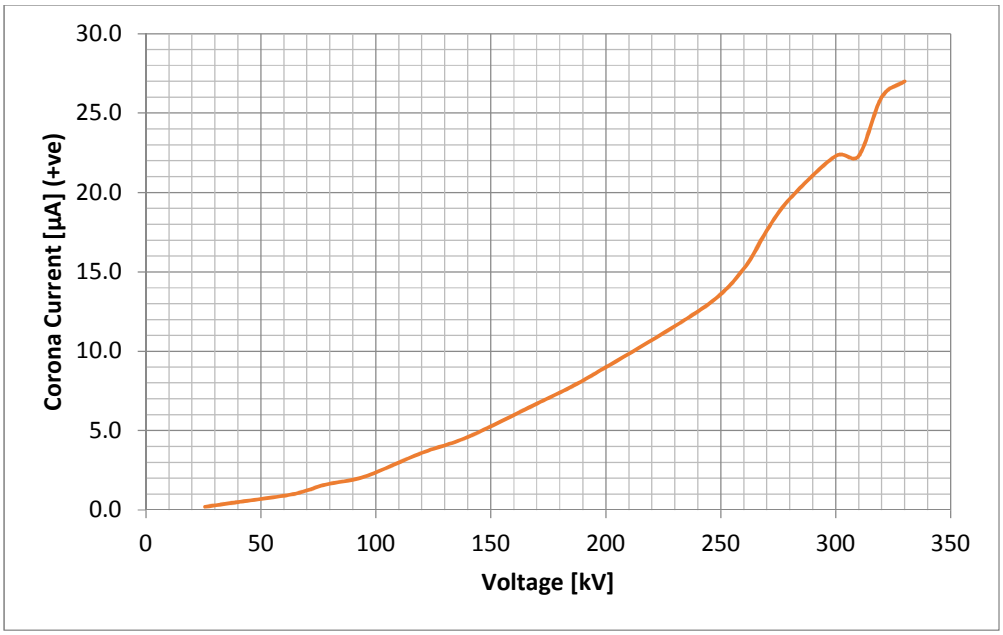

Figure D4.4: I-V Characteristic For 73 cm Grass Height Under 4 Wire Positive Pole

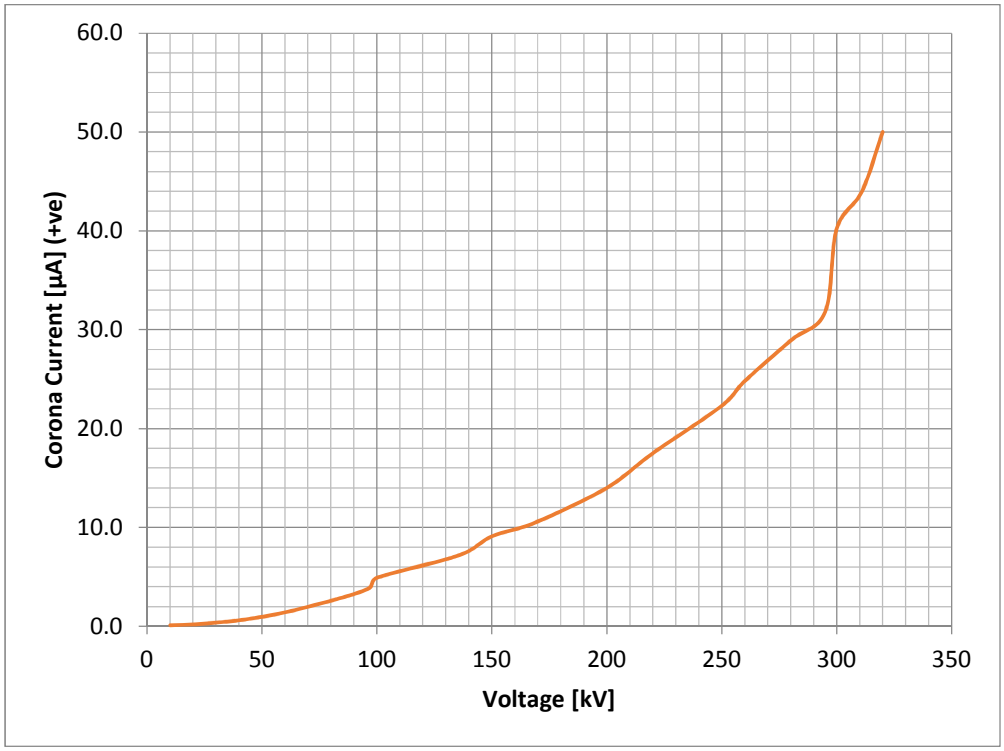

Figure D4.5: I-V Characteristic For 80 cm Grass Height Under 4 Wire Positive Pole

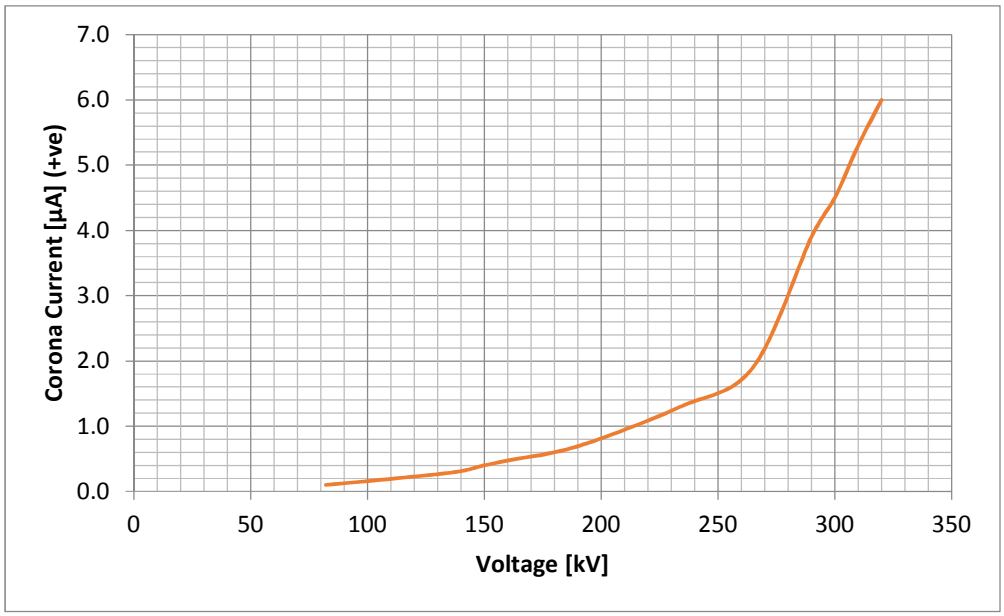

Figure D4.6: I-V Characteristic For 96 cm Grass Height Under 4 Wire Positive Pole

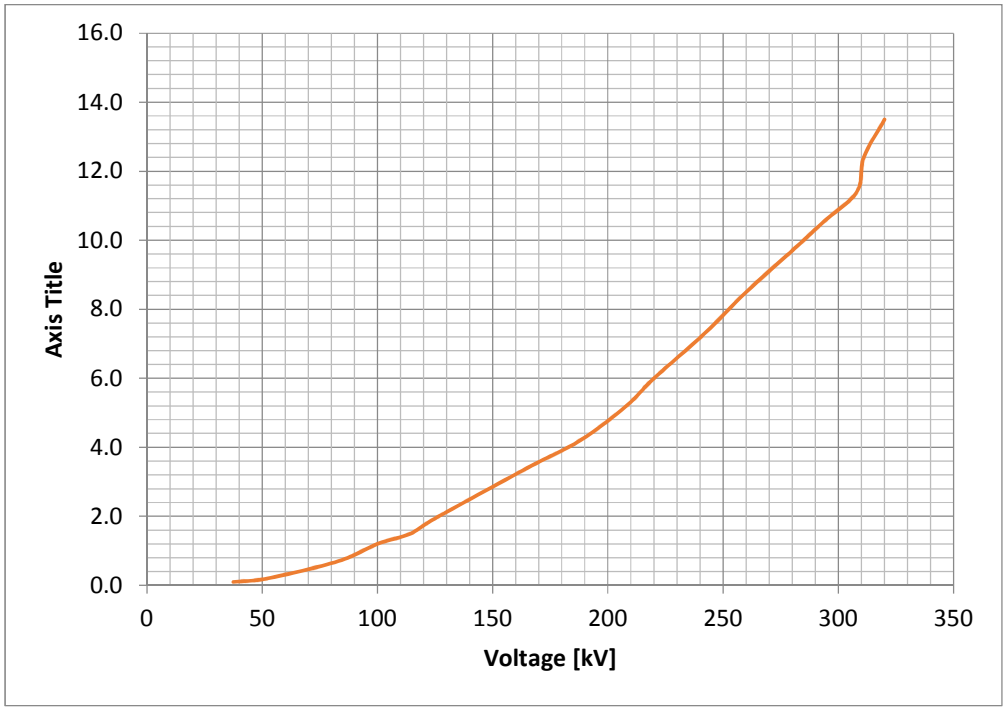

Figure D4.7: I-V Characteristic For 110 cm Grass Height Under 4 Wire Positive Pole

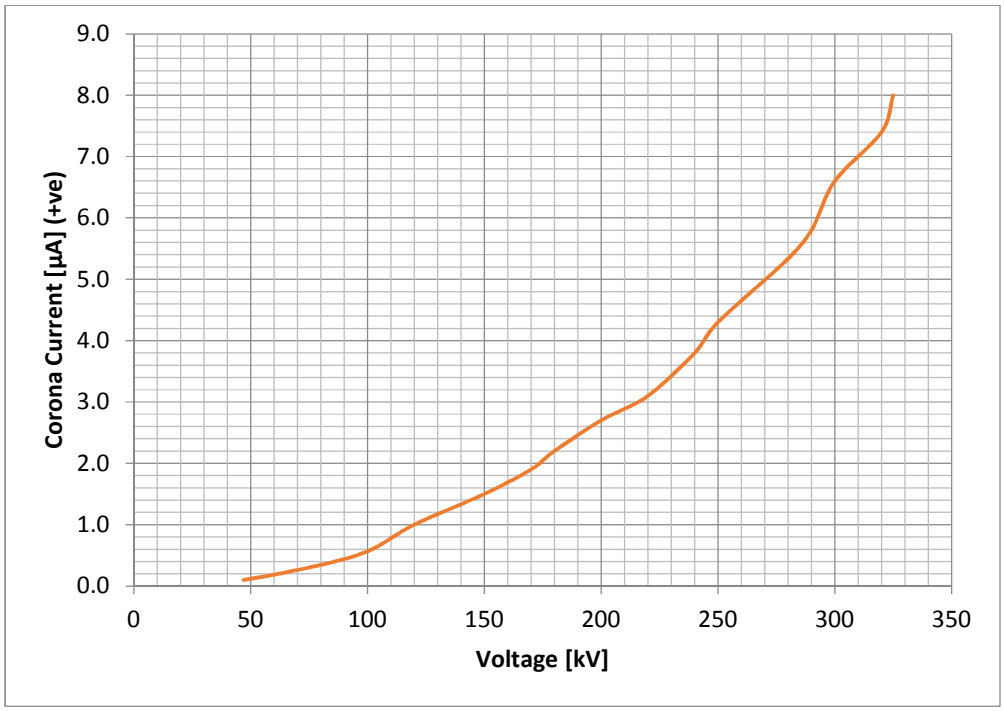

Figure D4.8: I-V Characteristic For 120 cm Grass Height Under 4 Wire Positive Pole

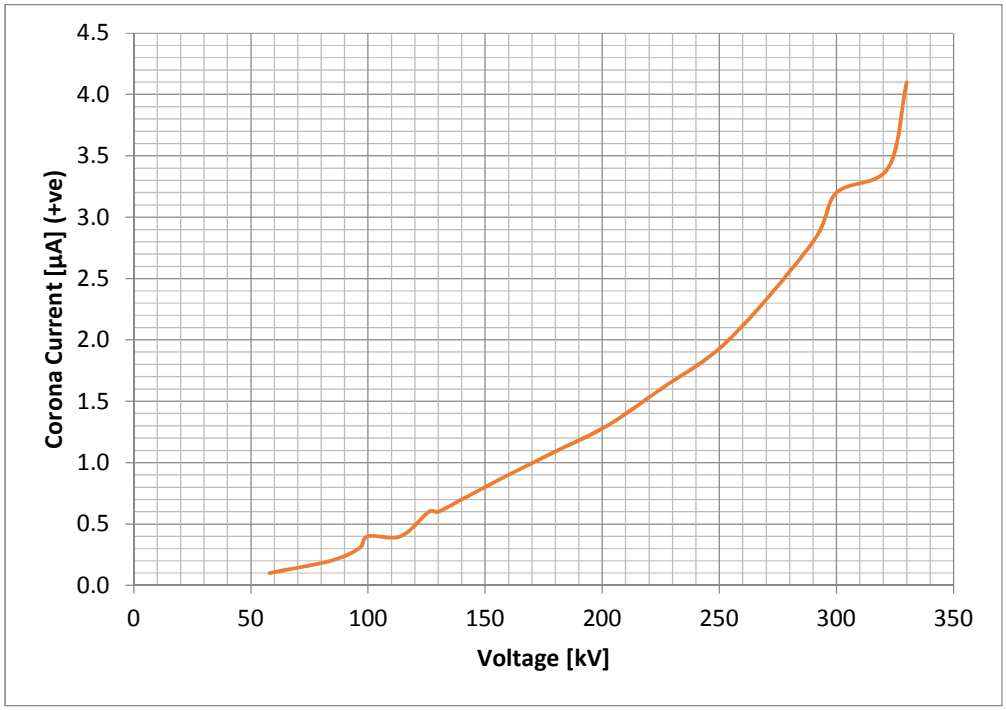

Figure D4.9: I-V Characteristic For 130 cm Grass Height Under 4 Wire Positive Pole

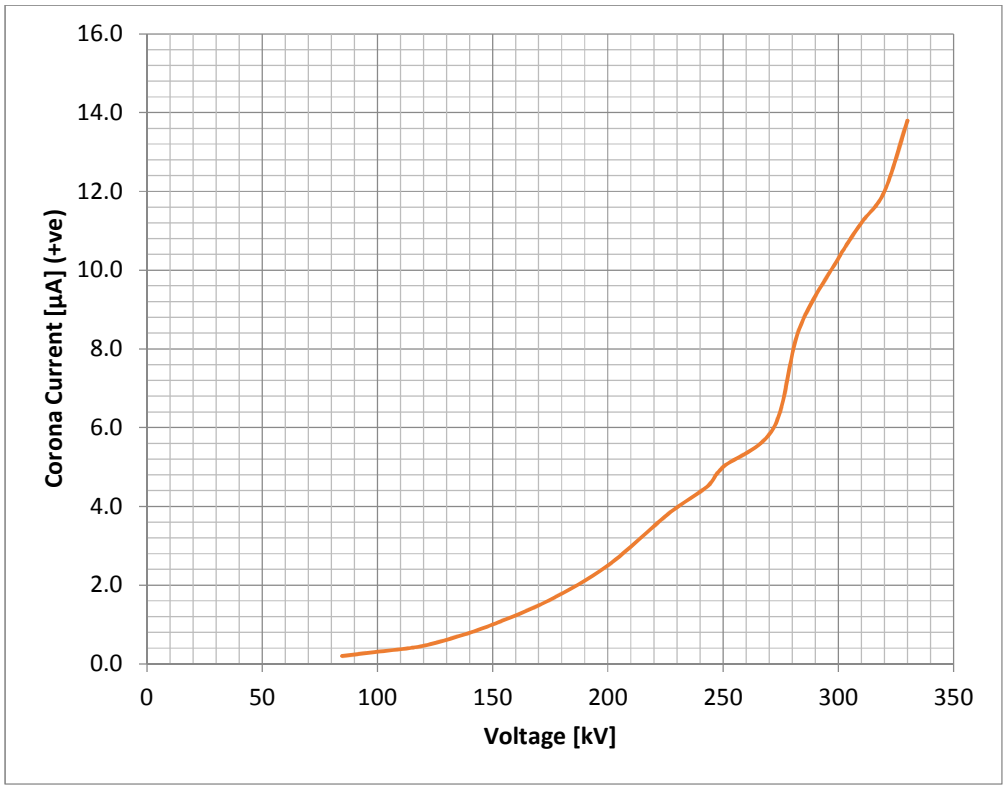

Figure D 4.10: I-V Characteristic For 145 cm Grass Height

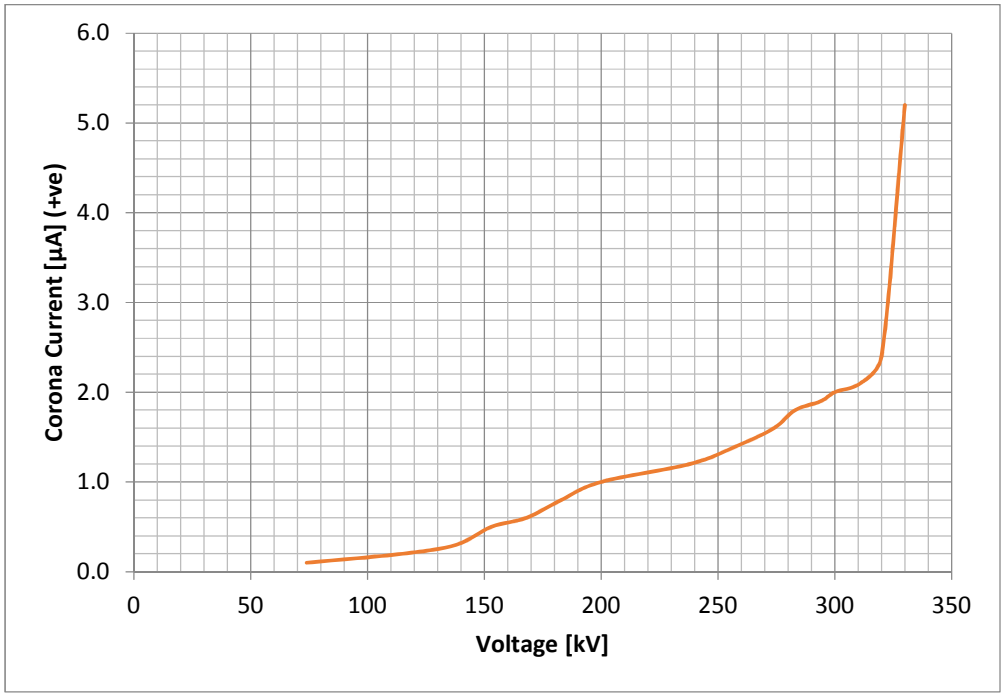

Figure D4.11: I-V Characteristic For 150 cm Grass Height Under 4 Wire Positive Pole

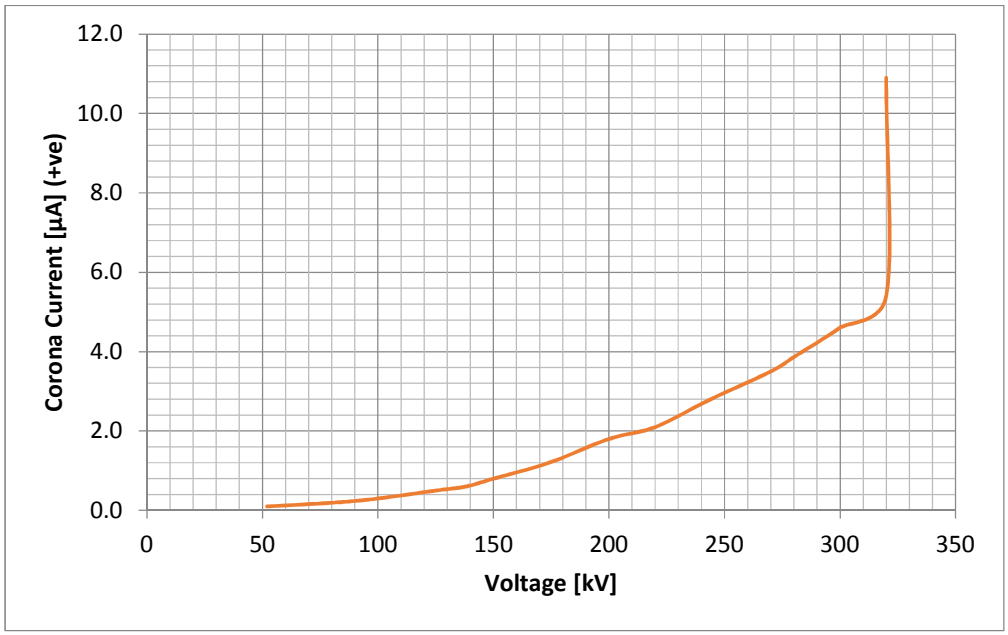

Figure D4.12: I-V Characteristic For 150 cm Grass Height Under 4 Wire Positive Pole

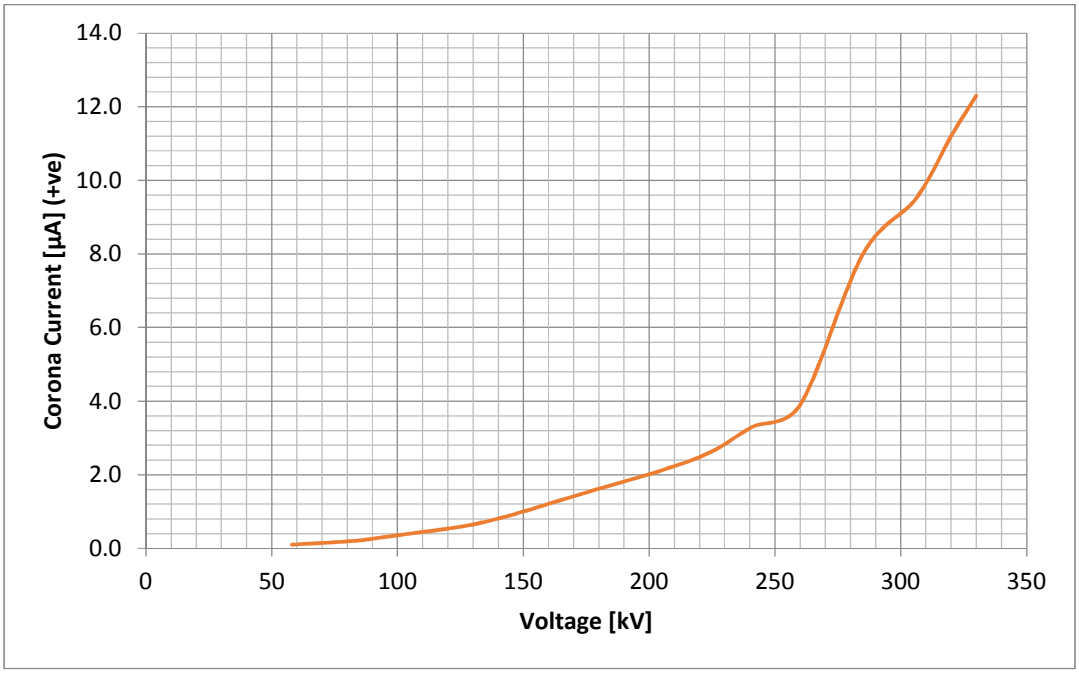

Figure D4.13: I-V Characteristic For 151 cm Grass Height Under 4 Wire Positive Pole

APPENDIX E ASSOCIATED PUBLICATIONS

Siame C, Chetty L, Ijumba NM, "Investigation of Corona Induced Fire in High Voltage DC Lines", *XVII International Symposium on High Voltage Engineering*, Hannover, Germany, August 22-26, 2011